LUT
Lappeenranta
University of Technology

Rotich Nicolus Kibet (Nicholas)

DEVELOPMENT AND APPLICATION OF COUPLED DISCRETE AND CONTINUUM MODELS IN SOLID PARTICLES CLASSIFICATION

Thesis for the degree of Doctor of Science (Technology) to be presented with due permission for public examination and criticism in the Auditorium 2310 at Lappeenranta University of Technology, Lappeenranta, Finland on the 9th of June, 2017, at noon.

Acta Universitatis
Lappeenrantaensis 745

Supervisor Professor Marjatta Louhi-Kultanen
Department of Chemical and Metallurgical Engineering
Aalto University
Finland

Supervisor Assoc. Professor Ritva Tuunila
LUT School of Engineering Science
Lappeenranta University of Technology
Finland

Reviewer Prof. Dr.-Ing. Ulrich Teipel
The Fraunhofer Institute for Chemical Technology (ICT)
Technische Hochschule Nürnberg
Germany

Reviewer Prof. Tomáš Svěrák
Laboratory of separation Processes
Faculty of Mechanical Engineering
Brno University of Technology
Czech Republic

Opponent Prof. Dr.-Ing. Ulrich Teipel
The Fraunhofer Institute for Chemical Technology (ICT)
Technische Hochschule Nürnberg
Germany

Opponent Prof Hylke J. Glass
Camborne School of Mines
The University of Exeter, England
United Kingdom

ISBN 978-952-335-078-6
ISBN 978-952-335-079-3 (PDF)
ISSN-L 1456-4491
ISSN 1456-4491
Lappeenrannan teknillinen yliopisto
Yliopistopaino 2017

Abstract

Rotich Nicolus Kibet (Nicholas)
Development and application of coupled discrete and continuum models in solid particles classification
Lappeenranta 2017
79 pages
Acta Universitatis Lappeenrantaensis 745
Diss. Lappeenranta University of Technology
ISBN 978-952-335-078-6, ISBN 978-952-335-079-3 (PDF), ISSN 1456-4491

Bulk solids handling play a critical role in modern industrial processes. Particulate classification is one aspect of materials (bulk solids) handling, the aim of which is to distinguish unique particles by virtue of predetermined criteria. Construction, foods, mining, pharmaceutical industries, power generation (e.g. the now versatile biomass-based co-generation plants), and waste management etc., often require sorting in terms of size, specific gravity, grain loading, shape, chemical composition, bulk density, resistivity, friability, wettability, cohesiveness, resilience etc., prior to end-use or further utilization in downstream unit operations. Moreover, bulk solids have been a complex material for several decades, as the process is often referred to as 'not fully understood'.

This dissertation is aimed at developing enhanced, and deeply understood methods for modelling the flow of particles during size classification, by incorporating modern study tools, including computer simulations, and experimental designs, targeted at improved processes. One key objective is to understand the dynamics of granular flow in depth, and to find ways to correlate the energy spent, and the efficiency in such solids classification, both with gravity and vibrated screening equipment. This direct link holds the key to a better understanding that may lead to optimal design and operation of particle classification equipment. The second objective is to address the inefficiency caused by operations at high capacity, through further development of the methods of determination of the rates and optimization of classification processes. The final objective is to simplify these models, to make them easy and applicable for rapid prototyping, fabrication and up-scaling in relevant the industries.

First order rate law (FORL) has been used for a long time to estimate the rate of particles' classification during screening. However FORL only calculates the current population of particle (overflow), but does not estimate the difference in particle population, or the underflow. In order to get the passage, the overflow must be subtracted from the original mass or the particle count. Due to this problem, there are only a few mathematical models (apart from some Weibull distribution functions), that can estimate underflow growth from zero. The existence (or non-existence), of such models is usually described as failure, as it censors some useful results. Secondly, FORL does not necessarily relate the moments or rate constants, to the key design parameters of the unit operation, such as screen dimensions and area, aperture sizes and shapes, and transient motion of particles along the

sieve lengths in general. These problems present a challenge for, and are a limitation of the FORL, and thus necessitates empirical, or data-driven modelling. In this thesis, all the components of particle population are estimated simultaneously, which seems to be a successful methodology for further development. An attempt is made to link these constants to the design parameters, used in a representative case study on designing the unit operation.

An improved theoretical model for the quantification of the rate of classification is postulated, based on discrete and continuum mathematical theories. These models are tested through a prototype screening equipment designed for studying the impacts of feed throughput, flowability, and screen deck declinations on the overall performance of the screen. Two extremes usually exist when considering rheology in fluid flow. Either it is assumed purely *compressible* or *incompressible*. Contrary to these assumptions, it is shown in this study that granular flows are divided into two regimes - the continuum constituting the middle of the flow cross-section, and the bulk flow around it. The specific gravity of the *particle fluid* tend to vary with the position (vector in space) in the continuum, but invariant with time. In the bulk region, however, the specific gravity varies more with time, but less with position, and thus the flow forms a quasi-compressible flow. Granular flow is therefore described in this study as turbulent, unsteady, Newtonian fluid flow (in a wide channel), with nominal to high densities, and generally low dynamic viscosities, and consequently even lower kinematic viscosities. It is therefore incompressible within the core continuum, but compressible around the bulk flow regime. The volume of the continuum changes with space, and thus the density varies only macroscopically, but remains nearly constant microscopically inside the continuum. The flow over the screens is classified as unidirectional subsonic, meaning that the flow velocity is low ($\leq 3.5\text{ms}^{-1}$) and only in one direction (downslope), giving Mach numbers below 0.011. On the other hand, when discrete models are considered, granular materials and powders are assumed to be incompressible, dry, non-cohesive, and rigid, in order to allow time averaging of the bulk velocity. Both models result in Newton's second law for variable masses, whose solution is found analytically and numerically. Obtaining and zeroing the gradient of the fluctuation velocity enables achieving the agitation force requirements in G-force.

A close correlation was found between the developed theoretical and simulation models, and experimental results. In general, dense screen loading is the main source of momentum accumulation that increases the underflow rates, rather the capacity in ton per hour, but reduces the flowability, and consequently the efficiency of size classification. For multi-sized screens, it was shown that up to 99.99% efficiency can be achieved for gravity separators while operating at low to medium capacity, but the same efficiency can only be achieved operating at low capacities in vibrated screens.

Keywords: Bulk solids; Classification; Continuum models; Discrete simulation; Sieve Screening; Numerical modelling; Solids separation; Material handling

Acknowledgments

I have had the pleasure of carrying out this doctoral dissertation in the School of Engineering Science of Lappeenranta University of Technology (LENS), Finland, between May 25, 2013 and June 24, 2016. During this period, I was guided, mentored and supervised by Prof. Marjatta Louhi-Kultanen and associate Professor Ritva Tuunila, whose time and support has been invaluable. I wish to express my sincere gratitude for all the support they have offered me during this period. I will be forever thankful.

Part of the concepts in the dissertation were developed in collaboration with the University of Waterloo, Canada, under the supervision of Prof. Ali Elkamel, whom I wish to thank for accepting my request to conduct a research visit for a period of one year, and for his unrelenting support.

I also wish to thank the key financiers of my doctoral thesis, the Finnish Cultural Foundation - South Karelia Regional Fund (in Finnish: Suomen Kulttuurirahasto, Etelä-Karjalan rahasto), which supported my studies for two full academic years. I also wish to recognize the support from the Research Foundation of Lappeenranta University (LUT tukisäätiö), the Alfred Kordelin - Gust. Kompan foundation and the Finnish Science Foundation for Economics and Technology (KAUTE).

I thank my colleagues at LENS, especially in loving memory of Mr Markku Maijanen who helped in building the prototype equipment I used for lab experiments, may his soul rest in eternal peace. I thank Mr Henri Vainio and Ms Minna Laitinen for helping me in conducting the necessary experiments. Much thanks also go to Peter Curran, Avery Drouillard, and Chris Chen of the University of Waterloo, for carrying out related studies that supported my work during the research visit in Canada. Thank you all for allowing me to count on you.

Lastly, I wish to thank my mom for her love, first for me, and for education, that compelled her to push me to these great heights. I thank all my siblings for accepting and understanding my struggles and time away from home. Finally, I thank my fiancéé Valentine, and my two lovely daughters, Natasha and Cassidy. Your love, support, and understanding have brought me this far. You mean the world to me, and I will always be indebted to all of you.

Nicolus Rotich
May 26, 2017
Lappeenranta, Finland

Contents

List of publications

Publication I

Rotich, N., Tuunila, R., and Louhi-Kultanen, M. (2013). Modeling and simulation of gravitational solid-solid separation for optimum performance. *Powder Technology*, 239, pp. 337-347.

In this publication, the author proposed the rate equation that was studied in the publication. The author also designed the prototype equipment used for the tests and carried out the modeling and simulation part. The manuscript was completed with the co-authors.

Publication II

Rotich, N., Tuunila, R., and Louhi-Kultanen, M. (2015). Empirical study on the effects of screen inclination and feed loading on size classification of solids by gravity. *Minerals Engineering*, 70, pp. 162-169.

All experimental work presented in this empirical study was carried out by the author with a little help from an undergraduate student under the supervision of the author. The manuscript was completed together with the co-authors.

Publication III

Rotich, N., Tuunila, R., Elkamel, A., and Louhi-Kultanen, M. (2016). Nonlinear optimization of gravity solids classification based on the feed and deck angles: a law of mass action approach. *Powder Technology*, 291, pp. 140-146.

The experimental work was carried out by the author with the help of an undergraduate student under the author's supervision. The computational study part was done by the author, with the help of an international supervisor, who was also a co-author. The manuscript was completed with all the co-authors.

Publication IV

Rotich, N., Tuunila, R., Elkamel, A., and Louhi-Kultanen, M. (2016). Dynamic population balance and flow models for granular solids in a linear vibrating screen. *AIChE Journal*, 62(11), pp. 3889-3898.

The experimental design and planning was carried out by the author with the help of an undergraduate student under the author's supervision in carrying out the experimental work. The computational study part was done by the author, with the help of an international supervisor, who was also a co-author. The manuscript completed with all the co-authors.

Publication V

Rotich, N., Tuunila, R., and Louhi-Kultanen, M. (2013). Nonlinear optimization of gravity separation, feed and deck angles with response surface methodology (Peer reviewed). In: Yianatos, J., ed., Proceedings of the XXVII International Mineral Processing Congress-IMPC 24th October 2014, Ch. 17, pp. 15-26. Santiago Chile: OneMine.

The author was responsible for formulating the optimization models and carrying out all the calculations. The experimental part was also done by the author with a little help from an undergraduate student. The conference paper was developed with and contributed to by all the co-authors.

Other publication(s)

Rotich, N. (2014). The fall and rise of gravity separation, vol. 9, Mining magazine. 68 Upper Thames Street, London, EC4V 3BJ: Aspermont media, pp. 60 - 65.

The author contributed to mining magazine, a major mining industry circular in the UK and around the world. The supervisors helped in reviewing the contribution.

Glossary

AEM Association of Equipment Manufacturers. 17

ANOVA Analysis of Variance. 58

CAE Computer Aided Engineering. 18

CD Contact Dynamics. 68

CDF Cumulative Distribution Function. 50

CFD Computational Fluid Dynamics. 18

DEM Discrete Element Method. 18

DoE Design of Experiments. 58

FEMAP Finite Element Method and Post-processing. 18

FORL First Order Rate Law. 3, 22

HAF Holed Area Fraction. 57

MIT Massachusetts Institute of Technology. 22

PBE Population Balance Equation. 45

PSD Particle Size Distribution. 45

TPHSM Ton Per Hour Square Meter. 65

VSMA Vibrating Screen Manufacturers Association. 17

Nomenclature

$\acute{P}$	Fluctuation linear momentum, Kgms^{-1}
$\acute{v}$	Fluctuation velocity
α_i	Model independent factors
$\bar{P}$	Mean linear momentum, Kgms^{-1}
$\bar{p}$	Mean compression stress, Nm^{-2}
$\bar{v}$	Mean velocity, ms^{-1}
$\bar{v}$	Mean velocity
β	Screen area allocation constant, s^{-1}
β_i	Statistical model coefficients
Δl	Distance along the incline length, m
ΔN	Number of collisions
Δp	Average energy loss due to collision, J
$\dot{\gamma}$	Shear rate, s^{-s}
η	Solids classification efficiency, dimensionless
Γ	G-force (from mechanical rotation), G's
γ	Damping coefficient, dimensionless
κ	Stiffness constant, Nm^{-1}
λ	Vibration amplitude, m
$\mathbf{b}$	Body force per unit mass, ms^{-2}
$\mathbf{M}$	Couple stress, Nm^{-2}
μ	Dynamic viscosity, Nsm^{-2}
μ_k	Kinetic friction coefficient, dimensionless
ν	Kinematic viscosity, m^{2}s^{-1}
ω	Angular velocity, s^{-1}
ω_i	Intrinsic angular velocity, Rad s^{-1}
$\overrightarrow{F}$	Force density (force per unit volume), Nm^{-3}
$\overrightarrow{u}$	Flow velocity vector field, ms^{-1}
ρ	Density of granular material, kgm^{-3}
σ	Grain-grain contact force, N
$\mathcal{T}$	Second-rank tensor field (Shear stress), Nm^{-2}
τ	Screening intensity surface area constant, sm^{-2}
θ	Deck inclination angle, Rads
θ_m	Angle of maximum stability, Rads
θ_r	Angle of repose, Rads
ε	Overflow fraction, dimensionless
ε_a	Alternating tensor, Nm^{-2}
ς	Body couple, Nm
A	Total screen area, m^2
a	Screen holed area, m^2
A_{di}	Aperture diameters, m
B	Number of births in population balance equation

C	Capacitance, μF
D	Number of deaths in population balance equation
D_i	Mass of desired product, kg
D_p	Mean particle diameter, m
d_{50}	50% pass particle size, m
D_θ	Apparent aperture diameter, m
D_{ap}	Aperture diameter, m
E	Loaded screen mass fraction, dimensionless
E_i	Accummulation at stage i, kg
f	Vibrating frequency, Hz
F_f	Friction force field, N
F_g	Gravity force field, N
F_r	G-force (From electrical circuit), G's
G	G-force, G's
g	Gravity acceleration, ms^2
I	Intrinsic inertia tensor, Nm^{-2}
K	Screening intensity length constant, m^{-1}
k	Screening intensity time constant, s^{-1}
L	Inductance, H
m	mass of granular material, kg
m_o	Overflow mass, kg
M_s	Mass of the screen structure, kg
M_T	Sample mass, kg
m_u	Underflow mass, kg
N	Number of particles (count)
P	Linear momentum
R	Rate of change in particles' population, s^{-1}
R_{ip}	Reynolds number of particles, dimensionless
s	Aperture spacing distance, m
T	Average particles runout time, s
t	time, s
U_o	Total batch mass, kg
V	Volume, m^{-3}
v	Granular flow velocity, ms^{-1}
v_f	Reduction in velocity due to friction, ms^{-1}
W	Power, W
x	A unit position vector in x-direction
y	A unit position vector in y-direction
z	A unit position vector in z-direction
F	Applied force field, N

1 Introduction

1.1 Granular solids classification: industrial significance

Granular solids and powders, commonly referred to as bulk solids, are an integral part of our day-to-day materials, from domestic use to industrial and raw material, and intermediate and end-user products. Bulk solids reportedly account for over 50% of the raw materials used in the chemical industry today. Raman and Aziz (2010). In fact 60% of the chemical industry products are sold as disperse or bulk solids, and another 20% are sold as gases or liquids, but involve solids in the production process (Feise, 2003). This makes bulk solids the most ubiquitous and the second most manipulated material in industry after water. Richard et al. (2005); Kamrin and Koval (2014). Notwithstanding this, large-scale granular solids plants presents a challenge of low *operating reliability*, standing at an average of 63%, compared to that of large-scale liquids processing plants, estimated at 84%. Massoudi and Boyle (2013).

Particulate classification is one aspect of bulk solids handling, whose aim is to distinguish a set of particles that are unique by virtue of predetermined criteria/on. Industries such as minerals and coal (i.e. dry beneficiation), food, chemical process, pharmaceutical, agricultural and farm productions, often require sorting of particles prior to utilization in downstream processes, or for final use. The most common form of sorting is by size, using screening units (see Fig.1.1), even though there are many other criteria that may dictate the classification process, e.g. density, resilience, shape etc., as described in **Publication I**. For instance in mining there is an intricate relationship between particulate classification, comminution, and recovery of the primary mineral product. Despite the fact it is difficult to estimate comminution energy consumption, a reliable source presented it to be an estimated 30 to 70% of the total plant energy (Nadolski et al., 2014). This is exacerbated by allowing excess earth and rocks, by improper classification. When strategically planned and executed, classification helps to weed out barren ore and gangue from a potential quality product. It therefore makes classification an important process that determines a bulk of mine profits. Albuquerque et al. (2008).

Like most industrial processes, particle classification is currently hindered by a number of challenges ranging from environmental problems to intensive energy requirements needed to drive 'phase' separation. Many unit operations are currently high contributors of carbon, atmospheric dust and other fugitive emissions that are detrimental to both human health and the environment. Minimal energy vibrating screens and gravity classification are considered in this study. Gravity is one of the oldest techniques of mechanical separation, often characterized by downward motion of particulates, long residence times, and low overall capacities. With the current need for low-energy low-carbon, but equally efficient operations, mimicking nature will in the long run become part of the solution. This implies that if these processes are expected to continue playing this important role in industry, improving and modernizing the old methods is of essence.

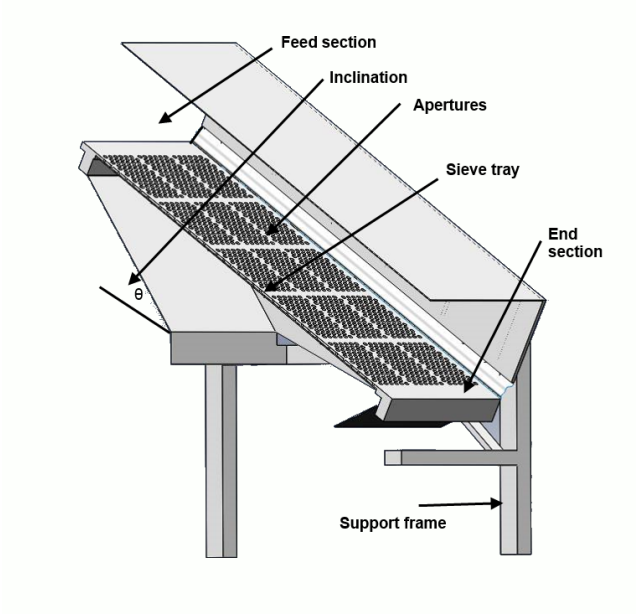

Figure 1.1: An illustration of the main parts of a screening equipment

Granular material in general portrays a mix of characteristics, a lot of which have not been fully understood (Behringer, 1996). For instance, just as fluids do, granular particles take the shape of the container, but also form heaps when poured on a flat surface (Jop et al., 2006). As such, it is a rapidly developing interdisciplinary research area that can be approached from many different angles. Zhu et al. (2007); Massoudi and Boyle (2013). Particles' separation and classification by using linear vibrating or stationary (gravity) screens is by far the most common way to achieve this goal. Makinde et al. (2016). Moreover, as dominant as they are, these processes still face vagueness posed by factors ranging from those affecting equipment design strategies, to those directly related to the physicochemical properties of the bulk solids in question. Li et al. (2002); Zhu et al. (2007); Albuquerque et al. (2008); Chen et al. (2010); Wang and Tong (2011); Li et al. (2015). Besides these obvious challenges, linear screens, like cyclones are faced with a unique problem, in which the processing capacity act as a critical limiting factor. There exists an antagonistic relationship between capacity in tonnage (ton m^{-2}hr) and the efficiency. This implies that maximum throughput capacities are only attainable at the expense of low efficiencies and vice versa (Wang and Tong, 2011; Ortega-Rivas, 2012; Wills, 2016; Olsen and Carnes, 2001). In gravity screening, this problem is largely caused by the lack of control of the bed thickness, which is in turn affected by the deck inclination and the surface characteristics of both the plate wall, and the solid particles. For vibrating screens, the total weight of the screen structure contributes to this problem, in addition to large bed thicknesses. In cyclone separators, capacity is a limiting factor that is more or less like an *opportunity cost* that must be foregone. (see Fig.1.2 cyclone efficiencies compared to their performance). Screen manufacturers have always got around this problems

by setting lower efficiency targets of 90 to 95%, in order to compensate for the lost capacities. Olsen and Carnes (2001). The particular problem of antagonism between capacity and efficiency was recognized as a common problem of *multistablity* in dynamic systems theory. An attempt to address these problems is being conducted by applying perturbation theory. Rotich et al. (n.d.).

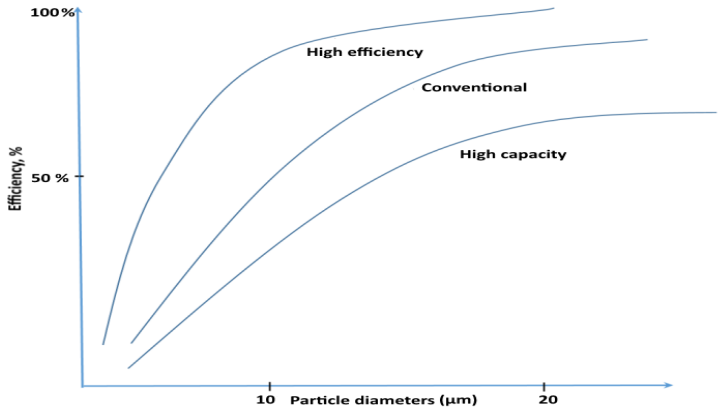

Figure 1.2: A generic plot illustrating *opportunity cost* problem in cyclones

The challenges discussed above have made the manufacturing of linear screens to be highly dependent on empirical methods, with the most common design handbook being the guide developed by the Vibrating Screens Manufacturers Association (VSMA) and distributed by Association of Equipment Manufacturers (AEM). Telsmith inc. is another prominent developer, with a readily available reference handbook. Other vibrating screen manufactures include Osborn (Pty) Ltd., Pilot Crushtec (Pty) Ltd., Tenova Mining and Minerals (Pty) Ltd., Weir Minerals Ltd., Joy Global (Pty) Ltd., Multotec (Pty) Ltd., VibraMech (Pty) Ltd., Shanghai Joyal Machinery Co. Ltd., and Karman Vibrating Technologies CC. Makinde et al. (2015). Very little design information for vibrating screens is available in the public domain, making it a highly commercialized industrial product with information about it even less accessible to researchers in many industries and academia. This necessitates the boosting of technology transfer and information exchange between entities through print media, e.g. industry journals and magazines, and expert gatherings, such as conferences and exhibitions. In October 2014, the author shared expertise with *Aspermont media*, a UK-based print media that has been disseminating industry information since 1909 (Rotich, 2014).

1.2 Motivation and objectives of the study

This study has been motivated by the fact that most of the existing methods to date are not able to characterize and assess several aspects of granular flows completely. These problems are reflected in the industry today through serious economic losses. The US pharmaceutical manufactures, for instance, reject about 5% of manufactured products, with the cost of losing a single batch of medication as high as $ 650,000. Fertilizer manufacturing plants worldwide know the importance of maintaining precise flow over agricultural equipment, and clean cut during size classification. In these industries, passing of oversized and/or retaining of undersized particles constitutes additional costs of re-manufacturing, e.g. grinding to reduce the upper cut-off diameter, and agglomeration to enlarge the lower cut-off diameter. Even with the advent of powerful Computer Aided Engineering (CAE) applications, such as Computational Fluid Dynamics (CFD), Finite Element Analysis and Post-processing (FEMAP), and the Discrete Element Method (DEM), among others, which have been vastly applied in particle technology within the last decade, success in understanding, and thus controlling their behavior is only possible with (1) developing sound mathematical models governing granular systems, (2) proper customization of CAE applications to mimic exact models developed, and (3) excellent interpretation of the results obtained from CAE, an aspect most CAE-based research lack. An attempt is made in this thesis, to conduct systematic derivation of mathematical models governing granular flow over size classification equipment, and solution strategies are formulated. Representative case studies are also presented, on direct applications of these models into the designing of particle size classification unit operation.

1.3 Previous approaches

A prominent challenge today is the fact that most contemporary experimental and numerical studies consider the flow of granular material along incline planes under a destabilizing (collapsing) force, without necessarily taking into consideration changing mass and density dynamics, an important aspect of classification. The following section discusses past models describing various behaviors of granular particulate systems.

1.3.1 Particulate system models: a literature view

The work of Jaeger et al. (1990) on friction in granular flows proposed that there exist stable and unstable flow regimes in granular material, for which they presented a method of quantifying the shear rate that separates them. The main variable was the inclination angle, which was established to be between the angle of repose, θ_r and the angle of maximum stability, θ_m. Jaeger et al. (1990); Silbert et al. (2001). They linked particulate momentum to the driving force F and other forces that results from the grain-grain contact force, σ. However, no consideration was necessary for changes in the total mass, since the study concerned friction in granular flows of constant masses, as shown in Eq.

(1.1).

$$m\frac{\partial v}{\partial t} = F - \sigma \tag{1.1}$$

In their generalized model of the motion of a single particle on a bumpy inclined surface made of other small particles, (Ristow et al., 1994) established that the ball quickly attains a constant mean velocity . Similarly, in this model there was no change in mass but only in velocity. The driving force, σ was taken as the force parallel to the incline, and at a constant velocity $\nabla v = 0$, with the external forces being those resulting from grain collision, Eq.(1.2).

$$mg\sin\theta = \Delta p\frac{\Delta N}{\Delta l}v \tag{1.2}$$

where Δp is the average energy loss due to collision, ΔN is the number of collisions, Δl is the displacement along the incline length, and v is the velocity of the grain.

Silbert et al. (2001) studied a set of numerical simulations of bulk granular flow down an inclined plane. They reported on the rheological effects of packing fraction, coefficient of friction, pile depth of particles, density, and velocity profiles on flow regimes and stability. However, this study did not take the possibility of flow with a dynamic change in mass into account.

Kruggel-Emden and Elskamp (2014) integrated Newton's and Eurler's equations for each particle trajectory explicitly. They used Newton's equation consisting of all contact forces, $\overrightarrow{F}$, and gravity as the main driving forces. The resultant force was quantified as the acceleration of the particle, obtained as a second derivative of its displacement position, x on the screen, Eq.(1.3).

$$m\frac{\partial^2 x}{\partial^2 t} = mg + F \tag{1.3}$$

The models discussed above are useful in describing individual particle behavior, trajectories, kinetic energies, collisions, and non-variable mass systems in general. These are mostly relevant in geological contexts, such as avalanche motion and the after effects of snow, sand and mudslides, fault zone evolution, and pipe formation (Hancock et al.,

2012), where the transient movements of granular slopes and heaps do not necessarily change in mass. In the industrial context, we refer to granular flows in material handling equipment such as chutes, hoppers, bins, etc., where the system mass is constant, and velocity and kinetic energies are the main variables.

1.3.2 Recent approaches to granular rheology

For over one and half decades up until now when this dissertation is concluded, application of fluid flow equations to model powders and particulate solids is a highly contested topic. The point of contest is particularly whether the analogy of constitutive equations used in fluid flow can be applied in granular flows and to what extent. Many researchers concur that the equations governing granular matter under shear, are still a matter of debate. Savage (1998); Aranson and Tsimring (2001); Mills et al. (1999); Bocquet et al. (2001); Ertaş and Halsey (2002); Mohan et al. (2002); Josserand et al. (2004); Kumaran (2004); Owens and Phillips (2002); Jop et al. (2006). In light of this thereof, it is reasonable to also imply that one of the essences of this dissertation is to serves as part of a large hypothesis (out there) that such constitutive relations may also be derived from a transport phenomena point of view, and in particular the Navier-Stokes equation.

In granular rheology context, it has been shown that the flow velocity of granules on a very fine scale can be divided into fluctuating and mean transport components and treated as a fluid, and on a somewhat larger scale, one can utilize analogous fluctuations in strain rates to assess the extent of dependence on viscosity in developing the constitutive equations Savage (1998). This is what was done in the second set of the models in this dissertation. Aranson and Tsimring (2001) showed that if granular flow continuum is to be described, it follows the Navier-Stokes equation.

$$\rho D v_i / Dt = \frac{\partial \sigma_{ij}}{\partial x_j} + \rho g_i, \; j = 1, 2, 3... \tag{1.4}$$

Eq.(1.4) is a form of Navier-Stokes that ignores the pressure drop and viscosity terms and assumes a constant material density throughout the flow. Mohan et al. (2002) supplemented generic linear momentum conservation equations with an angular momentum balance term.

$$\begin{aligned} \frac{D\rho}{Dt} + \rho \nabla . u &= 0 \\ \rho \frac{D\mathbf{u}}{Dt} + \nabla . \sigma - \rho \mathbf{b} &= 0 \\ \rho \frac{D(I\omega_i)}{Dt} + \nabla . \mathbf{M} - \varepsilon_a \colon \sigma - \rho \varsigma &= 0 \end{aligned} \tag{1.5}$$

Here I is the intrinsic inertia tensor, ω_i is the intrinsic angular velocity, $\mathbf{M}$ is couple stress,

ε_a is the alternating tensor and ς is the body couple. $\mathbf{b}$ is the body force per unit mass and the rest of the symbols take the usual meanings. It can be seen that the second part of Eq.(1.5) is Navier-Stokes with isentropic pressure and viscosity terms dropped.

In order to dissect the granular flow in general, a number of assumptions are necessarily guided by the material and flow characteristics. If the flow is *inertia* dominated then $\rho\frac{Du}{Dt}$ plays a greater role compared to the rest of the forces, if the flow is *friction* dominated, then kinetic theory is sufficient to describe the motion as collision can be factored into these equations Josserand et al. (2004). It has become customary within the last few years to assume that the properties of a flow are close to Newtonian fluid if we are describing a dense flow of fine granular solids. Once this assumption is made, it obviously mean that shear stress, τ can be expressed as a function of shear strain, $\dot{\gamma}$, and by implication it's flow can be estimated using Navier-Stokes equations. In reviewing these models, it can be seen that the most important aspect is what approximations and/or assumptions are made to the generic models in question. For instance in the general conservation of momentum equation Eq.(1.6):

$$u\frac{\partial\rho}{\partial t} + \rho\frac{\partial u}{\partial t} = -\nabla p - \mu\nabla^2.u + \overrightarrow{F} \tag{1.6}$$

If in a certain particle system the density is found to be constant, and the viscosity, and the isentropic pressure are negligible, where $\overrightarrow{F}$ is body force per unit volume, the equation can be reduced to the well known form of Newton's first law **F**=m**a** by multiplying through by V. Obviously this means the kinetic regime takes over, and friction coefficients must be introduced. An it also implies that the generic force **F** can still be split into various components provided they are known. For instance, Kruggel-Emden and Elskamp broke down theirs to gravity (m**g**) and other forms of **F** and assumed no density variations Kruggel-Emden and Elskamp (2014) as seen in section 1.3.1.

In the current study it is noted that most models fail because of oversimplification, especially the assumption of total continuity i.e. $\nabla.(\rho v) = 0$, as though the granules directly emulates the liquid fluid element. It therefore necessitates an approach that the particle fluid is sectioned into two: the center referred to as the continuum, and the outer surface of the element referred to as the boundary or bulk region. Take for instance the Portland cement or corn starch which you can insert an object. At the boundary of the powder matrix, it is much easier to push but only up to some point where it becomes much dense and difficult to do push further. This analogy was tested by Seguin et al. (2011). At this point, it is reasonable to assume that the powder is less dense around it but much denser into the continuum (due to solid packing fraction). When this situation is pictured as the powder flows the density definitely lessens but the trend still exists and thus it is not sufficient to assume that the density is invariant, but vary with space (into the powder) but not necessarily with time. The foregoing argument leads to the modification of the continuity equation to $v\nabla\rho_b + \rho_b\nabla v = 0$, where ρ_b is the bulk density as a function of the packing fraction, ϕ so that $\rho_b = \rho\phi$. This is done with considerations that the packing fraction, and therefore volume, is a function of position vectors (x, y, z) in the granular matrix. In particle classification the packing fraction increases as the mass of the overflow is dimin-

ished. On the other hand, the mean bulk velocity, $\bar{v}$ and total force of the material varies along the screen length.

In general, more research efforts today are concentrating on unifying the constitutive equations for liquid and granular matter, and also suspension in granular rheology Boyer et al. (2011). However, at the moment there is no general equation of motion that describes granular flows, and until recently there were few indications of any sort of universality among different systems. Some researchers are currently (2016) working towards developing models for a general understanding and are at advanced stages of investigation, notably Heinrich Jaeger at the University of Chicago, and the Ken Kamrin research group at MIT. It is therefore hoped the analysis given in the current dissertation will make a contribution that will provide a different angle to look at flow over particles classification equipment as a unit operation.

1.3.3 The generic model of solid particles classification

The use of first order rate law (FORL) has for long been seen as a conventional way of describing the screening dynamics.

$$\begin{aligned} \frac{\partial m(t,x,...)}{\partial t} &= -km, \text{ for time rate, t or} \\ \frac{\partial m(t,x,...)}{\partial x} &= -Km, \text{ screen lenght, x} \end{aligned} \tag{1.7}$$

However, these methods present a challenge as they do not quantify the effect of velocity on the intensity (rate) and efficiency of classification when each equation is solved inherently. The assigned rate constants lumps the effects of all factors, i.e. screen area, deck inclination, force applied, friction coefficients, etc., into one parameter (K,k), making it difficult to assess the individual effects of the factors, both qualitatively and quantitatively. The random path model by Jansen and Glastonbury (1968) showed that first order rate laws become deficient, when high probability particle passage is required and screen loading is thick. The use of first order rate in the forms of Eq.(1.7) also constitutes a problem of implementing an additional apertured boundary, and algorithms to allow passage of particles and rebounding when approaching the screen surface in DEM (Li et al., 2002). In addition, FORL only estimates the rate of classification, either as a function of time or screen length, but not both.

As a result, there is a general lack of concrete kinetic models in the industry today that describe the complexities of granular flow (Henann and Kamrin, 2013), let alone the flow over classification equipment. No model today can explain the quantitative considerations of key important parameters, such as time, deck inclination, friction, screening energy, available spatial domain, particle size distribution, length, and the screening rate itself (as a constraint), all in one go. It was observed in this study that expressing the change in

mass as a function of flow velocity and current mass would capture both the length and time dependence depicted in Eq.(1.7) at the same time. The study therefore focused on the hypothesis that the dynamics of solids classification vary greatly and instantaneously, with both flow velocity (downslope) and mass, and thus inertia plays a greater role, compared to inter-particle collisions, or normal stresses, and velocity in the perpendicular direction is negligible (compared to the flow downslope). This description led to the postulation of our rate Eq.(1.7), which was described, tested, simulated and verified experimentally in the appended **Publications I, II, III, IV, V**, and Rotich et al. (2015).

$$\frac{\partial m}{\partial t} = -\tau \frac{a}{D_p} m \frac{\partial v\left(x,t\right)}{\partial t} \tag{1.8}$$

Apart from time, the velocity component, v is calculated as a function of the remaining factors, namely: deck inclination, θ, applied force, F, and friction coefficients, μ_k.

1.3.4 Model-based designability

While empirical studies have resulted in good methods in a the past, they lack universality in practice, hence replicating the models in different situations makes it almost impossible to obtain authentic results. Empirical formulae have in fact been reported in the past to have produced results deviating by up to a factor of three (Li et al., 2002). However, it is worth noting that computer algorithms have made enormous contributions which have brought about development of less time-consuming analysis through discretization of the particulate systems. Saravacos et al. (2002); Li et al. (2002); Zhu et al. (2007); Li et al. (2003).

Pure reduction in computation time does not, necessarily imply ultimate efficiency in terms of eliminating flow prediction errors. Even with the significant improvements mentioned above, there still exists a gray area when it comes to process engineering-based design of particle classification systems. By this we refer to design criteria that focus, not on physical, structural or mechanical integrity only, but a holistic one, covering process efficiency, capacity and energy (efficiency), in addition to structural integrity. For instance, it is surprisingly difficult to estimate the comminution energy portion as a fraction of total energy in a solids processing plant, even though many have tried (Napier-Munn, 2015). Even more surprising, is the missing link between particle size separation efficiency, and the amount of vibration energy required, apart from other major constraints, such as deck inclination, perforated/holed area fraction, screening time, particle size diameters, bulk flow velocity of the material, and even the classification capacity itself. In that regard, there seems to have been a bias in the design process that has greatly limited optimal performance of this unit operation.

In their paper titled 'Dynamic design theory and application of large vibrating screen', Yue-min et al. (2009) focus mainly on the reliability of the mechanical structure, e.g. maximum dynamic stresses, amplitudes, frequency and total mass. Iizuka and Delfim (2010) presented an introduction to the design and application of a high capacity vibrating screen used in coal processing. This study discusses some important process related variables qualitatively, such as attaining a good screening efficiency by correct dimensioning of the screen area, choice of media type, and the choice of amplitude and frequencies as a function of the screened material. They also state that the particle should move over the screen surface without hitting the same opening repeatedly, but also without surpassing several openings ahead, as this will deter the achievement of a clean cut. The engineering design strategy itself, however, focuses on the performance mode, shape, static and dynamic stresses, and their overall influence on the structural design. Even though the study did not cover each factor in detail and how to manipulate in order to enhance the separation rates and efficiency, it provided a qualitative basis for the current work.

Another promising research is that carried out by Baragetti and Villa (2014), who optimized the load carrying capacity of a generic vibrating screen used in asphalt screening. The result of this study led to the development of an algorithm that helps designers to assess and optimize the dynamic behavior of the fatigue resistance of a vibrating screen, based on different geometric and inertial properties. Baragetti (2015) later applied the previously developed algorithm to provide an innovative structural solution for heavy loaded vibrating screens, which have the same geometry as the traditional ones and almost the same mass, but with higher dynamic structural resistance at frequencies, loads and amplitudes much higher than the nominal ones. This new solution has been patented Baragetti et al. (2006).

1.4 Novelty of the present approach

Separation processes, such as screening, cause dynamic changes in the momentum due to change in total mass and bulk flow properties, which are primarily important when evaluating the success of screening processes. In the current study, attempts have been made to derive discrete and continuum models that estimate the required particle classification energy (in G-force) as a function of important process parameters, namely the deck inclination angle, θ, coefficient of kinetic friction between the screen plate wall and the granular material, μ_k, classification efficiency, η, holed area of the screen, a, particle mean diameter, D_p, bulk flow velocity, v, and the total mass of the screen structure, M_s, all at once. Methodologies for optimizing these process parameters were also developed as part of the study in **Publications III, IV** and **V**.

1.4.1 Research objectives and hypotheses

The key hypothesis that yielded the objectives to this study was that particle classification by size over the screen plate is driven by a continuous change in the total momentum of the particulate system, rather than the change in mass and/or velocity inherently, as often perceived. This regime treats screening as a variable mass system, which bundles up the effect of change in mass and velocity together (as momentum), instead of treating the two as independent variables affecting the screening process. This change in momentum therefore affects the rates and efficiencies of classification directly, and consequently the design methodology of the material handling equipment (screen). It was foreseen that by solving Eq.(1.8) and monitoring the change in the bulk velocity with mass, separation efficiency and rates may be inferred from the varying mass. Upon successful development of these models, the mass flow rates may be used to estimate the required feed rate capacities, and used to determine related dimensions that give optimal efficiencies.

Throughout this study, I have characterized multi-size, mono-shaped particles and used the outcomes of the process to gain new information into the physical separation world. This has been done with regard to the postulated variable mass regime. The objectives were divided into various tasks which constituted at least one publishable research:

i To come up with new theoretical models for studying the motion of granular particles during classification.

ii To simplify and interpret the models to make them applicable for rapid prototyping in relevant industries.

iii Design and development of prototype particle separation equipment, based on the models.

iv Fabrication of up-scalable pilot/lab scale prototype of the developed equipment.

v Process optimization of solid classification based on the developed unit operation.

vi Further development of other comparable models to study the existence of trends in the different methods for the chosen solutions.

1.4.2 Research methods and collaborations

The research was done by experimentation, coupled with theoretical and computational modeling by which the particles can be separated from a mixture and classified into the required classes for further use or final disposal, with minimum environmental problems and less intense energy requirements. I collaborated with the university professors (supervisors) at Lappeenranta in Finland, and in the University of Waterloo in Ontario, Canada, where I conducted a one-year international research visit.

1.5 Organization of the thesis

This thesis is organized into five chapters: the introduction and two chapters on model development named the development of kinetic flow models and population balance models. The next two chapters concern experimental verification and model-based design considerations, before the concluding chapter. The first part introduces the thesis by giving an overview of particulate systems and the rationale for conducting the study. It also presents the hypothesis of the study, the extent of novelty involved, and the expected outcomes. The second chapter begins with the development of the models, in particular derivation from conventionally known equations of conservation of momentum. This chapter only deals with kinetic flow models named the continuum and discrete models. The third chapter is meant to act as a supplementary to the reader, as it relates the already derived models in the second chapter to the population balance model, a strategy that has been used frequently to describe particulate systems and others in systems theory in recent times. The fourth chapter explains how the experiments were conducted and the data analyzed, to conform to the standard scientific procedures. Finally, in chapter five a study is done to show that the formulated strategies can be used, especially to guide the design and development of sound and modern particle classification systems in industry today. The last chapter is an assessment of the hypothesis and a summary of the findings of the study.

2 Development of kinetic flow models

2.1 The continuum model

Understanding the qualitative description or the classification of flows is the first step in developing sound models. In this study, the flow regime is seen to be constituted by two main regions, the middle section of the flow cross-section - here referred to as the continuum, and the exterior bulk flow region, whose properties are seemingly diluted by those the surrounding fluid - air in this case. The process is therefore described as turbulent, unsteady, Newtonian fluid flow (in a wide channel), with nominal density ~ 1600 kg/cm^3, and very low dynamic viscosity, and consequently even lower kinematic viscosity. It is incompressible within the core continuum, but compressible around the bulk flow regime. The volume of the continuum changes with the position, and thus the density varies only macroscopically, but remains nearly constant microscopically inside the continuum. The flow over the screens is classified as unidirectional subsonic, meaning that the flow velocity is low (typically 0 to 3.5 m/s) and only in one direction (downslope), giving a Mach number up to 0.0109. A summary of the flow classification of fluids in terms of shear stress versus shear strain is shown in Fig.2.1.

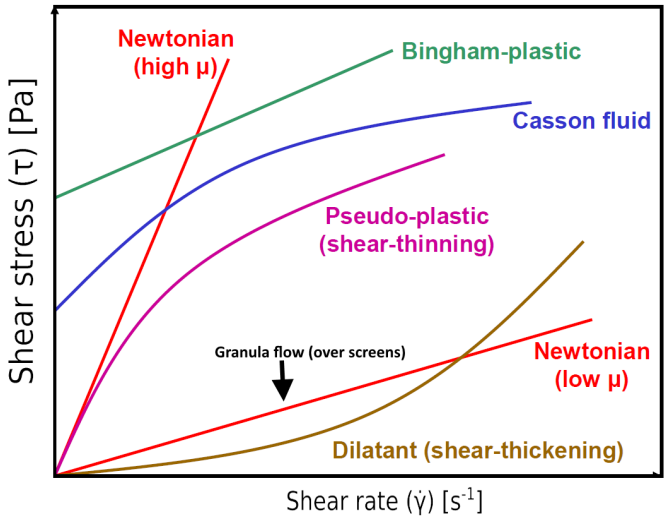

Figure 2.1: Flow regimes classification in terms of shear stress versus shear strain

2.1.1 Constitutive equation for deviatoric stress

The description presented in section **2.1** makes it possible to develop the constitutive equations, for each diffusive component of the flow, with the field variable being the velocity vector field, $\overrightarrow{u}\,(s, y, z)$. Momentum density, $\rho\overrightarrow{u}$ is the easiest to represent, as it captures

two main aspects capable of manipulation and *designability* in bulk solids processing. It therefore starts with an expression for shear rate within the bulk, say in the x axis, so that:

$$\frac{\partial\left(\rho\overrightarrow{u}\right)}{\partial t}_{shear} = -\frac{\partial\mathcal{T}_{xx}}{\partial x} - \frac{\partial_{\mathcal{T}_{yx}}}{\partial y} - \frac{\partial\mathcal{T}_{zx}}{\partial z} \tag{2.1}$$

where $\mathcal{T}$ is a second-rank tensor field. We like completeness, so that even though it maybe unnecessary, we introduce the pressure drop term, ∇p to cater for the *Stokes flow*. This is done by simply adding the term to the right-hand side of Eq.(2.1).

$$\frac{\partial\left(\rho\overrightarrow{u}\right)}{\partial t}_{shear} = -\frac{\partial p}{\partial t} - \frac{\partial\mathcal{T}_{xx}}{\partial x} - \frac{\partial_{\mathcal{T}_{yx}}}{\partial y} - \frac{\partial\mathcal{T}_{zx}}{\partial z} \tag{2.2}$$

2.1.2 Conservation of momentum equation

The pressure drop contributes to momentum accumulation by providing an extra inertial force, in the direction of the pressure gradient. We add all these forces to give a rough estimate of the equation of conservation of momentum in the x-axis.

$$\frac{\partial\left(\rho\overrightarrow{u}\right)}{\partial t}_{shear} = -\nabla p - \nabla\cdot\mathcal{T} + \overrightarrow{F} \tag{2.3}$$

2.1.3 Expression for density

Eq.(2.3) is still open, until when the shear stress is expressible in terms of velocity in the constitutive equation, and an expression for density is derived. Luckily, there is a widely applicable analogy that unifies *particle-particle* interactions both in solid mechanics and fluid flows. While mechanics deals exclusively with *stress* and *strain*, fluid dynamics involves their respective *rates* of occurrence. Newtonian fluids exudes a linear relationship between shear stress and velocity gradient, so that:

$$\mathcal{T}_{yx} = -\mu\left(\frac{\partial u_x}{\partial y} + \frac{\partial u_y}{\partial x}\right) \tag{2.4}$$

The proportionality constant μ is referred to as *viscosity*. Non-Newtonian fluids however do not exhibit this linear relationship, but takes a more complex form. Solids alike have their true area of atomic contact increasing *linearly* with the normal force, with the widely known correlation to frictional (shearing) force $F_f = \mu_k N$. $\mathcal{T}_{yx}$. Eq.(2.4) therefore represents the constitutive equation for the local shearing force, per unit volume.

Over-simplification of the bulk density is one reason for most failures in handling flow problems. While the variation in density is perceived in most cases as constant in order to simplify incompressible flow models, boundaries, especially in granular flows, lead to non-uniformity in equilibrium systems. Take for instance *powders whose specific gravities are much higher beneath and within the continuum, but nearing the density of the surrounding fluid properties at the boundaries* (see Fig.2.2). The equation of conservation

of mass also known as *continuity equation* is written as shown in Eq.(2.5) below:

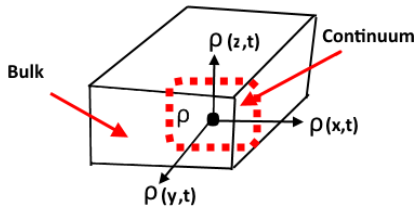

Figure 2.2: Representation of density variation in the continuum

$$\begin{aligned} \frac{\partial \rho}{\partial t} &= -\nabla \cdot (\rho u) \text{ or} \\ \frac{\partial \rho}{\partial t} + \overrightarrow{u} \cdot \nabla \rho + \rho \nabla \overrightarrow{u} &= 0 \end{aligned} \tag{2.5}$$

Where ρ implies the density within the continuum. In these instances, Eq.(2.5) must be simplified with precaution. Indeed, if the flow is steady, there is no variation in density with time inside the continuum. This reduces the first term effectively to zero. However, when bulk density is referred to, e.g. in geology and petrology, density is estimated as a function of matrix density and the surrounding fluid density. Thus, mass varies e.g. with position and time in the matrix that has different mineral ores, gases, liquids, etc., and fixed volume of the reservoir, or any other enclosed space. This concept forms the basis for well logging or density logging, used to calculate porosity within reservoirs during oil and gas exploration. The second term therefore does not certainly reduce to zero, due to the conditions explained above. The usual presumption that the first two terms automatically vanishes (for incompressible flows) and thus $\overrightarrow{u} \cdot \nabla \rho = 0$, does not surpass, especially for multiphase mixtures. We therefore take note of Eq.(2.6) as the continuity in granular flow:

$$\overrightarrow{u} \nabla \rho + \rho \nabla \cdot \overrightarrow{u} = 0 \tag{2.6}$$

The general form of continuity Eq.(2.6), also referred to as the mass balance equation can be expressed as follows:

$$u \frac{\partial \rho}{\partial x} + v \frac{\partial \rho}{\partial y} + w \frac{\partial \rho}{\partial z} + \rho \left(\frac{\partial u}{\partial x} + \frac{\partial v}{\partial y} + \frac{\partial w}{\partial z} \right) = 0$$

Mechanical pressure, $\bar{p}$ is the non-thermodynamic component of strain, defined as *negative one-third the sum of the normal stress tensors in all three directions*. In solids, mechanical pressure makes a little difference in the entire bulk flow since there are very few flat surfaces (at the atomic level) that touch in granular flows, and if any, this could

cause bonding. These are referred to as areas of 'true contact'. The component $\bar{p}$ therefore represents a mean compression stress on each continuum element, and is given by Eq.(2.7):

$$\bar{p} = -\frac{1}{3}\left(\mathcal{T}_{xx} + \mathcal{T}_{yy} + \mathcal{T}_{zz}\right) \tag{2.7}$$

2.1.4 Convective acceleration

Convective transport can occur in the event of convergence, which is not a common term in fluid mechanics, but is used here casually, to imply the opposite of divergence. In simple terms, it is time-independent acceleration, with respect to space (inside the continuum) which causes accumulation, and thus a negative term, $-\nabla \cdot (\rho \overrightarrow{u}\,\overrightarrow{u})$ - in expanded form, is added to the right side of Eq.(2.3).

$$\begin{gathered}\frac{\partial\left(\rho\overrightarrow{u}\right)}{\partial t}_{shear} = \left(-\overrightarrow{u}\,\overrightarrow{u}\nabla\rho - \overrightarrow{u}\,\rho\nabla\overrightarrow{u} - \rho\left(\nabla\overrightarrow{u}\right)\overrightarrow{u}\right) - \nabla P - \nabla\cdot\mathcal{T} + \overrightarrow{F} \\ \rho\left(\frac{\partial\overrightarrow{u}}{\partial t} + \overrightarrow{u}\cdot\nabla\overrightarrow{u}\right) + \overrightarrow{u}\left(\frac{\partial\rho}{\partial t} + \overrightarrow{u}\nabla\rho + \rho\nabla\cdot\overrightarrow{u}\right) = -\nabla P - \nabla\cdot\mathcal{T} + \overrightarrow{F}\end{gathered} \tag{2.8}$$

2.1.5 Simplified Navier Stokes equation for granular particles classification

Simplification is advanced by fixing the shear rate and the density functions in Eq.(2.3) (ignoring $\bar{p}$). Note that the two last terms of the second parenthesis on the L.H.S of Eq.(2.8) encloses Eq.(2.6), and thus it all reduces to zero. In this flow regime, the *convective acceleration* term is zero, so that $u.\nabla u = 0$ in the first part of Eq.(2.8). Eq.(2.9) thus constitutes a complete (closed) Stokes general equation for momentum conservation in granular flow over perforated surface in one direction.

$$\rho\frac{\partial v}{\partial t} + u\frac{\partial\rho}{\partial t} = -\nabla p + \mu\nabla^2 u + \overrightarrow{F_x} \tag{2.9}$$

In Cartesian plane, Eq.(2.9) can be represented in 3D as follows:

$$\left.\begin{aligned}\rho\tfrac{\partial u}{\partial t} + u\tfrac{\partial\rho}{\partial t} &= -\tfrac{\partial p}{\partial x} + \mu\left(\tfrac{\partial^2 u}{\partial x^2} + \tfrac{\partial^2 u}{\partial y^2} + \tfrac{\partial^2 u}{\partial z^2}\right) + \rho g_x \\ \rho\tfrac{\partial v}{\partial t} + v\tfrac{\partial\rho}{\partial t} &= -\tfrac{\partial p}{\partial y} + \mu\left(\tfrac{\partial^2 v}{\partial x^2} + \tfrac{\partial^2 v}{\partial y^2} + \tfrac{\partial^2 v}{\partial z^2}\right) + \rho g_y \\ \rho\tfrac{\partial w}{\partial t} + w\tfrac{\partial\rho}{\partial t} &= -\tfrac{\partial p}{\partial z} + \mu\left(\tfrac{\partial^2 w}{\partial x^2} + \tfrac{\partial^2 w}{\partial y^2} + \tfrac{\partial^2 w}{\partial z^2}\right) + \rho g_z\end{aligned}\right\} \text{3D momentum}$$

The postulate presented in **Publication I** that change in momentum is the key driving force of particle separation, came from the consideration of granular flow as inertial. Rather, the inertia force is much higher than the viscous term in Eq.(2.9), and thus the term with viscosity is ignored. We also need to consider the rheology of bulk flows. In-

ertial rheology has been known to work well for uniform flows over a wider range of flow rates. Kamrin and Koval (2014). These flows are characterized by low viscosity, high Reynolds numbers (> 1), and generally slow to fast flows, depending on the external forces involved. The Reynolds number of particulates, R_{ip} is calculated from the bulk flow densities, ρ and a viscosity, μ. In their study to characterize the rheology of a gas fluidized granular bed involving glass spheres, (Conway et al., 2004) observed that particle separation occurred within the range of Reynolds numbers from $R_{ip} = 36 - 50$. The Reynolds number is an indication of the flow regime, and is obtained by estimating the ratio of inertial to viscous forces.

Upon neglecting the viscous forces, we remain with dynamic pressure and momentum density due to external forces. The pressure drop term is eliminated (as is done conventionally) for inertial flows. As some particles are ejected to the underflow, there is a relative reduction in mass and density downslope. This necessitates quantification of the 'extra' force seen as momentum accumulation due to *density gradient*, which can be modeled by considering the change in the mass with the position of particulates in time. Due to the explanations presented above, the momentum density Eq.(2.9), can be simplified further:

$$\rho \frac{\partial u}{\partial t} + u \frac{\partial \rho}{\partial t} = \overrightarrow{F} \tag{2.10}$$

Idealize a local population of particles of mass, $m\,(x,t)$ flowing through a control volume, $V\,(x)$, with a velocity , $v\,(x,t)$, so that only momentum in x is conserved. With the prior induction that the bulk density may vary owing to the fact that rheology changes within the continuum, the continuity equation Eq.(2.6) in one direction can be written as follows:

$$\rho \frac{\partial v_x}{\partial x} + v_x \frac{\partial \rho}{\partial x} = 0 \tag{2.11}$$

Note that the assumption $\partial\rho/\partial t = 0$ is only permitted for microscopic mass balance with the continuity equation inside the continuum. There are two main characteristics of compressible flows when carrying out material balance:

i The volume varies with the position, $V(x,y,z)$

ii The fluid density varies with time, $\partial\rho/\partial t$

As a specific case in this study, the first assumption is taken as positive for continuity within the fluid particle, but not in the bulk flow. Similarly, the second assumption is taken in the bulk flow but not inside the continuum (see Fig.2.2 for the description of fluid flow regimes). With these assumptions, the density of the control volume is defined as:

$$\rho\left(x,t\right)=\frac{m\left(x,t\right)}{V\left(x\right)} \tag{2.12}$$

Replacing Eq.(2.12) in Eq.(2.10) and evaluating the partial derivative with respect to time, t:

$$\begin{aligned}\left[\frac{m(x,t)}{V\left(x\right)}\right]\frac{\partial v_x}{\partial t}+u_x\frac{\partial}{\partial t}\left[\frac{m(x,t)}{V\left(x\right)}\right]&=\overrightarrow{F}\\ \left[\frac{m(x,t)}{V\left(x\right)}\right]\frac{\partial v_x}{\partial t}+u_x m\left(x,t\right)\frac{\partial}{\partial t}\left[\frac{1}{V\left(x\right)}\right]+\frac{u_x}{V\left(x\right)}\frac{\partial}{\partial t}m(x,t)&=\overrightarrow{F}\\ \left[\frac{m(x,t)}{V\left(x\right)}\right]\frac{\partial v_x}{\partial t}+\frac{u_x}{V\left(x\right)}\frac{\partial}{\partial t}m(x,t)&=\overrightarrow{F}\end{aligned} \tag{2.13}$$

Taking note of the constant component of velocity in Eq.(2.13), this value is denoted as u. When the solution used in the discretization of the flow space and time domain is a structured grid e.g. in the finite difference method (FDM), it is possible to make time and space homogeneous so that: $\Delta x=\Delta t$ as described by (Popescu, 2014), (see Fig. 2.3). A 1D continuum model for granular flow in classification equipment may therefore be constituted by multiplying the momentum density in Eq.(2.13) by the control volume, V.

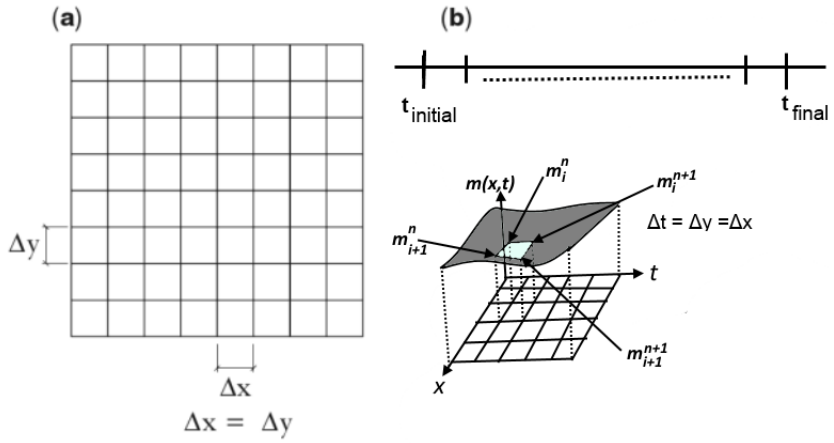

Figure 2.3: Space and time discretization of the fluid flow domain with function

$$m\frac{\partial v}{\partial t}+u\frac{\partial m}{\partial t}=F \tag{2.14}$$

Eq.(2.14) is a statement of Newton's second law for variable mass systems.

2.2 Discrete model

The numerical and experimental discrete model used here is based on solid-solid separation. It was conceptualized in Publication I that even simple processes such as granular particles classification are driven by a continuous change in the momentum of the bulk of particles, resulting from velocity fluctuation. This particular description is illustrated schematically in Fig.2.4. This postulate was subsequently refined, tested and used in conducting various studies forming a part of this thesis. In general, the model seeks to assess individual (discrete) particle characteristics, and the aim was to eventually apply the model throughout bulk flow characteristics, such as velocity, friction, and overall force balances. Once realistic models were achieved, they were then generalized and applied to the entire bulk flow of the solids in question. A successful application of these models can be used to study the potential changes in the mass of the screen loading and the overall performance of the equipment. In these studies, particle classification rates and efficiency were the main two factors, which in turn were controlled by other sub-variables. Qualitative and quantitative assessment was carried out on these variables, either numerically or experimentally, whenever possible. These studies form a part of this thesis, **Publications I, II, III, IV, V** and Rotich et al. (2015) as supporting publications.

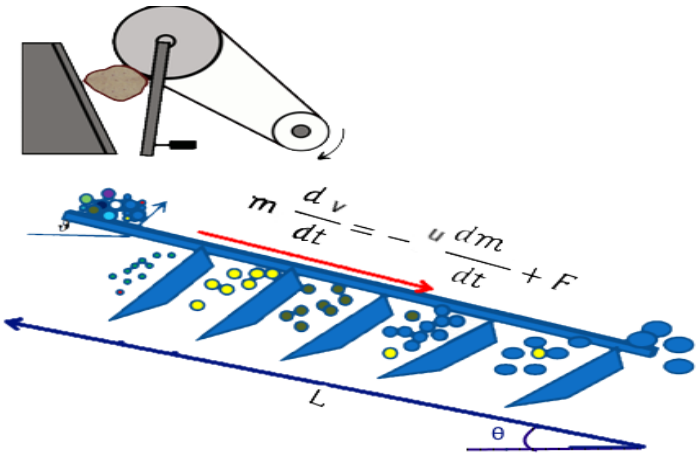

Figure 2.4: Schematic representation of the postulated kinetic model

2.2.1 Numerical setup

Consider a lump of dry granules of mass m_0 and a uniform particle size distribution (PSD), flowing down a surface inclined at angle, θ to the horizontal as illustrated in Fig. 2.4, starting to flow with an initial velocity, v_0, to attain a the bulk average velocity $\bar{v}$, after time t. The mass is under the influence of force(s), F. The surface is made of a material which exerts kinetic friction μ_k on the particles, and is perforated with triangular-patterned circular apertures increasing uniformly in diameters down the incline. The smallest aperture is half a diameter larger than the smallest particle size, and the same applies to the largest aperture. The spacing between the apertures is structured to half a diameter apart, so that the holed area fraction is 40.31% of the total . The falling mass of particles, also referred to as *underflow* get trapped and collected, while the remaining group of particles, referred to as *overflow* continue downslope. Some of the forces acting on the system can be approximated easily by using simple calculators, while others may require more powerful numerical tools. At any given time, each of the masses can be expressed as fractions of the original mass so that the underflow fraction, η represent the amount collected and the overflow, ε represents the continuing particles' fraction. The perforated surface releases the underflow with resolved velocities $v_f(t)$, $t \in [t_0, t]$ parallel to the screen. The original mass, m_0 of the system of particles therefore decreases to $m(t)$ with time. The total force, F is the sum of all the external forces that stimulate the screen, e.g. mechanical or electrical vibration, gravity, friction, collision, etc. In this case study a generalized single degree oscillator is considered, with negligible air resistance on the bulk of particles. An illustration of the forces and velocities is given in Fig.2.5.

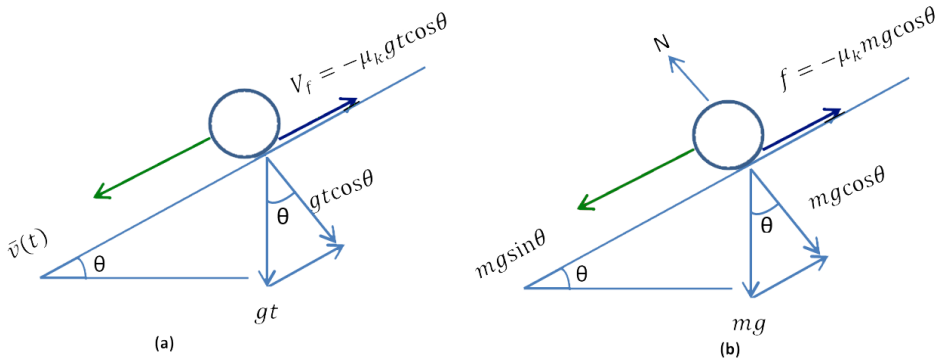

Figure 2.5: Vector diagram illustration of (a) velocity and (b) forces on the particles

2.2.2 Bulk flow characterization

The current study views particle classification not only as a function of time, but also dependent on turbulent fluctuating bulk flow velocity. As the particle sizes are reduced, the granular material flow properties also change from macro to micro and eventually nanoscales, and the flow tend to attain fluid properties. This makes Reynolds decomposition

possible, allowing sectioning of the velocity profile into two discrete components, a time averaged mean velocity , $\bar{v}$, and a fluctuating component $\acute{v}$. Particulate movement over screens can therefore be characterized as laminar or turbulent, depending on the extent of disturbances caused by collision, friction, as well as other forces acting on the particle fluid.

2.2.2.1 Laminar flow velocity

In general, a foreign component (e.g. a dye trace) injected into the flow would trace a straight line if the flow is laminar (see Fig.2.6). At this point the flow is streamlined, and the overall velocity equals the mean, so that $v = \bar{v}$ for all t. This is ideally the description of flow within the continuum as explained in Chapter I.

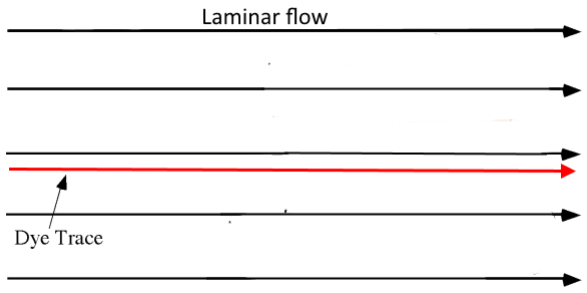

Figure 2.6: An illustration of laminar flow velocity

2.2.2.2 Fluctuation (turbulent) velocity

In the turbulent regimes, flow velocity is estimated as a sum of both the mean and fluctuation components of velocity by using Eq. (2.15) below. The flow is illustrated in Fig. 2.7.

$$v(t) = \acute{v}(t) + \bar{v} \tag{2.15}$$

In order to estimate the fluctuation velocity described in section **2.2.2**, a definition of linear momentum is provided as follows: for a dynamic system, the linear momentum P is determined by the velocity, $v\,(t)$, and mass, m of the system, given by Eq.(2.11).

$$P(t) = mv \tag{2.16}$$

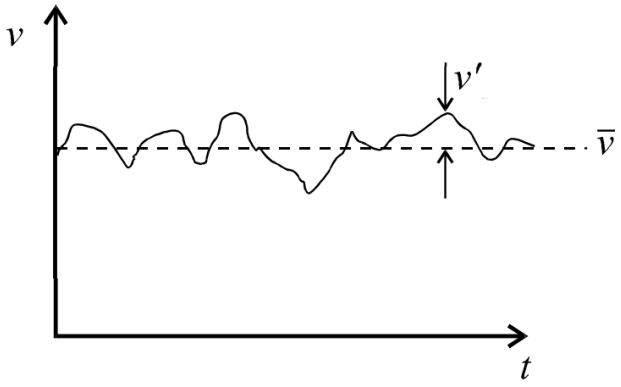

Figure 2.7: Illustration of laminar flow velocity

Where the two independent variables, v and m are parametric functions of time, it follows the dependent variable; P is also a function of time. Fluctuation in velocity affects the momentum so that fluctuations may also be represented as shown in Eq.(2.17).

$$P(t) = \acute{P}(t) + \bar{P} \tag{2.17}$$

The mean values in Eq.(2.15) and Eq.(2.17) are constant, hence taking the fluctuation components, the change in momentum can be expressed by using the chain rule, stated as:

If $\acute{P} = f\,(m, \acute{v})$, but $m = c(t)$ and $\acute{v} = h(t)$, then $\acute{P} = q(t)$, where the small brackets imply 'function of'. This makes it possible to write the differentials of $\acute{P}$ shown in Eq. (2.18).

$$\delta\acute{P} = \frac{\partial\acute{P}}{\partial\acute{v}}\delta\acute{v} + \frac{\partial\acute{P}}{\partial m}\delta m$$

Taking limits as $\delta\acute{v}$ and $\delta m \to 0$

$$\frac{\partial\acute{P}}{dt} = \frac{\partial\acute{P}}{\partial\acute{v}}\frac{\partial\acute{v}}{\partial t} + \frac{\partial\acute{P}}{\partial m}\frac{\partial m}{dt} \tag{2.18}$$

taking the partial derivative of Eq.(2.16) you obtain:

$$\frac{\partial\acute{P}}{\partial t} = m\frac{\partial\acute{v}}{\partial t} + \acute{v}\frac{\partial m}{\partial t}$$

Taking note that $\acute{v}$ in the last term of Eq.(2.18) is no longer time-dependent, if this value is taken as the velocity at which the underflow particles are rejected *relative* to the velocity of the continuing overflow mass fraction. This component of velocity can then be renamed $\acute{v} = u$, and Eq.(2.13) can be written as shown below in Eq.(2.19). Otherwise Eq.(2.18) remains as it is, for instances where a particle in the overflow fraction is to be tracked.

$$m\frac{\partial \acute{v}}{\partial t} = F - u\frac{\partial m}{dt} \tag{2.19}$$

Eq.(2.19) is essentially Newton's second law for variable masses under external force(s), illustrated in Fig. 2.1. $F = \frac{\partial \acute{P}}{\partial t}$ is the vector sum of all body forces acting on the system, including gravity, Lorentz, electromagnetic forces etc. A detailed account on the use (and abuse) of Eq.(2.14) has been given by Plastino in Plastino and Muzzio (1992). The relative velocity of falling mass with respect to continuing mass, u is given by evaluating the difference between the overflow velocity and the resolved component of the falling mass, v_f in Fig.2.2 to obtain a stationary quantity as shown in Eq.(2.15).

$$\begin{aligned} u &= v\,(t) + v_f, \\ \text{where } v_f &= -\mu_k g t cos\theta \\ u &= v\,(t) - \mu_k g t cos\theta \end{aligned} \tag{2.20}$$

The three most significant external forces are the friction forces retarding the bulk solids Fig.2.2 (b) and the gravitational force and vibration, in addition to the 'thrust' force due to inertia, $-u\frac{\partial m}{\partial t}$. The rest of the external forces are perceived negligible. At the rate determining stage, F is set to zero in Eq.(2.19). For significantly small particles the system is more accurately modeled with continuum models, such as the complete form of the Navier Stokes' equation in Eq.(2.9). We therefore consider here the forces due to gravity field, F_g, friction force, F_f, and resonance to be caused by the oscillator (vibration), F_r as shown in Eqs.(2.21)-(2.24).

$$F_f = -\mu_k m g cos\theta \tag{2.21}$$

The force due to friction, F_f, acts opposite to the average tangential velocity field and is governed by the total pressure and the coefficient of friction during bulk flow (Mangeney

et al., 2007).

$$F_g = mgsin\theta \tag{2.22}$$

In mechanical systems, vibration force is produced by rotational motion e.g. of motors, and quantified as G-force (G), denoted by the Greek capital letter gamma ($F_r = \mathbf{\Gamma}$). 1G is approximately 9.81 m/s^2 and is calculated for and the amplitude λ and frequency f, producing angular velocity ω as shown in Eq.(2.18). The physical meaning of G-force, however, is the ratio of the force to the weight of the accelerating mass.

$$\begin{aligned} \Gamma &= \frac{\lambda\left(\omega\right)^2}{9.81} \\ \omega &= 2\pi f \\ F_r &= \frac{\lambda\left(2\pi f\right)^2}{9.81} \end{aligned} \tag{2.23}$$

In electronic dynamic systems, the vibration force is represented with the second order linear differential equation shown in Eq.(2.24), as a function of time, oscillating body mass M, stiffness constant κ, and the damping coefficient, γ. In principle, vibrating screens are rigid, undamped bodies, leading to negligible stiffness coefficients.

$$\begin{aligned} F_r &= -M\frac{d^2\lambda}{dt^2} + \kappa\lambda + \gamma\frac{d\lambda}{dt} \\ F_r &= -M\frac{d^2\lambda}{dt^2} \end{aligned} \tag{2.24}$$

Notice the (-) in Eq.(2.19), which accounts for simple harmonic motion acceleration. The use of a solenoid to cause accurate motion and efficiency in heavy vibrating machines has also appeared within the last decade. In these circumstances, the solenoid design equation is used. Vibrations are generated through a simple Inductor-Capacitor (LC) circuit operating at its resonant frequency (see Fig.2.8). The magnitude of the vibrations is proportional to the maximum charge in the capacitor, or the voltage and the size of the capacitor in farads. In solenoids at resonance, frequency is a function of inductance, L, and capacitance, C, i.e. $f = h\left(L, C\right)$. The design equation for a solenoid is given in Eq.(2.25).

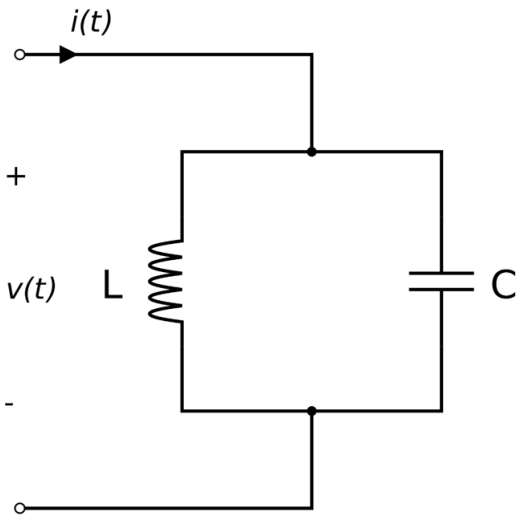

Figure 2.8: LC circuits used in solenoid design

$$f(L,C) = \frac{1}{2\,\pi\,\sqrt{C\,L}} \tag{2.25}$$

The dynamic change in mass also affects the stability of the sum of forces acting on the system. The total energy requirement lessens as the bulk mass diminishes. By first assuming a rate of reduction in the overflow as a first order rate law, which is a monotonically decaying function that depends only on the mass, m and constant k, as shown in Eq.(1.7), the fluctuation velocity component in Eq.(2.15) may then be estimated as shown in Eq.(2.26) to Eq.(2.28) below.

Eqs.(2.20)-(2.22) are substituted in Eq.(2.19), to obtain the simplest form of the discrete model describing macroscopic fluctuation of bulk velocity in granular flows.

$$\frac{d\acute{v}}{dt} + uk = -\frac{F}{m} + gsin\theta - \mu_k gcos\theta \tag{2.26}$$

Integrating Eq.(1.7) gives k as:

$$k = -\frac{\ln \varepsilon}{t}, \text{ where } \varepsilon = \frac{m\,(t)}{m_o} \tag{2.27}$$

Substituting Eq.(2.20) and Eq.(2.27) in Eq.(2.26) and solving for $\acute{v}$ gives the fluctuation velocity of the bulk flow shown in Eq.(2.28).

$$\acute{v} = \frac{-\frac{Ft}{mg} + t\left[sin\theta - \mu_k cos\theta\left(1 + \ln\varepsilon\right)\right]}{\frac{1}{g}\left(1 - \ln\varepsilon\right)} \tag{2.28}$$

Noticeably, $\frac{F}{mg} = G$ is the G-force, defined as the numerical ratio of any applied force to the gravitational force.

2.2.2.3 Estimating mean velocity

The mean velocity component may be obtained empirically or by taking measurements. It can also be achieved numerically, for instance by assessing the variation of velocity with the change in mass and momentum. The latter option has been chosen in this study. It was proposed in **Publication I** that the rate of particle screening may be determined at the steady state by using Eq.(2.29) and also by rewriting Eq.(1.5) in section **1.3.1**.

$$\begin{aligned} \frac{\partial m}{\partial t} + \beta m \frac{\partial v}{\partial t} &= 0 \\ \text{where } \beta &= -\tau \frac{a}{D_p} \end{aligned} \tag{2.29}$$

The model estimates the mean bulk flow velocity through time integration of Eq.(2.29).

$$\begin{aligned} \int_{m_0+M_s}^{m(t)+M_s} \frac{dm}{m} &= -\int_0^{\bar{v}} \beta dv \\ \bar{v} &= -\frac{1}{\beta} \ln\left[\frac{m\left(t\right) + M_s}{m_0 + M_s}\right] \\ &= -\frac{\ln E}{\beta} \end{aligned} \tag{2.30}$$

Where

$$E = \frac{m\left(t\right) + M_s}{m_0 + M_s} \leq 1, \text{ and}$$

M_s, is the mass of the sieve plate

This is done with the expectation that by the end section of the screen, there will be no overflow, and the only mass remaining is the sieve plate, i.e., M_s, and $m\,(t) = 0$. The overall velocity may then be expressed by substituting Eq.(2.20) and Eq.(2.27) in Eq.(2.26) so that:

$$v\,(t) = \frac{-Gt + t\,[sin\theta - \mu_k cos\theta\,(1 + \ln\varepsilon)]}{\frac{1}{g}\,(1 - \ln\varepsilon)} - \frac{\ln E}{\beta} \tag{2.31}$$

Upon attaining a stationary value of velocity, system stability is also achieved. At this point the time-dependent part of Eq.(2.31) is expected to be equal to zero. This implies that the total velocity only equals to the mean component.

$$v\,(t) = \bar{v} = -\frac{\ln E}{\beta} \tag{2.32}$$

The variable E is expected to be minimal at the end section of an ideal (efficient) screen, as it constitutes the rejects or overflow.

$$\eta \;\; = 1 - e^{-\bar{v}\left[\tau\frac{a}{D_p}\right]} \tag{2.33}$$

It can be seen in Eq.(2.33) that low values of overflow are achieved by maximizing the product βv. It was shown in this study that the overflow fraction, ε can be practically minimized (close to zero), by keeping $\beta v \simeq 2\pi$. The smaller the overflow, the higher the system efficiency, since η is an inverse function of E. Eq.(2.33) therefore represents the screen classification function of this kinetic model, and gives the efficiency of transfer of particles of size D_p to the undersized.

When the above kinetic models are implemented and Eq.(2.33) solved properly, more insight into important structural parameters may be achieved. As a representative case study, a finite element analysis was carried with *COMSOL Multiphysics* (COMSOL, 2012), to estimate the extent of vibration (amplitudes), yield stresses, and agitation force needed for a 15 mm thick, 5 m long and 2 m wide (a= 0.4031×10 m^2= 4.031m^2 screen plate effective area), tilted at 30° to the horizontal. The deck had a *sweep* ranging from 10 to 30 mm, under a total load of 22 kN i.e. M_s= 400 and m_0= 1800 kg, respectively - reference to Eqs.(2.25) to (2.29). The mean particle diameter, D_p = 1.05×10^{-1} mm, target efficiency, η= 90%, and the wall friction were set to μ_k= 0.69 - typical μ_k values were picked with

reference to Jaeger et al. (1990); Silbert et al. (2001); Mangeney et al. (2007); Artoni and Richard (2015) and Mutabaruka et al. (2015). The simulation results are shown in Fig.2.9.

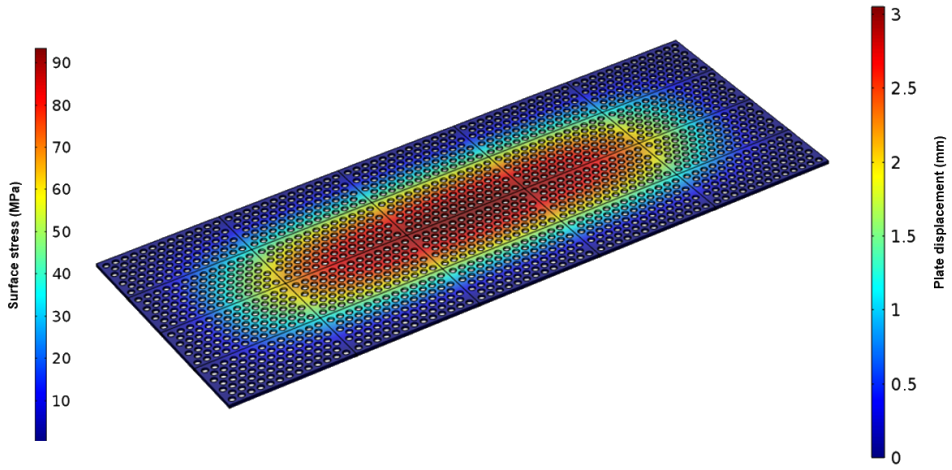

Figure 2.9: Estimated vibration amplitudes and yield stresses obtained through simulation

By fixing the boundaries of the tray, yield stresses of up to 90 MPa, and amplitudes ranging from 0 - 3 mm at the center of the plate were observed. The vibration energy needed to effect the simulation parameters was 1.28 G, the optimal bulk flow velocity $\bar{v}$= 22 cms^{-1}, and an amplitude of 1 mm and a frequency of 18.9 Hz was required.

The screen classification function was originally identified by Fréchet (1927), a French mathematician. It was however first applied by Rosin-Rammler in 1933 to describe particle size distribution (PSD) in minerals processing. His function was based on d_{50} of the particles, besides the particles' diameters, D_p. The Rosin-Rammler function is given in Eq.(2.34) below. Notice its comparison with Eq.(2.33).

$$\eta \quad = 1 - e^{-0.693\left[\frac{D_p}{D_{50}}\right]^{5.9}} \tag{2.34}$$

The limits of both Eq.(2.33) and (2.34) as D_p and D_{50}, respectively tend to zero yields $\eta \simeq 100\%$. These equations also explains the variability in the efficiency models with particle sizes depicted in Fig.1.2.

2.3 Summary: Coupling the discrete and continuum models

There exists a unified approach to get between the continuum model and the discrete model. For specific application to solids classification equipment, this study proposes the following summary of simplifications to the continuum model in Eq.(2.9):

i Noticing that Eq.(2.9) is on a 'per volume density' basis, multiply it by flow volume, V to convert the units to force, N

$$m\frac{\partial u}{\partial t} + Vu\frac{\partial \rho}{\partial t} = -V\nabla p + \mu V\nabla^2 u + F \tag{2.35}$$

ii Exclusion of the viscous and pressure drop terms, since the flow is inertia-dominated.

iii Pressure fluctuation in granular flows is small (Swinney, 2007). However, in particles classification there is variation in density around the continuum. These slight variations from the center of the continuum outwards are caused by the *multiphase* effect due to the interface (of air and solid particles) explained in section **2.1.5**. The additional force is thus seen as momentum accumulation due to the density gradient.

$$uV\frac{\partial \rho}{\partial t} = u\dot{m} = u\frac{\partial m}{\partial t} \tag{2.36}$$

This methodology therefore accurately converts in between the continuum model and the discrete model. The above steps transforms Eq.(2.35) to the form in Eq.(2.37):

$$m\frac{\partial v}{\partial t} = -u\frac{\partial m}{\partial t} + F \tag{2.37}$$

Eq.(2.37) provides an estimate of the Navier Stokes equation. When momentum is conserved by attaining continuity, the net external forces sums to zero, i.e. $F = 0$. To determine the time rate of particles classification, setting the third term (sum of external forces) to zero, reduces the equation into the form of a 'first order rate law' written as:

$$\begin{aligned} \frac{dm}{dt} &= -km \\ \text{where } k &= \frac{1}{u}\frac{dv}{dt} \end{aligned} \tag{2.38}$$

iv Equations (2.19) and (2.37) are just statements of Newton's second law until the constant velocity u, usually referred to as 'relative' is defined. The hypothesis was stated in **Publication I** as follows: *the rate of particle classification is proportional to the rate of change in momentum and the screening open area, but inversely proportional to the particle size*. Mathematically, this is done by introducing important aspects of this thesis into the flow equations, 'open' area, a and the particle size

mean diameter, D_p.

$$\begin{aligned} \beta &\propto \frac{t}{\bar{v}} \propto \frac{a}{D_p} \\ \beta &= \frac{kt}{\bar{v}} = \tau \frac{a}{D_p} \\ \beta \bar{v} = kt &= \frac{\rho \bar{v}}{\mu} \left(\frac{a}{D_p} \right) \end{aligned} \tag{2.39}$$

From Eq.(2.39), it can be shown by dimensional analysis that $\tau \simeq 1/\nu$, and thus for a continuous process the rate of classification can be expressed as a function of the driving force, F, the length characteristic, $L = a/D_p$, and the kinematic viscosity of a particulate system.

$$\dot{m} = -\frac{FL}{\nu} \tag{2.40}$$

Most important and perhaps challenging is to note that the Reynold's number of this particulate system is not constant as explained throughout this text, that the density is a discrete function of position vectors x, y and z (voidage, ϕ) in the matrix, referred to as bulk the density ($\rho_b = \phi\rho$). The velocity is also averaged, to mean bulk characteristic flow. The mass rate of separation therefore varies at each section of the screen but constant when the total is estimated as a function of time only.

The Reynold's number of particulate system flow in a perforated screen surface is estimated by first calculating the flow area, which corresponds to the un-holed surface represented as a fraction of the total screen area:

$$\begin{aligned} R_{ip} &\simeq \frac{\rho \bar{v}}{\mu} \left[\frac{A\,(1 - HAF)}{D_p} \right] \\ &\text{merging in Eq.(2.39)} \\ R_{ip} &\simeq \beta \bar{v} \left[\frac{1 - HAF}{HAF} \right] \end{aligned} \tag{2.41}$$

A simplified empirical model for optimal value of Reynold's number can therefore be estimated from the fact a maximum value of $\beta v \simeq 2\pi$ and with known HAF e.g. 0.4031 as applied in this thesis, $R_{ip} \simeq 9.304$. Such a low value of particulate Reynold's number simply imply that the flow velocity, holed area fraction, inclination and all rate factors must be controlled in order to attain an optimal process.

3 Population balance models

The population balance phenomenon has accounted for many applications in systems theory in recent times. In fact it has gathered unprecedented attention in the past few years, as it has proven applicable in many academic and industrial quarters, and in particular, areas involving particulate matter (Ramkrishna and Mahoney, 2002; Bayraktar et al., 2008). Today, population balance modeling is undergoing phenomenal growth in areas such as transport, nucleation, crystal morphology, cell growth and differentiation, gene regulatory processes, and transfer of drug resistance (Ramkrishna and Singh, 2014), and in assessing the changes in Particle Size Distribution (PSD) as a function of time in processes such as agglomeration, aggregation and breakage (Maurstad, 2002; Moussa, 2008). These models have also been applied to aid product and process design in various industries, such as comminution in minerals processing, cereal plants etc., (King, 2012; Johanson, 2016). The following sections detail how the population balance models have been applied to explicate the flow dynamics of particle size classification in this thesis. Particular attention is paid to a novel *law of mass action* approach that is conceptualized around the analogy of a series of parallel chemical reactions giving 'birth' to underflow ('offspring') with subsequent 'death' of the initial feed mass of materials ('parents'), while at the same time having a functional dependence on each other, called aggregation through classification.

3.1 First order rate law

The Population Balance Equation (PBE) is a statement of continuity applied widely in particulate systems (Nicmanis and Hounslow, 1998), e.g. to model the rate limiting regimes (LeBlanc and Fogler, 1987). From the kinetics of particle classification for instance, the mass balance of particles by-passing a screen section of length, x in Fig.3.1 is described by the PBE, stated in Eq.(3.1):

$$m\left(x+\Delta x, t+\Delta t\right) R\left(x\right)|_{x+\Delta x} - m\left(x,t\right) R\left(x\right)|_{x} = \frac{\partial}{\partial t}\left[R\left(x\right) m\left(x,t\right)\right] + B\left(x\right) - D\left(x\right) \tag{3.1}$$

The rate of change in particle population, $R\left(x\right)$ expressed as dx/dt, is described by solving the PBE at *steady-state*. Steady-state conditions imply stable population, meaning that the carrying capacity is within the limit, so that the number of 'births', $B\left(x\right)$ equal that of 'deaths', $D\left(x\right)$. In this particular context, it requires that no accumulation of mass or energy occurs over the time period of interest i.e., $B\left(x\right) = D\left(x\right)$.

3.1.1 The steady-state solution of population balance equation

Theoretically, the steady state solution of population balance equation (PBE) is obtained by setting the result of the last two terms of Eq. (3.1) equal to zero, $B\left(x\right) - D\left(x\right) = 0$,

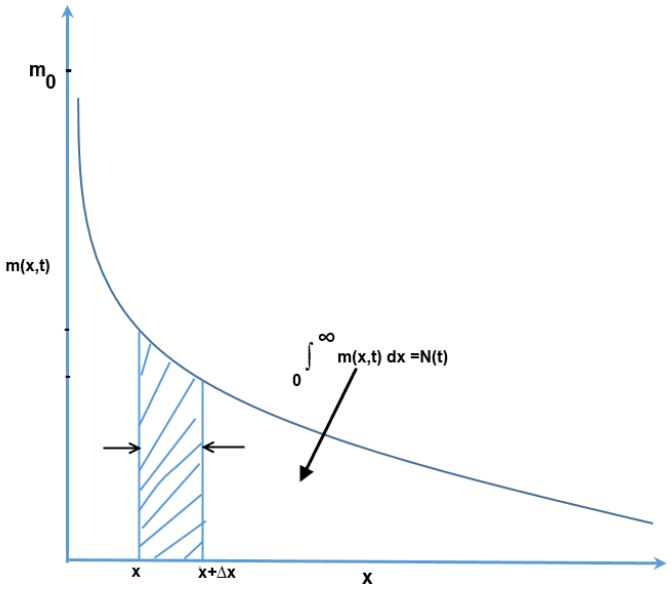

Figure 3.1: Illustration of population balance formulation

and applying boundary conditions. At the beginning of the batch process, the following apply: $t = 0$, $\Delta x = \Delta t = 0$, $m\left(x, 0\right) = m_0$.

After t seconds: $m\left(x + \Delta x, t + \Delta t\right) - m\left(x, t\right) = dm/dt$. PBE in Eq.(3.1) can be expanded by substituting all the terms, so that:

$$\begin{aligned} -\frac{\partial}{\partial x}\left[m\left(x,t\right)R\left(x\right)\right] &= m\left(x,t\right)\frac{\partial}{\partial t}R\left(x\right) + R\left(x\right)\frac{\partial}{\partial t}m\left(x,t\right) \\ -m\left(x,t\right)\frac{\partial}{\partial x}\left(\frac{dx}{dt}\right) - \frac{dx}{dt}\left[\frac{\partial m\left(x,t\right)}{\partial x}\right] &= m\left(x,t\right)\frac{\partial}{\partial t}\left(\frac{dx}{dt}\right) + \frac{dx}{dt}\left[\frac{\partial m\left(x,t\right)}{\partial t}\right] \end{aligned} \tag{3.2}$$

Noting that $R(x) = dx/dt = v$ (velocity):

$$\begin{aligned} \frac{dx}{dt}\left[\frac{\partial m}{\partial x}\right] = \frac{\partial}{\partial x}\left(\frac{dx}{dt}\right) &= 0 \\ m\frac{\partial v}{\partial t} &= -v\frac{\partial m}{\partial t} \\ \frac{\partial m}{\partial t} &= -km \\ \text{where } k = \frac{1}{v}\frac{\partial v}{\partial t} & \end{aligned} \tag{3.3}$$

Notice the change in notation of the variable component of velocity, $\partial u = \partial v$. Since quantities are conserved in this case, the mass, k, is referred to as the moment of mass. The remaining form of Eq.(3.2) is a function of time only, and thus it still holds when written as a fully derivative function as follows:

$$\frac{dm}{dt} = -km$$

Notice that Eq.(3.3) is comparable with Eq.(1.7). The *first order rate law* is therefore better understood when viewed as a *truncation*, or the simplest form of the PBE.

3.1.2 Application of the first order rate law

In practice steady-state assumptions are not always true, and thus accumulation (in the case of PBE) always occur. The challenge with particle classification like with many processes is predicting the amount of overflow particles accurately. With population balance modeling, the particle classification process can be modeled for its components, i.e. the underflow, overflow and when well applied, first order rate law may show the dynamic population e.g. of the accumulation. When the first order rate law is applied as is, the decrease in the initial batch masses may be predicted with some accuracy. For instance, in a representative case in which the feed batch of 50 kg was run, and the weight of the underflow particles, m_u of a certain mean particle diameter, D_p could be measured within a time interval (2 minutes in this case) and used to estimate the constant k experimentally to gage the performance of the classification process, i.e. the ability to reduce the overflow significantly, e.g. by lengthening the screening time, and screen, widening the sieve, or manipulating other screening variables.

Table 3.1: A representative experimental procedure using the PBE model

t (min)	0	2	4	6	8
$m_u(t)$ kg	0	31.606	43.23	47.51	49.084
$m_o(t)$ kg	50.0	18.3940	6.7668	2.4894	0.9158
$m(t)$ kg	0	2.8	2.2	1.3	0.7

The following procedure was followed.

i Use the population balance equation to estimate the overflow $m_o(t)$ and k for the feed amount of 50 kg.

$$m_o(t) = 50\,\mathrm{e}^{-0.5\,t}$$

ii Estimate and monitor the accumulation rate through the material balance

$$m(t) = 50 - [m_u(t) + m_o(t)]$$

iii Estimate ε and η at the end of the separation period, t

$$\varepsilon = \frac{50 - 49.084}{50} = 0.03,\ \eta = 1 - \varepsilon = 0.97$$

iv Plot the results

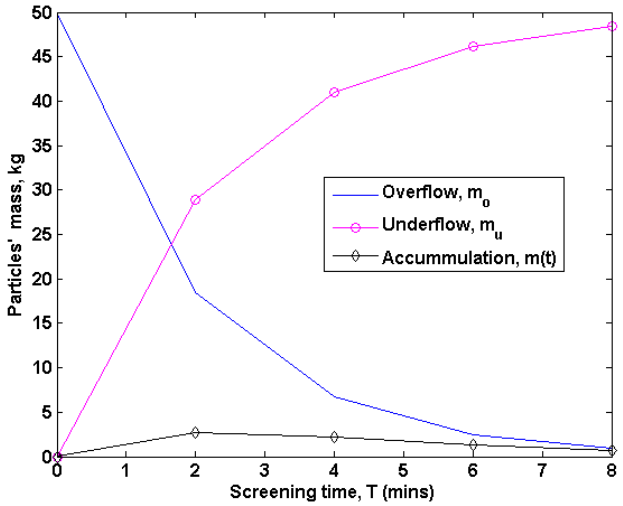

Figure 3.2: Illustration of population balance equation application

v Relate the time constant k to screen area intensity τ, and average screening time, t

$$\beta = -\frac{\ln \varepsilon}{\bar{v}},\ \tau = \frac{ktD_p}{\bar{v}a},\ R_{ip} = \frac{\bar{v}\tau}{D_p} A\,(1 - HAF)$$

vi Adjust parameters a, β, D_p, and τ appropriately to achieve the desired values of k, ε, and the flow regime R_{ip}.

The last two items in the above description are a contribution of this thesis, aimed at relating the separation intensity to the manipulable design variables.

3.2 Statistical model

It is also possible to characterize a particulate system to achieve a generalized statistical model, based on the mass of a particle count. Consider a group of particles, U_o discharged from a hopper to a series of n stationary (for gravity) or vibrating screens of increasing aperture sizes, D_{ap} downslope. The number of particles falling through to the underflow in each of the n screen sections at a time interval t_i is represented by, D_i, while those proceeding to the next screen are given as intermediate products, U_i, where i represents the current stage number. With statistical inference, a generalization for the intermediate particle count or overflow at each separation stage can be expressed algebraically as shown in Eq.(3.4). This methodology was detailed in **Publication IV**.

$$U_i = U_o - \sum_{i=1}^{n} D_i(t_i) \tag{3.4}$$

Dividing Eq. (3.4) by U_o normalizes the equation to yield the system efficiency η, and the overflow fraction ε of the screening unit Eq.(3.5).

$$\begin{aligned} &\frac{U_i}{U_o} = \frac{U_o - \sum_{i=1}^{n} D_i(t_i)}{U_o} \\ &\text{or } \eta_i = 1 - \varepsilon_i \end{aligned} \tag{3.5}$$

where ε_i is the oversized fraction, and η_i the undersized fraction, at section i of the screen. At the end section of the screen (see Fig.1.1), $i = n$, it is expected that $U_n = 0$. With some optimization strategy, e.g. least squares (LSQ), U_n can be driven to zero, so that the cumulative particle count of D_i roughly equals the original number of particles, U_o. This is done by taking the residual particles count E_i as an objective function (or error) that needs to be minimized, as shown in Eq.(3.6).

$$\begin{aligned} f(t_i) &= \sum_{i=1}^{n} {E_i}^2 \\ \text{where } E = E(t_i) &= U_o - \sum_{i=1}^{n} D_i(t_i) \end{aligned} \tag{3.6}$$

E_i corresponds to accumulation in the PBE. Eq.(3.6) forms an underdetermined optimization strategy. The best way to solve these problems is to find an approximate function that minimizes E_i. Linear models have been used widely in describing most systems and they

seem to work quite well. Computing the first derivative of the error function, $f(t_i)$ in Eq. (3.6), and setting it to zero, yields the minimum value of E_i, in Eq. (3.7).

$$\hat{Y}\left(\alpha\right) = \sum_{i=1}^{n} D_i(\alpha) \simeq \beta_0 + \sum_{i=1}^{h} \beta_i \alpha_i(t) \tag{3.7}$$

$$\begin{aligned} &\frac{df}{d\beta_i} = 2\sum_{i=1}^{n}\left[U_o - \left(\beta_0 + \sum_{i=1}^{h}\beta_i\alpha_i(t)\right)\right](-1) \\ &\left(\mathbf{t^T t}\right)\hat{\beta} = \mathbf{t^T} U_o \end{aligned} \tag{3.8}$$

where $\hat{\beta}$ are the optimal coefficients of the function, $D(\alpha)$, obtained by solving the *normal* equation (3.8). In most cases particulate systems are continuous functions of time and can be described by using Eq.(3.9).

$$U\left(t_i\right) = U_o - \frac{i}{h}\int_0^{\alpha_{th}} \sum_{i=1}^{h} \beta_i \alpha_i(t) \tag{3.9}$$

The accumulation term, $E(t_i)$ can be minimized by checking the differences in Eq. (3.4) at any given time. Simultaneous solutions of Eqs. (3.5), (3.6) and (3.9) yield a the steady state solution of PBE. U_o decays exponentially, as the cumulative undersize increases with a Cumulative Distribution Function (CDF). The accumulation, $D(t_i)$, takes a temporary growth before dying out, as shown on Fig. 3.3. This trend can also be observed in the representative case study presented in Table 3.1. The difference E_i also dies out, and is minimal for highly efficient systems.

The sum of the undersized with the oversized masses gives the total amount of particles, obeying the ideal material balance equation with no losses, $E_i(t_i)$. However, this is not true in real systems, due to imperfections and particles clinging to the tray blinding the screen, and thereby preventing passage to the underflow. This situation constitutes inefficiency of the screening process quantified by E_i.

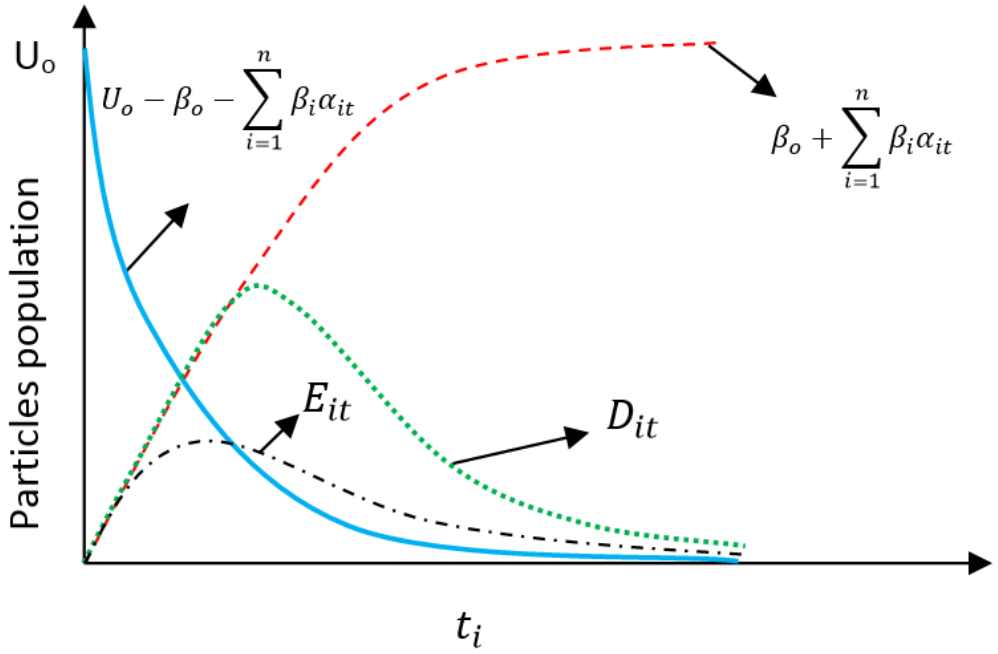

Figure 3.3: An illustration of a typical particle screening model

3.3 A Novel law of mass action model

Statistical models are convenient in the sense that only the underflow is needed in order to come up with a complete model, including expected oversized particles and accumulation, as seen in section **3.2**. It was found in this study, however, that multi-sized screening is one of most exciting not only for grading products into several particle sizes, but when well implemented it also provides a clean cut, thus reducing economic losses in re-manufacturing, as well as efficient ore/gangue separation in the mines, and fertilizer plants as discussed in section **1.2**. This makes it necessary to understand the dynamic quantification of not only the oversized and undersized particles simultaneously, but also to estimate the intermediate amounts between the initial feed and the overflow product at any given time.

Many attempts to describe screening processes kinetically have ended up adopting either probabilistic or empirical approaches (King, 2012; Karra, 1979; Subasinghe et al., 1989). However, it is possible to use one set of experimental data to build and train a general model that can be used to up-scale a process. The model uses the analogy of an extended Guldberg-Waage network of nested irreversible parallel chemical reactions as shown in Fig. 3.4. A detailed account of this intuitive method was given in **Publication III** for gravity particle classification, and in **Publication IV** for forced vibration screening. The constants $k_i s$ are empirically related to the screening process factors discussed in **Publication V**, and *not* the usual reaction kinetics constants in chemical reactions. The same

constants are referred to as *moments* in the PBE.

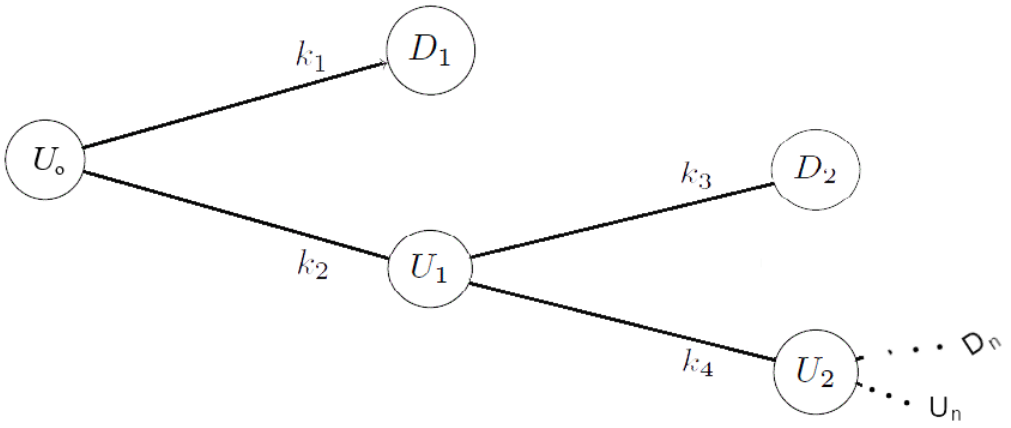

Figure 3.4: Nested parallel chemical reaction analogy of multi-sized screening

The screening system in Fig. 3.4 *decomposes* U_o into its components of underflow, $D_i s$, intermediate products, $U_i s$, and oversized, U, by using the set of state equations in Eq.(3.10). When well implemented, it also estimates the dynamic quantities of accumulation.

$$\left.\begin{aligned} \tfrac{dU}{dt} &= -(k_1 + k_2)\,U \\ \tfrac{dD}{dt} &= k_1 U + k_3 U_1 \\ \tfrac{dU_1}{dt} &= k_2 U - k_3 U_1 - k_4 U_1 \\ \tfrac{dU_2}{dt} &= k_4 U_1 \ldots \end{aligned}\right\} \text{Nested parallel chemical reactions analogy} \qquad (3.10)$$

Coincidentally the system of equation in Eq.(3.10) is identical to a Guldberg-Waage network of irreversible chemical reactions. The scheme of consecutive reaction pathways in the above system can be extended so that there are as many equations as the separation stages. A typical solution of a parallel reaction yields the desired product D and a side or intermediate accumulation product E, and also gives the dynamics of the original mass, U_o. Similarly, the results of the above system of equations in Eq. (3.10) are exactly the same as those of the statistical model discussed in section **3.2** and illustrated in Fig. 3.3. It is also possible to estimate the extent of separation efficiency by using this model. Taking the ratios of derived constants, from Eq.(3.10), the performance in terms of η_n for n

stages can be estimated by using Eq.(3.11).

$$\eta_n = \frac{\sum_{j=1}^{n} |k_{(2j-1)}|}{\sum_{j=1}^{n} k_j} \tag{3.11}$$

3.4 Summary: Key applications of population balance models

Statistical and law of mass action models were derived in this chapter. The models are accurate and work very well, i.e., when used for specific processes and equipment, e.g. when testing already fabricated particle classification units to estimate separation rates and efficiencies. However, the results obtained can easily mislead if applied blindly on other particulate systems. As discussed in section **1.3.4**, empirical models lack universality in providing tangible design information that can be applied across all unit operations. Even though they may not provide for initial design considerations, population balance models are still versatile when evaluating the performance of unit operation. Statistical inferences also form a basis for control and optimization, e.g. through the use of models to establish optimal operating conditions and when considering redesign. The first order rate law (FORL) only calculates the current population of particles (overflow), but does not estimate the difference in particle population, or the underflow. In order to get the passage, the overflow must be subtracted from the original mass or the particle count. For instance, there are few sufficient mathematical models (apart from the Weibull distribution function) that can estimate underflow growth from zero. The existence (no non-existence) of such models is usually described as failure. These problems therefore present a challenge and limitation of the FORL, and necessitate empirical or data-driven modelling. With the mass action model, all the components of particle population can be estimated simultaneously, proving it to be a successful methodology upon further development.

4 Experimental verification

While computer modeling and simulations have been widely accepted as engineering study tools nowadays, there still exist the need to complement their results by carrying out experiments, to authenticate the consistency of the models developed, and to ensure the relevance of the processes in the industry. As of today, computer modeling and simulation are still under huge discourse pertaining to their applicability and shortcomings, and are increasingly becoming a question of epistemic or philosophical issues, rather than those of a core engineering discipline (Grim and Rescher, 2013). The aim of this section is to describe the experimental procedures, planning, setup, and designs used, both for gravity and vibrated solids separation.

4.1 Gravity solids separation

Gravity-driven solids classification was covered in **Publications I, II and III**. The objectives of **Publication I** were set as follows:

i To study the motion of particles along inclined screens under the force of gravity

ii To Propose a new mathematical model to quantify solids separation rates and efficiency

iii To propose the three most important parameters for equipment design, and to test them by computer simulation

iv To carry out experimental verification and report the results through a journal publication

Publication II was aimed at achieving the following:

i To explore the theory on the dynamics of dry solids classification

ii To study the effects of more variables such as screen loading, inclination on the separation intensity and efficiency.

iii To assess whether the models developed in **Publication I** were still consistent and

iv To refine the models as necessary

The aims of **Publication III** were as follows:

i To develop a methodology for enhancing gravity solids classification through selection of optimized screen design and feed rates control.

ii To formulate and apply the newly founded *law of mass action* model discussed in section **3.3**.

4.1.1 Apparatus, experimental setup and procedure

For the study presented in this section, the following apparatus was required: a stopwatch, a porcelain bowl, an electronic weighing balance, 16 100 cc beakers, and four samples of 100 grams of glass beads of diameters 0.75, 1, 2 and 3 mm. The four samples of glass beads were uniformly mixed in a porcelain bowl. 16 samples (see **Publication I**) of the mixture were weighed to the beakers, with masses increasing at an interval of 10 g, from 10 up to 160 g. The prototype screen measured 30 cm $\times$ 46 cm, i.e. approximately 1380 cm^2 in total area. The perforated area was calculated to be about 40.31%, reducing the effective screening area to 556.28 cm^2 (see Fig. 1 in **Publication III**).

The prototype device was hinged at an angle of 15° from the horizontal, with the smallest sieve (1 mm) highest and the largest (4 mm) lowest. Each of the 16 mixture samples, one at a time, were carefully distributed at the width of the feed Fig.4.1, smallest sieve), before allowing the particles to roll down the sieves. For all the samples, the stopwatch was started upon discharge and stopped roughly when the last particle hit the oversize collection box at the end section. The following measurements were taken and recorded: sample mass m_T, mass of the undersize collected on the 1, 2, 3 and 4 mm sieves (m_1, m_2, m_3, m_4 and oversize m_n), and total runtime, T. In this case $n = 5$.

The following values were calculated directly from the collected data: total undersize masses (m_u), separation efficiency, η computed as the ratio of total mass of undersize m_u, to the sample mass m_T, overflow fraction, ε computed as the ratio of mass of oversize mass collected at the screen end section to the starting batch mass, m_T, and the mass of un-separated particles (accumulation), m_{un} calculated by subtracting the sum of undersize and oversize mass from the total sample mass, m_T. The results were tabulated and presented in Table 2 in **Publication I**.

The same experimental procedure was repeated for **Publication II** with five more angles, 10.5, 12.5, 14, and 20, with the aim of experimenting with more angles of inclinations and feed batch masses to ensure consistency. A typical table of sampled results were tabulated in Table 1 in **Publication II**. Three more angles, 5, 10 and 17.5 were tested in **Publication III** with results tabulated in Table 2 of the same publication. These results were used to formulate optimization regimes, which formed the basis of the mass action models.

4.1.2 Results and discussion

The postulated rate determining strategy seemed to mimic the solids classification well. As expected, smaller particles were separated at a higher rate than the larger ones, in both the simulation studies and the experiments. The total masses collected from each successive sieve were plotted against the aperture diameters on the prototype experiment, which also showed that smaller particles were collected at a higher rate. It can be seen in the rate equation Eq.(1.5) that the particle size diameter is inversely proportional to the rate of classification. Nevertheless, the proposed model is ideal in that it assumes a perfect

situation in which all the overflow has sunk to the underflow collection channels by the end of the runout time, or the length of the classification equipment. In reality, however, there existed un-separated particles unaccounted for. This is the group referred to as accumulation in the PBE. It constitutes the overall drop in the efficiency of the process. In the physical sense, accumulation is caused by the clinging of particles to the surface of the screen, and those that 'fly off' the screening tray. There are other situations that lead to reduction in the efficiency of the unit, e.g. adjusting the deck angle too high, which has two effects: causing a virtual reduction in the projected area from a 10% reduction in the aperture diameters at an angle of 20°, to almost 100% diminished apertures at 70°, as will be shown in the next chapter. Secondly, as the inclination angle increases, the particle flow velocity becomes difficult to regulate. Higher bulk velocities are detrimental to the efficiency of particle classification. While excess loading of the screen is known to cause multi-layered flow and possible blinding, this study has shown that a substantial amount of screen loading is required to increase the transport momentum, which has been found to be the main driving force behind inclined deck screening in both gravity and vibrated solid particle classification.

A controlled change in the momentum of the granular flow on a perforated inclined surface is enough to cause sufficient classification of particles by size. The rates of classification achieved depend heavily on the momentum (mass and velocity), the screening area and particle sizes and shapes. It is difficult to quantify the effects of mass and velocities separately on screening, since a larger mass becomes more complex to separate, as it tends to create a thicker layer, while a smaller mass correspondingly reduces the total force of separation (as per the rate model). At high velocities, particles move too fast to 'fall', while low velocities imply a reduction in the overall rate of separation, excessively long residence times, and increased probability of sieve blockage, commonly referred to as 'blinding'. Nevertheless, gravity solids classification is favorable since no agitation is needed, and hence energy is optimized at nominal efficiencies. The new model developed here also implies that it is possible to achieve up to 100% efficiency with gravitational solids classification, as it makes the granular flow less turbulent, and thus the flow velocity becomes easy to control by just adjusting the deck inclinations and the perforations on the sieve tray. The disadvantage with this system is that the lack of agitation may result in slow operations, and possible increase in the overflows if optimum inclinations and the Holed Area Fraction (HAF) is not well calculated. Fig. 4.2 shows a comparison of the mixed particles to the output of the size classification using the prototype vibrating screen.

4.2 Vibrated solids separation

Publication IV was an extension of (Rotich et al., 2015), presented in the physical separation conference held in Fallmouth, UK in June 2015. In general, vibrating screens were covered in **Publication IV**. The main objectives of this **Publication IV** were as follows:

i To derive in details models used to predict single layer flow of granular material on inclined, vibrating screens.

ii To test the applicability of the gravity classification models derived in **Publications I, II and III**.

iii To create a methodology for mathematical optimization of particle size classification through screening.

iv To use kinetic models to derive an estimation of the relationship between the required energy in solids classification and target efficiencies.

v To conduct Design of Experiments (DoE) and Analysis of Variance (ANOVA), in order to assess the significance of the manipulated variables, and their interactions, and to ensure statistical significance, due to the many variables involved.

4.2.1 Apparatus, experimental setup and procedure

The apparatus required for the experiments were the same as that in section 4.1.1, with an additional 100 W motor and a frequency controller to adjust the frequencies. In these sets of experiments, the number of runs per batch mass were planned by using the DoE strategy reduced to 8 and carrying out 3×3 sets of each batch, making a total of 72 experiments. The deck inclinations, θ, were varied over three angles (7.5,12.5 and 17.5°), and the vibration frequencies, f, varied over 7, 15 and 20 Hz, running a total of 8 feed batch masses, U_o of 10-80g at an interval of 10g with a constant power of 50 W. The prototype screen had a total area of 1380 cm^2 and effective (holed) area of 556.28 cm^2. The apertures were placed strategically half a diameter a way from each other to constitute a total HAF of 40.31%. On average it took $2 \sim 2.5$ seconds for complete classification of each batch. Fig.4.1 shows the schematic of the prototype screen used for experimental validation.

Figure 4.1: Schematic of the prototype screen used for experimental validation, 1) Multi-sized sieve plate, 2) 100 Watt tumbler motor, 3) FC-MTY4 IP54 motor frequency controller, 4) Underflow collection troughs below the sieves

4.2.2 Results and discussion

The rate determining equations used for gravity solids classification were also applicable with the vibrating screens. Even though the rates improved significantly, the relative classification efficiency dropped slightly. The planning and setup of the experiments with the DoE strategy helped to reduce the number of experimental runs needed to obtain useful information. Upon carrying out the DoE, the linear model in Eq.(4.1) was fitted to the results. More details were presented in **Publication IV**.

$$\hat{Y} = 27.03 + 21U_o + 3.8f - 3.1\theta f + 3.0U_o f - 2.4\theta U_o f \tag{4.1}$$

It became clear that some factors were far more significant than others. For instance, the most significant of all was the screen load or feed rate, having a large positive effect judged from the coefficients of the model in Eq.(4.1). This is no surprise, as it confirms the hypotheses that the greater the load, the higher the momentum, and thus the driving force. The general statistical model is shown in Eq.(4.2)

$$\begin{aligned} \hat{Y}(\alpha) &= \beta_o + \sum_{i=1}^{6} \beta_i \alpha_i \\ \text{Where } \beta_0 &= 27.03; \beta_1 = \beta_4 \simeq 0 \\ \text{and } \beta_2 &= 21; \beta_3 = 3.8; \\ \beta_5 &= -3.1; \beta_6 = 3.0; \beta_7 = -2.4; \end{aligned} \tag{4.2}$$

Surprisingly, deck inclination had no relative effect on its own, but only in combination with the rest of the factors, f and U_o. The f-value limit used in this study was 0.07. Even

though the model suggests that increasing the screen load would improve the screening process, attention must also be paid to the negative effect of aperture blockage and low flowability, when low deck inclinations and vibration frequencies are used.

4.3 Summary: Main results of experimental verification

In summary, the developed models worked for both gravity and vibrating screens, the only differences being intensity and efficiencies. In gravity separation, the efficiencies were quite high at median angles but the screens were blinded at lower angles. With vibrating screens, the rate was much higher but the clean cut was lost and the efficiency diminished. In general, the study proved that when multi-sized screens are well implemented, it is possible to obtain reasonable capacities, rates and a clean cuts, important factors in the relevant industries. Fig. 4.2 shows the products obtained from the vibrating screen prototype equipment with the deck inclined at 12.5° and the frequency set to 20 Hz, with a batch feed mass of 80 g.

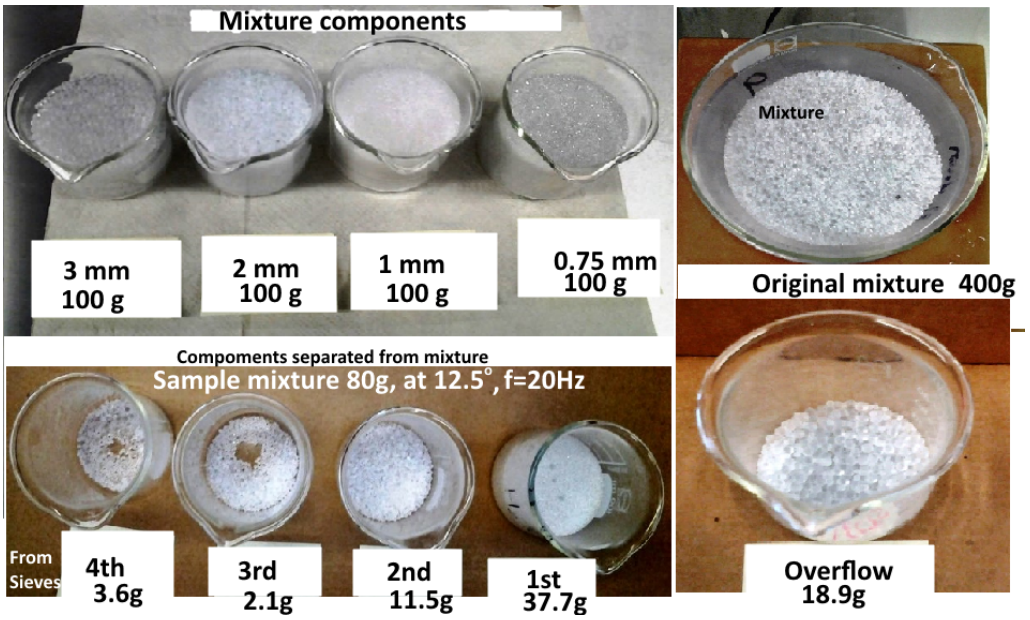

Figure 4.2: The results of screening at 12.5° and the frequency set to 20 Hz

5 Model-driven design considerations

5.1 Screening energy calculation

Benchmarking process energy is an important dictum in today's industry dynamics. The screening force, Γ, depends on the type of energy and the screen geometry, as well as the weight and the material of construction, among other factors. A direct correlation to estimate the screening force (also referred to as the screen factor) as a function of vibration amplitudes, z, and frequencies, f, is discussed qualitatively by (Wills, 2016), estimating $\Gamma \simeq 7G$. Iizuka and Delfim (2010) assigned this value a range of $\Gamma = 4 \pm 1G$. Jaeger et al. (1996) noted that when Γ is a bit larger than unity, the granular material tend to rise above the surface of the vibrating equipment, causing dilation and macroscopic flow in the process.

While such empirical correlations are useful in determining the screen factor towards mechanical engineering design, they barely give an indication of the required process parameters, e.g. energies relative to the expected screening efficiencies. Furthermore, they are only locally applicable in the test equipment, and thus have limited universal applications (**Publication III**). Some researchers have also pointed out that some screening charts and formulae have in the past produced results deviating by up to a factor of three (Li et al., 2002).

Kinetic models, on the other hand, have their own flaws. Laminar flow systems are easily predictable in theory, but their occurrence in practice is seldom. For instance, to maintain a constant value of $\beta v \simeq 2\pi$ as stated in section **2.2.2.3**, constant bulk velocity, v, must be maintained, i.e. Eq.(2.31) must always be satisfied. This means that the time dependence of velocity must be eliminated, which always present a difficulty in most process industry settings. However, the system can be stabilized forcefully by imposing certain conditions and assumptions to achieve useful estimations that may predict the system dynamics. One important condition for granular materials and powders is that of incompressibility ($d\rho/dt = 0$) in Eq.(2.9) when a discrete model is used as described in Chapter 2. In addition to the qualitative description given in section **2.1**, it is assumed that the granular material is dry, non-cohesive, and rigid in order to allow time averaging of the bulk velocity as presented in Fig.2.4. The discrete model estimates the convective acceleration using Newton's second law by assuming that the gradient of velocity is zero. The derivative of the fluctuating function in Eq.(2.31) may therefore be constrained to zero as shown in Eq.(5.1).

$$\begin{aligned} &\nabla . v = 0 \\ &\frac{dv}{dt} = -\frac{1}{\rho}\nabla p + \nu \nabla^2 v + \frac{\overrightarrow{F_x}}{\rho} = 0 \end{aligned} \tag{5.1}$$

The first two terms of the RHS of Eq.(5.1) are negligible from prior considerations leaving $\overrightarrow{F_x}$, the force per unit volume divided by ρ which yield nothing but the G-force ($F/V\rho = F/mg = G$). This results in the screening force as a direct function of deck inclination, coefficient of kinetic friction and the overflow fraction, as seen in Eq.(5.2).

$$G = sin\theta - \mu_k cos\theta \left(1 + \ln \varepsilon\right) \tag{5.2}$$

Eq.(5.2) may also be evaluated as a function of the screening efficiency, η, as shown in Eq.(5.3).

$$G = sin\theta - \mu_k cos\theta \left[1 + \ln \left(1 - \eta\right)\right] \tag{5.3}$$

The value of G obtained in Eq.(5.2)/(5.3) is therefore the force/energy in G-force required to stabilize the system by eliminating its time dependency, and thereby minimizing turbulence. This stabilization equalizes the bulk flow velocity to the mean at any given time, and gives the desired system efficiency upon substitution in Eq.(2.33).

5.2 Distinction between gravity and agitated screen models

When no vibration is induced in particle classification, the process is referred to as gravity solids classification. There are a couple of reasons that dictate this industrial situation. **Publications I, II and III** were dedicated to gravity solids classification. Even though gravity classification may be slow, it is natural. This means that it is nature-driven, and thus mimics nature by being less energy-intensive, allows remote area operations in mining, agriculture, etc., and sometimes it is just inevitable. Some processes with high density differences, such as rare earth minerals e.g. Wolframite (with specific gravity ~ 7.5), necessitates the use of gravity concentration for higher recovery - this was discussed briefly in **Publication III**. In fact, gravity solids classification might be the only one that can be pushed to yield 100% efficiency. This is an aspect that was also shown mathematically in this study. In agitated solids processing, a certain energy is lost just to vibrate the screening equipment itself, leading to less overall performance in general.

While the use of E in Eq.(2.30) is not obvious, it shows the effect of using heavy construction material on the overall performance of the screen. If the limits are taken as $M_s \to \infty$, $E \sim 1$, making $\beta v \sim 0$, thereby reducing the system efficiency to $\eta \sim 0$ in Eq.(2.33). This implies that, there is a force needed to agitate the screen structure, even when no

actual separation occurs. This can be seen by taking the limits of Eq.(5.3) as $\eta \rightarrow 0$. Thus the use of heavy construction material must be matched by application of greater agitation energy (G-force), and lower operational efficiencies in general. An alternative form of Eq.(5.3) can be obtained for gravity classification, by setting $G = 0$ as shown in Eq.(5.3) and using $E = \varepsilon = \frac{m(t)}{m_0}$.

$$\begin{aligned} \sin\theta &= \mu_k \cos\theta \left(1 + \ln\varepsilon\right) \\ \tan\theta &= \mu_k \left(1 + \ln\varepsilon\right) \end{aligned} \tag{5.4}$$

Eq.(5.4) defines the limitation of gravity separation, as it implies that the overflow fraction, $\varepsilon \sim 1$ and thus the condition $\frac{\tan\theta}{\mu_k} < 1$ must be maintained.

5.3 Screen dimensioning

The dimensioning of the screen must not be considered as an isolated or inherent process, but highly controlled by other key design constraints, such as the force and the screen work expected, for instance the load capacity and particle shapes and sizes. It also depends on the overall operational conditions, which in general affect the efficiency of separation. The dimensioning task is subdivided into the following subsections, each with described implications.

5.3.1 Screen length

The length of the screening equipment controls two important aspects of the process: efficiency and cut. In multi-sized screens, when the screen length is controlled properly in synchrony with aperture diameters, a clean cut is easily achieved. Screen length is also directly linked to the efficiency of separation, in fact according to (Wang and Tong, 2011), there is a functional, exponential relationship between efficiency of separation and the screen length. In general, the screening efficiency increases with the length .

Length is in turn controlled by the mean bulk flow velocity of the particles, and the mean runout time taken by the oversize mass of particles to traverse the entire length of the screen. For time-averaged bulk flow velocity, $\bar{v}$ Eq.(2.32) and the mean time, T, this functional relationship can also be described mathematically as follows:

$$\begin{aligned} dL &= v dt \\ \int_0^L dL &= \int_0^T \bar{v} dt \\ L &= -\frac{T}{\beta} \ln\left[\frac{m\left(T\right) + M_s}{m_0 + M_s}\right] \end{aligned} \tag{5.5}$$

It can be seen in Eq.(5.5) that the smaller the overflow required (inside square brackets), the greater L is, for constant β and T. This further supports the claim of (Wang and Tong, 2011) on the existence of an exponential relationship between the length and the efficiency. The minimum screen length is estimated by computing the minimum runout distance of the particles on the screen using Eq.(5.6) for $m\,(T) = 0$.

$$L_{min} = -\frac{T}{\beta} \ln \left[\frac{M_s}{m_0 + M_s} \right] \tag{5.6}$$

5.3.2 Screen width

Screen width not only affects the screening efficiency in general but also influences the operational capacity directly. For a fully loaded screen of bed thickness t_b, screen width w, bulk density ρ, flow velocity v, consider a section of an inclined screen with granular solids of bulk density ρ, depicted in Fig. 5.1.

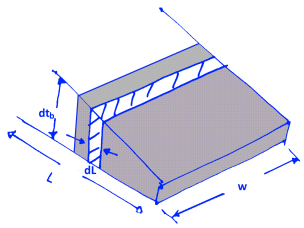

Figure 5.1: Illustration of a fully loaded section of inclined screen

Suppose that the bed thickness, dt_b of the material is to be estimated across the section dx. An element of a mass, dm, and volume dV, passing through section dx within a residence time dt s is considered in Fig.5.2.

$$\begin{aligned} dm &= m_i - m_o \text{ material blance in and out} \\ dm &= \rho dV \\ dV &= w dx dt_b \text{ estimate elemental volume} \\ dm &= \rho w dx dt_b \end{aligned} \tag{5.7}$$

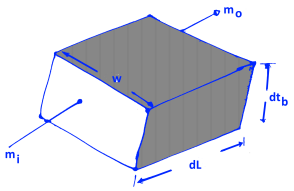

Figure 5.2: Elemental material passing through the section dx in dt s

For mass flow per unit time, Eq.(5.7) is divided by the residence time dt to estimate the mass flow rate or to estimate bed thickness t_b for a known mass flow rate, bulk density, width, and travel speed.

$$\begin{aligned} \dot{m} &= \int_0^{t_b} \rho w \frac{dx}{dt} dt_b \\ \frac{dx}{dt} &= v = \bar{v} \text{ from Eq.(3.1)} \\ t_b &= \frac{\dot{m}}{\rho w \bar{v}} \end{aligned} \tag{5.8}$$

The mass flow rate in Eq.(5.8) has also used by (King, 2012) and (Fuerstenau, 2003). The implication of this model is that the mass flow rate increases with the width. However, large screen widths also limit the capacity of the screen, measured in Ton Per Hour Square Meter (TPHSM). TPHSM is estimated as follows:

$$\frac{\dot{m}}{t_b w} = \rho \bar{v} \tag{5.9}$$

To address this problem, empirical studies have shown that an optimum bed thickness at the discharge end should not exceed four times the mesh size (King, 2012). With regard to the current model, the screen capacity in Eq. (5.9) may then be expressed by substituting in the time averaged velocity obtained in Eq.(2.32).

$$TPHSM = \frac{\dot{m}}{t_b w} = -\frac{\rho_B}{\beta} \ln \left[\frac{m\,(T) + M_s}{m_0 + M_s} \right] \tag{5.10}$$

5.3.3 Screen open area

The total open area, also referred to as 'free area' is an important design parameter in solid particles classification. A large free area is required to ensure effective transfer of particles to the underflow. The free area is controlled by aperture shapes and sizes. Excessive free surface area can be detrimental to the achievement of a clean cut, and thus careful consideration must be given to it. Different aperture shapes and sizes are suited for different processes, and are sometimes dependent on the physicochemical properties of the particles themselves.

For this study, circular apertures were considered owing to the fact that the most common particle shape is rounded. For the motion on the screen, triangular pattern shaped positioning of the apertures was used, with each aperture placed half an aperture diameter a way, $s = 0.5A_{di}$ at 60° apart, as this is a common pattern (Gupta and Yan, 2006). For this strategy, the holed area fraction (HAF) equation used is given in Eq.(5.11).

$$HAF = \frac{\pi \frac{D_{ap}}{8}}{\frac{1}{2}\sin 60\left(s + {D_{ap}}^2\right)} = \frac{0.907{D_{ap}}^2}{\left(s + D_{ap}\right)^2} \tag{5.11}$$

This design yielded a multi-sized screen with linearly increasing apertures downslope, with a total open area of 40.31%, which is by default a representative fraction of the open area for circular apertures half a diameter apart. As a guide, the particle diameters were used to estimate the aperture sizes. Depending on the screen inclination angles, the largest particle size was used as the aperture size of the last sieve downslope, with the largest aperture and smallest particle diameter used for the first sieve size. In general the aperture sizes must be slightly bigger than the particle size diameter expected at that screen section so that:

$$0.95 \leq \frac{D_p}{D_{ap}} < 1$$

5.4 Deck angle of inclination/declination

In controlling the aperture sizes, there exist the problem of 'virtual' reduction in the projected hole area that controls the entrance of the particle. The higher the inclination, the smaller the projected area, and thus due consideration must be given. The percentage effective aperture diameter, Y followed a quadratic function while apparent aperture diameters, D_θ followed a trigonometric function. Both equations are shown below Eq.(5.12).

$$\begin{aligned} D_\theta &= 0.5D_{ap}\left(3\cos\theta - 1\right) \\ Y &= 100\% - 0.018\theta^2 - 0.164\theta \text{ where} \\ Y &= \frac{D_\theta}{D_{ap}} \times 100\% \end{aligned} \tag{5.12}$$

It can be seen from Eq.(5.12) that when the plate is not tilted, i.e. $\theta = 0$, $D_\theta = D_{ap}$,

and $Y = 100\%$. As a result of this effect, at zero inclination, i.e. when the tray is placed horizontally, the projected area of the apertures remain constant. When the tray is tilted at 20° to the horizontal, effective aperture diameter is reduced by 10%, and diminishes to zero at 70° inclination. Fig. 5.3 shows a simulation of the reduction in aperture size with inclination.

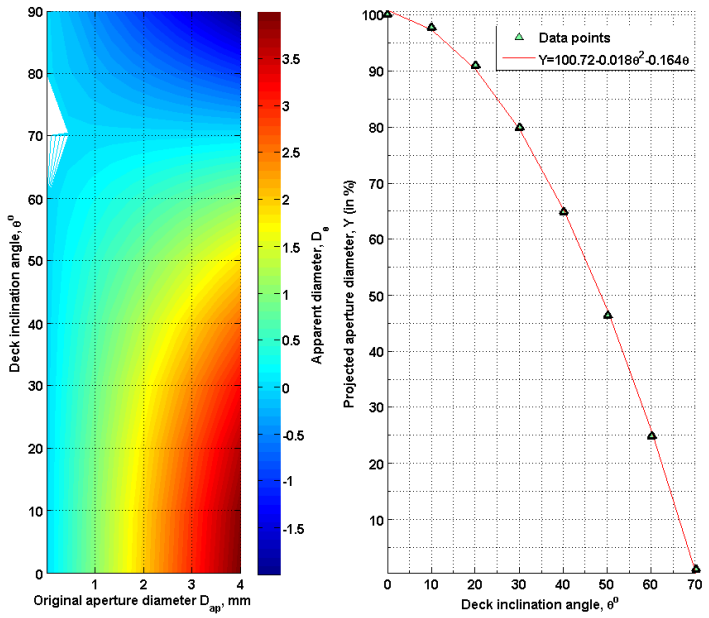

Figure 5.3: Simulation of reduction in the projected area with deck inclination

5.5 Screen load

Screen load or feed throughput in continuous processes is an important design parameter. It is sensible that overloading the screen could increase the chances of blinding of the apertures. However, from the main hypothesis that the screening process is driven by the change in momentum across the feeding point and the exit, it was shown both theoretically (in Section 2.1.5), empirically, and experimentally in **publications II** and **IV**, that the load on the screen helps to creates a transport momentum between any two points downslope, and thus is a positive contributor of the driving force for particles classification.

5.6 Particle-particle and particle-wall friction

The friction coefficient affects granular flow in many ways. There are two ways to look at friction in the bulk flow: particle-particle friction, which acts between the layers of particles, and particle-wall friction, acting between the surface of the equipment where granular flow occurs. Jaeger et al. (1990) proposed a method for the quantification of friction in granular flows. They observed that dimensionless friction force had a nonlinear relationship with dimensionless shear rate. In a numerical study down an inclined plane (usually referred to as 'chute flow'), Silbert et al. (2001) showed that the typical values of grain friction ranged between 0.4 and 0.6. In their numerical study using Contact Dynamics (CD) simulations, Mutabaruka et al. (2015) used typical values of 0.1, 0.4, and 0.7 to represent the friction coefficient, μ_k. Particle-particle and particle-wall frictions do not differ much. In their numerical study, on friction between two flat frictional sidewalls, Artoni and Richard (2015) used representative range values of 0.05. 0.1, 0.2 and 0.3. Therefore due to the difficulties involved in quantifying friction coefficients, this study applied a range between 0 and 4.5 for possible values of μ_k. It should be noted, however, that these values are not limited to the chosen range but can go over, depending on the nature of the surfaces of the walls or particles. The screening sieve material also matters when considering particle-wall friction. Screen selection, strength and limitations have been presented in detail by Makinde et al. (2015).

5.7 Vibration Sources

Determination of the optimal G-force precedes the selection of the vibration source. The sources of vibration can either electrical motors or electronic solenoids. A detailed procedure for this process is given in section 5.8. The use of solenoids is recommended in this study, as it makes it possible to vary the vibration intensities at different sections of the screen. For instance, in a batch process where fluctuation in feed occurs, vibration can be intensified where the bed thickness is the highest and vice versa. Today, however, electrical motors are the most common sources of vibration in vibrating screens. Upon knowing the value of G-force, Eq.(2.23) is used to estimate the values of λ and f for the selected electrical motor. In the case of electronic vibration, the values of inductance and frequencies are estimated from Eq.(2.25).

5.8 A case study on model-based design

To successfully conduct a model-based design Eqs.(2.32), (2.29), (5.2) and Eq.(2.31) in that order are first solved.

Scenario

Consider the following constrained design scenario. A company dealing with bulk solids processing have recently approached an engineering firm with the following requirement for a small vibrating screen: the mass of the structure, M_s must not exceed 5 kg, as it will be processing a batch of 50 kg every 8 minutes, or feed rate of 0.1042 kg/s. The company desire to achieve a minimum of 97% solids classification efficiency without using up a total floor area greater than 2m^2. They have determined that the mean particle size diameter of the solids is about 3.25mm and the value of the friction coefficient between the solids is determined as 0.32. The task is to design this unit operation in order to achieve the required capacity and efficiency. This is a kinetic model based problem setting of the example given in section 3.1.2, with the same feed rate and same time, t. Table 5.1 presents the solutions of all design equations generated in this study.

Design procedure

The following steps are involved:

i Calculate stable v and β based on the ε from Eq.(2.32).

ii Estimate the required area a, and τ, given D_p from Eq.(2.29).

iii Use the given μ_k to estimate the required optimal energy in G-force for agitation and deck inclination to overcome the time-dependent velocity. Obtain the implicit solutions of Eq.(5.2).

iv Estimate the amplitude λ and frequency f required to produce mechanical agitation from an electrical motor by using Eq.(2.23).

v Obtain electronic (solenoid) vibration parameters, i.e. inductance L and capacitance C by solving Eq.(2.25)

vi Verify the velocity calculated in item i by using ε and β

Fig.5.5 to Fig.5.7 are charts created from all relevant equations to aid quick design calculations.

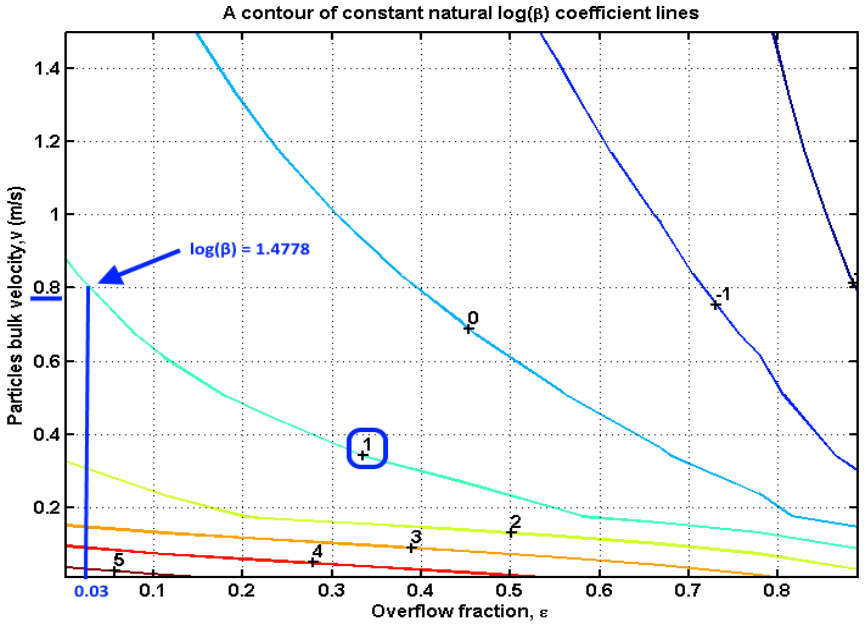

Figure 5.4: A chart for calculation of v and β for given ε

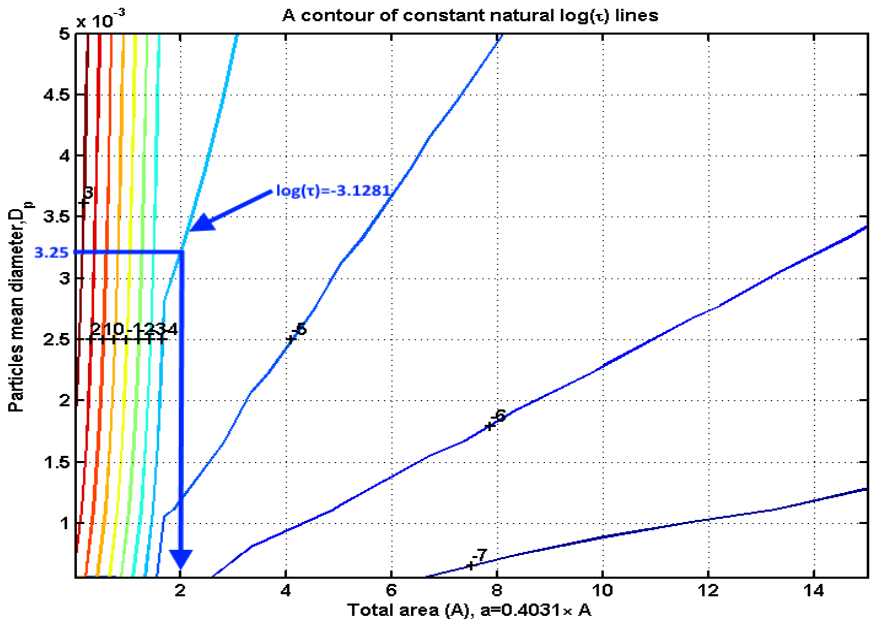

Figure 5.5: Chart for estimating a, and τ, given D_p

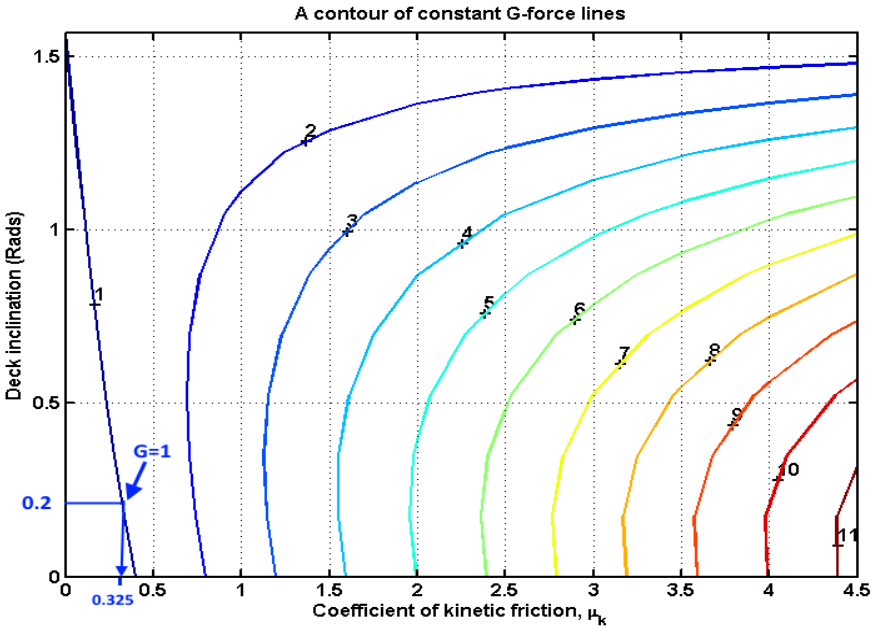

Figure 5.6: Estimation of G-force, G, for all given coefficients of friction, μ_k

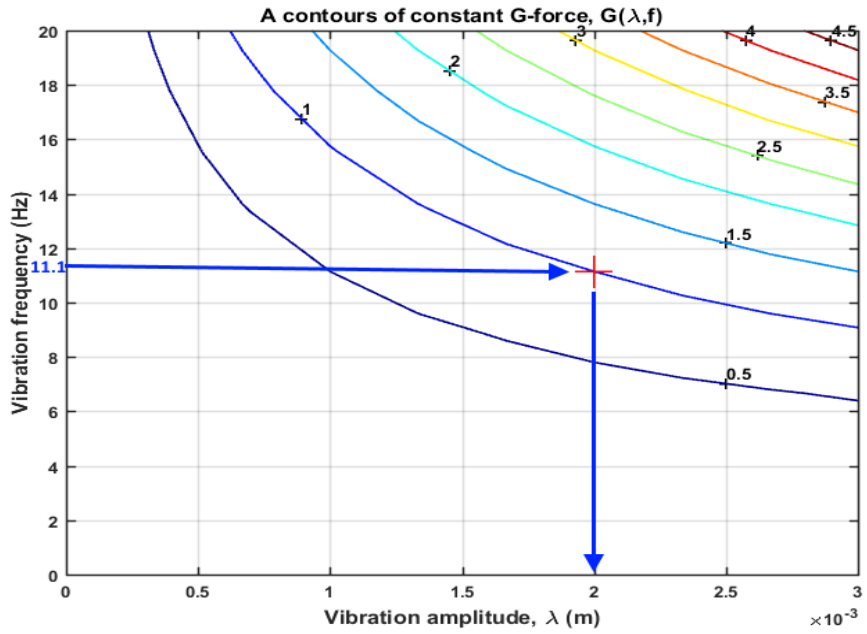

Figure 5.7: A chart used to estimate the amplitude λ and frequency f for optimal G

Table 5.1: Tabulated values that satisfy the design equations

$\theta = 0.2$ rad	$G = 0.9971$ G
$\lambda = 0.002$ m	$f = 11.11$ Hz
$M_s = 5$ kg	$C = 3.6633$ μF
$m_o = 50$ kg	$L = 55.9956$ H
$\varepsilon = 0.03$	$v = 0.8$ m/s
$\mu_k = 0.32$	$\eta = 0.97$
$D_p = 0.00325$ m	$a = 0.8036$ m^2
$b = 4.3832$ sm^{-1}	$\tau = 0.0438$ sm^{-2}
$HAF = 0.4031$	$A = 2.0$ m^2

5.9 Summary: Key design parameters

It was shown in this study that even though there are numerous factors to consider when designing solids classification equipment, only a few factors are significant and need careful considerations. These are the total open area, angle of inclination, and aperture diameters, since particle sizes are rarely classified as a controlled variable. These parameters in general determine the required driving force to causes agitation. While there are many ways of creating this force, the end result is the change in momentum that truly drives the classification process. In vibrating screens, the same factors are also considered, in addition to the total weight of the screen structure. It was noted that for gravity classification, the total weight of the screening equipment is not important as it requires no vibration. However, in vibrating screens, much energy goes to vibration in such a way that even if ultimate classification has been achieved, some energy is spent purely on agitating the screen frame, which does not necessarily translate to higher efficiencies. The developed kinetic model was able to show that if the weight of the screening structure, M_s is too high, the efficiency of solids classification diminishes substantially. Vibration frequencies are also key as they complement the inclination angles, so that with higher frequencies, lower inclinations are required to achieve higher efficiencies, since the projected area of the apertures is not significantly affected. Most importantly, the design method developed can be generalized for use with other physical separation units such as spiral concentrators and banana screens.

6 Conclusion

Two broad categories of models were built in this thesis, whose aim was to find a precise mathematical way of describing mechanical separation of solid particles through screening. A theoretical description of the motion of particles down inclined screens was done. This resulted in the development of a mathematical model for approximating the classification rate. Upon formulation, these models were tested by computer simulations, and also through experimental verification. The first set of models, kinetic by nature, were derived from the physical laws of science, while the population balance model relied mostly on the statistical characteristics of the particulate system. Within the kinetic models, a continuum model based on the fluid dynamics of the granular flow, and a discrete model based on the classical dynamics of single particle trajectories were derived.

The second set of models were largely based on the population balance equation (PBE). Within this set, a new intuitive method called the *law of mass action* was discovered. This set of models tried to describe each group of particles in a single tray of a multi-sized screen. It employed the analogy of parallel chemical reactions to estimate instantaneous and dynamic population of particles along the screen downslope by using the steady-state solution of PBE. Even though all these models differed in the methodology, they reproduced the results seamlessly.

It was observed that even though empirical models are successful in predicting the flow of material to an accuracy of less than 3% relative error, they are specific to processes and equipment. They lack universality in providing tangible design information that can be applied across all unit operations. Kinetic models, on the other hand, make it possible to come up with useful artifacts for process design and improvements through optimization. Based on the Newtonian conservation of momentum, kinetic models use targeted results as constraints to come up with a design strategy. For instance, the input parameters for this kind of a model are: available screen area, target efficiency or threshold limit overflow allowed (in percentage), mean particle diameter, and the surface coefficient of kinetic friction between the screen and granular material. With a well-defined model that satisfies the design equations, important outputs such as flow velocity of material, deck inclination angle, and the required vibration force (in G-force) are obtained as outputs, and can be used during fabrication stages.

This study therefore combined the flow *predictability* provided by empirical models and the optimal *designability* of linear vibrating screens. The study also forms a basis for process control uncertainty calculations with selected modern rigorous regimes, such as perturbation analysis, in the future. The development of the kinetic model based on the variable mass system provided a preliminary result for a direct correlation between the screening efficiencies and the energy used in solid particle classification by size, which is a significant missing link at present.

References

Albuquerque, L., et al. (2008). Application of high frequency screens in closing grinding circuits. In: *Proceedings of the Vth International Mineral Processing Seminar, Procemin 2008, Santiago, Chile*.

Aranson, I.S. and Tsimring, L.S. (2001). Continuum description of avalanches in granular media. *Physical Review E*, 64(2), p. 020301.

Artoni, R. and Richard, P. (2015). Effective Wall Friction in Wall-Bounded 3D Dense Granular Flows. *Physical review letters*, 115(15), p. 158001.

Baragetti, S., et al. (2006). *High-performance vibration screen*. Google Patents. url: `https://google.com/patents/EP1719560A2?cl=fi`. EP Patent App. EP20,060,006,669.

Baragetti, S. (2015). Innovative structural solution for heavy loaded vibrating screens. *Minerals Engineering*, 84, pp. 15–26.

Baragetti, S. and Villa, F. (2014). A dynamic optimization theoretical method for heavy loaded vibrating screens. *Nonlinear Dynamics*, 78(1), pp. 609–627.

Bayraktar, E., et al. (2008). *Modeling and Numerical Aspects of Population Balance Equations in Gas Liquid Liquid Two Phase Flows*. Techn. Univ., Fak. für Mathematik.

Behringer, R.P. (1996). *Dynamics of Granular Materials*. Technical report. NASA.

Bocquet, L., et al. (2001). Granular shear flow dynamics and forces: Experiment and continuum theory. *Physical review E*, 65(1), p. 011307.

Boyer, F., Guazzelli, É., and Pouliquen, O. (2011). Unifying suspension and granular rheology. *Physical Review Letters*, 107(18), p. 188301.

Chen, Y.S., et al. (2010). Size separation of particulates in a trommel screen system. *Chemical Engineering and Processing: Process Intensification*, 49(11), pp. 1214–1221.

COMSOL (2012). *COMSOL Multiphysics*. Burlington, MA 01803: COMSOL, Inc.

Conway, S.L., Shinbrot, T., and Glasser, B.J. (2004). A Taylor vortex analogy in granular flows. *Nature*, 431(7007), pp. 433–437.

Ertaş, D. and Halsey, T.C. (2002). Granular gravitational collapse and chute flow. *EPL (Europhysics Letters)*, 60(6), p. 931.

Feise, H. (2003). On the future of solids processing. *Chemical Engineering Research and Design*, 81(8), pp. 837–841.

Fuerstenau, M.C. (2003). *Principles of mineral processing*. SME.

Grim, P. and Rescher, N. (2013). How Modeling Can Go Wrong. *Philosophy & Technology*, 26(1), pp. 75–80.

Gupta, A. and Yan, D.S. (2006). *Mineral processing design and operation: an introduction*. Elsevier.

Hancock, W., Weatherley, D., Wruck, B., and Chitombo, G. (2012). Numerical investigations on flow dynamics of prismatic granular materials using the discrete element method. In: *EGU General Assembly Conference Abstracts*, vol. 14, p. 13288.

Henann, D.L. and Kamrin, K. (2013). A predictive, size-dependent continuum model for dense granular flows. *Proceedings of the National Academy of Sciences*, 110(17), pp. 6730–6735.

Iizuka, E.K. and Delfim, O.J. (2010). High capacity vibrating screens. In: *Proceedings of International Coal Preparation Congress*, pp. 257–265.

Jaeger, H.M., Nagel, S.R., and Behringer, R.P. (1996). Granular solids, liquids, and gases. *Reviews of Modern Physics*, 68(4), p. 1259.

Jaeger, H., Liu, C.H., Nagel, S., and Witten, T. (1990). Friction in granular flows. *EPL (Europhysics Letters)*, 11(7), p. 619.

Jansen, M. and Glastonbury, J. (1968). The size separation of particles by screening. *Powder Technology*, 1(6), pp. 334–343.

Johanson, K. (2016). *Using a population balance model coupled with structural effects to aid product design of bran cereal*. Technical report. Material Flow Solutions, Inc.

Jop, P., Forterre, Y., and Pouliquen, O. (2006). A constitutive law for dense granular flows. *Nature*, 441(7094), pp. 727–730.

Josserand, C., Lagrée, P.Y., and Lhuillier, D. (2004). Stationary shear flows of dense granular materials: a tentative continuum modelling. *The European Physical Journal E*, 14(2), pp. 127–135.

Kamrin, K. and Koval, G. (2014). Effect of particle surface friction on nonlocal constitutive behavior of flowing granular media. *Computational Particle Mechanics*, 1(2), pp. 169–176.

Karra, V. (1979). Development of a model for predicting the screen performance of vibrating screens. *CIM Bulletin*, pp. 168–171.

King, R.P. (2012). *Modeling and simulation of mineral processing systems*. Oxford, UK: Elsevier.

Kruggel-Emden, H. and Elskamp, F. (2014). Modeling of Screening Processes with the Discrete Element Method Involving Non-Spherical Particles. *Chemical Engineering & Technology*, 37(5), pp. 847–856.

Kumaran, V. (2004). Constitutive relations and linear stability of a sheared granular flow. *Journal of Fluid Mechanics*, 506, pp. 1–43.

LeBlanc, S. and Fogler, H.S. (1987). Population balance modeling of the dissolution of polydisperse solids: rate limiting regimes. *AIChE journal*, 33(1), pp. 54–63.

Li, J., Webb, C., Pandiella, S., and Campbell, G. (2002). A numerical simulation of separation of crop seeds by screening-effect of particle bed depth. *Food and bioproducts processing*, 80(2), pp. 109–117.

Li, J., Webb, C., Pandiella, S., and Campbell, G. (2003). Discrete particle motion on sieves - a numerical study using the DEM simulation. *Powder Technology*, 133(1), pp. 190–202.

Li, Z., Tong, X., Zhou, B., and Wang, X. (2015). Modeling and parameter optimization for the design of vibrating screens. *Minerals Engineering*, 83, pp. 149 – 155. ISSN 0892-6875.

Makinde, O., Ramatsetse, B., and Mpofu, K. (2015). Review of vibrating screen development trends: Linking the past and the future in mining machinery industries. *International Journal of Mineral Processing*, 145, pp. 17–22.

Makinde, O.A., Mpofu, K., and Ramatsetse, B. (2016). Mining business optimisation through a reconfigurable vibrating screen design. *African Journal of Science, Technology, Innovation and Development*, 8(1), pp. 88–96.

Mangeney, A., Staron, L., Volfson, D., and Tsimring, L. (2007). Comparison between discrete and continuum modeling of granular spreading. *WSEAS Transactions on Mathematics*, 6(2), p. 373.

Massoudi, M. and Boyle, E.J. (2013). A continuum kinetic theory approach to the rapid flow of granular materials: the effects of volume fraction gradient. *International Journal of Non-Linear Mechanics*, 36.

Maurstad, O. (2002). *Population balance modeling of agglomeration in granulation processes*. Ph.D. thesis. Norwegian University of Science and Technology.

Mills, P., Loggia, D., and Tixier, M. (1999). Model for a stationary dense granular flow along an inclined wall. *EPL (Europhysics Letters)*, 45(6), p. 733.

Mohan, L.S., Rao, K.K., and Nott, P.R. (2002). A frictional Cosserat model for the slow shearing of granular materials. *Journal of Fluid Mechanics*, 457, pp. 377–409.

Moussa, A.S. (2008). *Experimental Investigation and Population Balance Modeling of Aggregation and Breakage of Polymer Colloids in Turbulent Flow*. Ph.D. thesis. The Swiss federal institute of technology (ETH Zurich).

Mutabaruka, P., et al. (2015). Transient dynamics of a 2D granular pile. *The European Physical Journal E*, 38(5), pp. 1–7.

Nadolski, S., Klein, B., Kumar, A., and Davaanyam, Z. (2014). An energy benchmarking model for mineral comminution. *Minerals Engineering*, 65, pp. 178–186.

Napier-Munn, T. (2015). Is progress in energy-efficient comminution doomed? *Minerals Engineering*, 73, pp. 1–6. doi:doi.org/10.1016/j.mineng.2014.06.009.

Nicmanis, M. and Hounslow, M. (1998). Finite-element methods for steady-state population balance equations. *AIChE Journal*, 44(10), pp. 2258–2272.

Olsen, L. and Carnes, B. (2001). *Screen capacity calculation*. 86470 Franklin Blvd., Eugene, Oregon, 97405: JCI an Astec Company.

Ortega-Rivas, E. (2012). *Non-thermal food engineering operations*. Springer 10013 NY, USA: Springer Science & Business Media.

Owens, R.G. and Phillips, T.N. (2002). *Computational rheology*, vol. 14. World Scientific.

Plastino, A.R. and Muzzio, J.C. (1992). On the use and abuse of Newton's second law for variable mass problems. *Celestial Mechanics and Dynamical Astronomy*, 53(3), pp. 227–232.

Popescu, I. (2014). Computational hydraulics: numerical methods and modelling. *Water Intelligence Online*, 13, p. 9781780400457.

Raman, A. and Aziz, A. (2010). Cohesiveness and flowability properties of silica gel powder. *Physics International*, 1(1), pp. 16–16.

Ramkrishna, D. and Mahoney, A.W. (2002). Population balance modeling. Promise for the future. *Chemical Engineering Science*, 57(4), pp. 595–606.

Ramkrishna, D. and Singh, M.R. (2014). Population balance modeling: current status and future prospects. *Annual review of chemical and biomolecular engineering*, 5, pp. 123–146.

Richard, P., et al. (2005). Slow relaxation and compaction of granular systems. *Nature materials*, 4(2), pp. 121–128.

Ristow, G.H., Riguidel, F.X., and Bideau, D. (1994). Different characteristics of the motion of a single particle on a bumpy inclined line. *Journal de Physique I*, 4(8), pp. 1161–1172.

Rotich, N. (2014). *The fall and rise of gravity separation*, vol. 9, Mining magazine. 68 Upper Thames Street, London, EC4V 3BJ: Aspermont media. 60–65 p.

Rotich, N., Tuunila, R., Elkamel, A., and Louhi-Kultanen, M. (n.d.). *Dynamic and perturbative system analysis of granular material's balance in a vibrating screen*. Under first review in *Advanced powder technology*.

Rotich, N., et al. (2015). New methods for granular-material flow prediction and design of efficient industrial screen. In: *Proceedings of Physical Separation '15*.

Saravacos, G.D., Kostaropoulos, A.E., et al. (2002). *Handbook of food processing equipment*. Springer.

Savage, S. (1998). Analyses of slow high-concentration flows of granular materials. *Journal of Fluid Mechanics*, 377, pp. 1–26.

Seguin, A., Bertho, Y., Gondret, P., and Crassous, J. (2011). Dense granular flow around a penetrating object: Experiment and hydrodynamic model. *Physical review letters*, 107(4), p. 048001.

Silbert, L.E., et al. (2001). Granular flow down an inclined plane: Bagnold scaling and rheology. *Physical Review E*, 64(5), p. 051302.

Subasinghe, G., Schaap, W., and Kelly, E. (1989). Modelling the screening process: A probabilistic approach. *Powder Technology*, 59(1), pp. 37 – 44. ISSN 0032-5910.

Swinney, H.L. (2007). *Dynamics of Granular Materials and Particle-Laden Flows*. Technical report. The University of Texas at Austin.

Wang, G. and Tong, X. (2011). Screening efficiency and screen length of a linear vibrating screen using DEM 3 D simulation. *Mining Science and Technology (China)*, 21(3), pp. 451–455.

Wills, Barry A., F.J.A. (2016). *Mineral Processing Technology: An Introduction to the Practical Aspects of Ore Treatment and Minerals Recovery*, 8th edn. Oxford, UK: Elsevier Science & Technology.

Yue-min, Z., et al. (2009). Dynamic design theory and application of large vibrating screen. *Procedia Earth and Planetary Science*, 1(1), pp. 776–784.

Zhu, H., Zhou, Z., Yang, R., and Yu, A. (2007). Discrete particle simulation of particulate systems: theoretical developments. *Chemical Engineering Science*, 62(13), pp. 3378–3396.

APPENDICES

Publication I

Rotich N., Tuunila R., and Louhi-Kultanen M.
Modeling and simulation of gravitational solid–solid separation for optimum performance

Reprinted from
Powder Technology,
Vol. 239, pp. 337–347, 2013.

Powder Technology 239 (2013) 337–347

Contents lists available at SciVerse ScienceDirect

Powder Technology

journal homepage: www.elsevier.com/locate/powtec

Modeling and simulation of gravitational solid–solid separation for optimum performance

Nicolus Rotich, Ritva Tuunila *,[1], Marjatta Louhi-Kultanen

Department of Chemical Technology, Lappeenranta University of Technology, P.O. Box 20, FI-53851 Lappeenranta, Finland

ARTICLE INFO

Article history:
Received 21 June 2012
Received in revised form 18 January 2013
Accepted 26 January 2013
Available online 8 February 2013

Keywords:
Gravitational classification
Modeling
Simulation
Solid–solid separation

ABSTRACT

Reichert cone separators have been used for classification in the mineral processing industry for over six decades now. However, their application has always been limited to wet processing. In this paper, we assess the potential of their modification and use in gravitational dry solid–solid separation. A theoretical model was formulated, describing the motion of particles along inverted cone-shaped series of inclined screens with increasing aperture sizes under the force of gravity. A mathematical model to quantify the rate of separation was also suggested based on the theory. Three important design parameters were proposed to aid the actual engineering design of the system. The two models were test-run by numerical simulation under computer-generated, uniformly distributed random sized particles on a hypothetical 0.254 m radius cone, from which a theoretical screening rate of 32.52 g/s was achieved. The simulations were verified experimentally by designing a prototype system of equal effective screening area, and with equal input masses of glass beads, an overall screening rate of 23 g/s and a maximum separation efficiency of 66.4% was achieved.

1. Introduction

Mechanical separation plays a critical role in modern-day industry. The construction, food, chemical process, pharmaceutical and many other manufacturing industries dealing with dry particulate solids require classification and sorting either in terms of size, density, shape or resilience, prior to utilization in downstream unit operations or in final use [1]. Classification by size is, however, most important, especially where density differences are not of significance in the succeeding industrial process. This is different in a case where variation in specific gravity is important e.g. in processes involving segregation in a fluidized bed [2]. It is well known that a certain intensity of vibration or velocity in at least one direction is required to drive 'phase' separation. Mechanical/electrical energy is usually required to shake and to disorient the particle order and to cause such sorting. Creating this motion is the main energy consuming operation in screening processes.

Solid–solid separation is characterized and determined by the chemical and physical properties of the material to be separated and is described by the direction of motion in which the particulates are accelerated to cause the desired separation. Throw-action sieving involves the upward and downward motion of particulates, causing collision and rotation before repeated interaction with the sieve surface, thus increasing the probability of eventual sorting. Horizontal sieving uses the same technique to disorient particles, but the particles are accelerated in a horizontal circular motion. The third method combines the two above techniques, and both vertical and horizontal circular motion is used. Other methods include sonic sieving, wet sieving and air jet sieving, which are beyond the scope of this work. Nevertheless, all these processes are carried out with mostly high-speed, low-amplitude vibrating machines which require enormous driving energies.

Gravitational separation is one of the oldest techniques of mechanical separation characterized by the downward motion of particulates, long residence times and low overall efficiencies. With the current need for low energy-low carbon, but equally efficient operations, mimicking nature will in the long run become part of the solution. Many unit operations are currently high contributors of carbon, atmospheric dust and other fugitive emissions that are detrimental to both human health and the environment. This implies that improving the old methods which almost equaled nature is of essence if these processes are to continue playing this important role in industry.

The objective of this study was to develop an improved Reichert cone separator (Fig. 1) for the gravitational screening of particulates for both separation and grading purposes and assess its usability in other industries. The study was divided into four parts: firstly, developing a theory describing the scenario of particulate motion along the perforated screens, secondly, generating a mathematical model to quantify the degree of solid-solid separation that can be achieved, followed by proposing important engineering design parameters of the unit, and finally designing a prototype system based on those

* Corresponding author. Tel.: +358 405296855.
E-mail addresses: nicolus.rotich@lut.fi, moininin@yahoo.co.uk (N. Rotich), ritva.tuunila@lut.fi (R. Tuunila), marjatta.louhi@lut.fi (M. Louhi-Kultanen).
[1] Tel.: +358 407018078.

0032-5910/$ – see front matter © 2013 Elsevier B.V. All rights reserved.
http://dx.doi.org/10.1016/j.powtec.2013.01.056

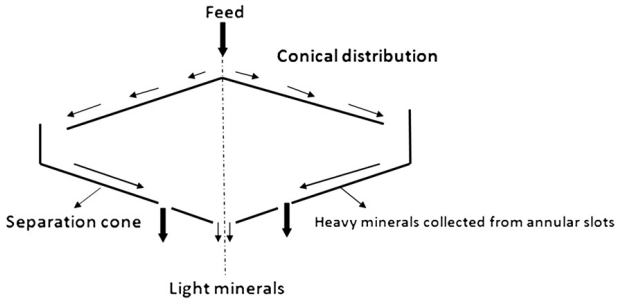

Fig. 1. Schematic side view of a Reichert cone separator.

parameters for use in experimental verifications. The model was then tested using MATLAB version R2012 (a) [3], to simulate before comparing the results to those achieved from the prototype experiment.

2. Methods

2.1. Theory

From the general theory of relativity, the inertial mass of a body is that which determines the acceleration of the body under the action of a given force, while the gravitational mass is that which determines the gravitational force between the body and other bodies. Originally tested by Galileo and most recently by R.H. Dicke in 1959, the principle of equivalence is the assertion that the gravitational mass exactly equals the inertial mass at any given time [4].

In this model, the total mass of solids M_T to be separated is moving down the inclined length of an 'inverted cone-shaped' series of screens of different (increasing) aperture sizes (D_{ap}) and widths, at a velocity $\mathbf{v}(t)$ and acceleration $\mathbf{a}(t)$. Below each width of the screens is a channel to tap the separated particles in every screen width. This mass consists of two components, the inertial mass and the gravitational mass. The motion of the particle along the length of the screens is retarded by the gravitational force until it comes to a stop. A certain weight fraction of the particles, ε continues to the next separation stage while the remaining fraction, 1-ε falls through the free area of the screens. This causes an overall change in the momentum of the system.

Several authors view screening as being identical to the first order chemical reaction which is directly proportional to the screening area and inversely proportional to the feed throughput [5]. Also in this model, separation is seen as a first order reaction, not only dependent on the screen free area but also driven by a continual change in momentum between the inertial and gravitational masses of the feed and the undersize. It is thus proportional to the rate of change in momentum (P) of particulates and the screen area A. It also implies that smaller particles are separated faster compared to relatively larger ones since aperture sizes increase down the incline screen. Screening is therefore inversely proportional to the diameters of the particulates D_p [6].

The weight fraction of the oversized particles proceeding to the next screen at any given time is

$$\varepsilon = \frac{W(t)}{W(0)}, \tag{1}$$

where $W(0)$ is the initial mass of a given size class of particles entering the screen, and $W(t)$ is the mass remaining on the screen at time t and only particulates of diameters smaller than the aperture sizes pass through as the undersize. The fraction of solids remaining on the screen at any given time can therefore be computed as a function of screening time t. [7].

2.2. Model formulation

Newton's second law of motion for objects on an inclined plane can be interpreted in this case as follows, particulates of a particular substance and nature would slide or roll down an inclined surface made of a particular material with a particular surface characteristic μ at a particular angle of inclination θ. The downward movement of the particle (by rolling or sliding) is determined by the shape of the particulate [8].

The following general assumptions are made;

- Non-slipping condition.
- The initial velocity ($\mathbf{v}_0$) is zero (at the feeding point).
- The particles are assumed to be dry, the angle of repose[2] is sufficiently low and the feed rate is controlled such that only one layer of particulates rolls down the surface at any given time.
- The average tilt angle of the mesh screen is 15°.
- Circular screen apertures are considered.

For the above arrangement, Newton's second law can be written as

$$\propto_c = \frac{-\mathbf{g}\sin\theta}{1 + {}^{I_c}/_{MR^2}}, \tag{2}$$

where $\propto \_c$ is the linear acceleration of the centre of mass of the particulate, I_c is the moment of inertia, M is the mass and R is the radius of the particulate and $\mathbf{g}$ is the acceleration due to gravity. It has been shown that I_c is proportional to the radius of the particle so that

$$I_c = \kappa MR^2. \tag{3}$$

where κ is the constant of the moment of inertia. For a sphere $\kappa = 2/5$ and 1/2 for a disk, particles of different sizes and shapes will thus have varying values of κ [9].

Leaving the final form of the Eq. (2) as

$$\propto_c = -{}^{\mathbf{g}\sin\theta}/_{1+\kappa}, \tag{4}$$

[2] The angle between the horizontal axis and the slope of a heap formed by a powder dropped from some elevation, e.g. a hopper.

Gravitational mass equals inertial mass (Galileo's theory of relativity), and the mass balance equation of this system can be conducted such that

$$M_T = m_g + m_i, \tag{5}$$

where m_i is the inertial mass of the particles that are remaining on the screen at any given time, while m_g is the mass fraction representing those falling by gravity and separated to the required groups. The two masses can each be represented as a fraction of the total as explained by Drzymala [10], with the main feature here being size and the splitting forces being gravitational and inertial forces. The mass fractions can then be represented mathematically as

$$m_i = M_T\varepsilon \tag{6}$$

$$m_g = M_T(1-\varepsilon). \tag{7}$$

Using Eqs. (4) and (5), a decomposed force equation can be written as

$$M_T a = m_g\mathbf{g} - m_i\mathbf{g}\left({}^{\sin\theta}\!/_{1+\kappa}\right). \tag{8}$$

The negative sign on the last term to the right of the equation serves to retard the particles. It is important to note that two forces acting in different directions are not summed, but one single force is decomposed into two components by virtue of gravity force, perpendicular to the horizontal and inertial forces parallel to the screens. By knowing the forces acting on the particle, the velocity and the trajectory of each individual particle can be computed by integration with time, as suggested by Li et al. [11].

Therefore, the force due to M_T of the system reduces, while that due to m_i and m_g is increasing with time as ε stabilizes. It also means that m_g is stronger than m_i in a free area of the screen depending on the diameter of the particulate. The difference in the rates at which the two forces change with time is the momentum P of the system [12]. Conventionally,

$${}^{dv}\!/_{dt} = a; \tag{9}$$

Therefore,

$$M_T\,{}^{dv}\!/_{dt} = M_T\mathbf{g}(1-\varepsilon) - M_T\mathbf{g}\varepsilon\left({}^{\sin\theta}\!/_{1+\kappa}\right). \tag{10}$$

The implication of Eq. (10) is that, at the start of the process (t = 0), no separation has occurred, the fraction ε is zero and the only force acting on the particles is gravity. However, this changes immediately when particles are released as ε starts with a high value of ~1 and reduces to a final value with time and therefore as ε approaches zero **a** ~ **g**.

2.3. Testing the validity of the model

The Galilean theory of relativity implies that Eq. (10) holds at any given time. This can be proved by obtaining a derivative of the equation to find out if there is any instantaneous change in acceleration $a(t)$ of the particulate. The derivative can thus be rewritten as

$$M_T\,{}^{da}\!/_{dt} + a\,{}^{dM_T}\!/_{dt} = \mathbf{g}\varepsilon\,{}^{dM_T}\!/_{dt} + \mathbf{g}M_T\,{}^{d\varepsilon}\!/_{dt} - \mathbf{g}S\,{}^{dM_T}\!/_{dt} - \mathbf{g}S\varepsilon\,{}^{dM_T}\!/_{dt} + \mathbf{g}M_T S\,{}^{d\varepsilon}\!/_{dt}$$

Where

$$S = \frac{\sin\theta}{1+\kappa}. \tag{11}$$

S is the retarding term on Eq. (10).

For spherical particulates $\kappa = 2/5$. The design tilt angle is 15°. Assuming that there is no generation or loss of mass, ${}^{dM_T}\!/_{dt} = 0$; Eq. (10) is reduced to

$${}^{da}\!/_{dt} = -\mathbf{g}\left(1 - {}^{\sin\theta}\!/_{1+\kappa}\right){}^{d\varepsilon}\!/_{dt}. \tag{12}$$

The solution of Eq. (10) gives

$$a(t) = 0(t) + 7.988. \tag{13}$$

This means that there is no instantaneous change in acceleration jerk (**j**). The physical meaning of jerk is described as a sudden change in acceleration with time and motion in a different direction from the earlier determined. As can be seen from Eq. (13), acceleration is not a function of time. We therefore assume that particles move only down the inclined screens with the constant acceleration determined. Consequently, the second derivative of momentum with respect to time yank **Y** is zero. This proves the theory of relativity is satisfied by the model, which forms a basis for this separation equipment. The value of **a** less than that of gravity simply implies the particle comes to rest faster than if it were under the influence of gravity only and no inertial forces.

Eq. (10) can thus be solved to obtain the velocities of the particulates as a function of time $\mathbf{v}(t)$. The tilt angle to the horizontal is important as it determines the acceleration of particulates down the screens. Previous designs, e.g. those used in feed concentration in the gold mines, had between 15 and 30° [13]. However, it is possible to design modern equipment to be adjustable depending on the nature of particles to be separated. This design is done at an optimum angle of 15° (π/12 radian), which is slightly above the angle of friction between most surfaces.

2.4. The rate of separation

Based on the description in Section 2.1, the rate of separation is then given by

$${}^{dM}\!/_{dt} \propto -A\frac{1}{D_p}M\,{}^{dv}\!/_{dt}. \quad \text{Therefore;} \quad {}^{dM}\!/_{dt} = -\tau\left(\frac{A}{D_p}\right)M\,{}^{dv}\!/_{dt}, \tag{14}$$

where A is the effective free area of the screen, M is the feed mass and τ is the screening rate constant with units of seconds per unit area (s/m^2), signifying the time the particles have to be in contact with a square unit of the screen surface to allow a unit mass of particles to pass through.

2.5. Design parameters

2.5.1. Tilt angle of screens

The first design parameter to determine is the tilt angle θ, which is approximated as slightly greater than the angle of friction between the particulate and most fabrication materials. This approximation is based on the ability of the particulate to roll down under the slightest force applied. It is also important in ensuring that particulates do not remain on the surface of the screen after the separation process.

2.5.2. Aspect ratio of the conical screen

The second important parameter is the aspect ratio[3] (AR), which determines the dimensions of the cone, i.e. the height, the hopper feeding point, the screening area and the overall space occupied by the unit. It therefore influences the efficiency of the cone directly, thus being an important factor in the design of the cone.

The aspect ratio of the cone is the height to diameter ratio (H/D):

$$L^2 = D^2/4 + H^2, \tag{15}$$

where L, D and H are the slant cone length, diameter and height, respectively. The equation can be re-written:

$$\left(\frac{L}{D}\right)^2 = \frac{1}{4} + (A.R)^2. \tag{16}$$

In addition,

$$\tan\theta = \frac{H}{D/2} = 2(A.R) \tag{17}$$

$$A.R = tan\ \theta/2$$

Eq. (17) can now be written as

$$\left(\frac{L}{D}\right)^2 = \frac{1}{4} + (tan\ \theta/2)^2. \tag{18}$$

L is determined by the velocities of particulates and can be found by calculating the furthest distances of the particle motion, after which the cone diameter is found using Eq. (18). Alternatively, depending on the space available, L or D is fixed and used to determine the rest of the design parameters.

2.5.3. Screening area

The slant area of a cone is responsible for separation. However, the net effective screening area is a fraction of the total surface area. In this design, holes are diagonally spaced 60° apart, which is very common [14]. It is important to note that the projected area is not of much importance since the particle is moving linearly down an incline; the most important is the path followed by the particle. The use of holes spaced at 60° is advantageous in this case, as the probability of particles falling is enhanced (Fig. 2(a)). If a particle did not fall in the previous hole, it will probably fall in the next one because of its optimized position and increased aperture size. The aperture size, D_a increases linearly down the incline, with the smallest being approximately equal to the smallest particle, D_p min and the largest aperture size, approximately equal to D_p max.

The percentage of the holed area (porosity) for diagonally spaced apertures is given by:

$$Holed\ Area = \frac{\frac{\pi d^2}{8}}{\frac{1}{2}\sin 60(s+d)^2} = \frac{0.907d^2}{(s+d)^2}, \tag{19}$$

where s is the spacing between holes and d is the diameter of apertures. For linearly increasing aperture diameters roughly from the smallest particle diameter to the largest, the value of s is related to that of d as e.g. half a diameter or a diameter distance away from each other. For demonstration purposes, this design is performed on a hypothetical cone of a radius of 0.2541 m. The holes are placed half a diameter away from each other ($s = 0.5d$), giving the holed area a maximum value of 40.31%. Therefore, the porosity is constant at 0.4031. Fig. 3 shows the side view of the proposed modified Reichert cone solid-solid separator.

[3] The aspect ratio of an object is the ratio of its longer dimension to its shorter dimension.

3. Simulation Results

3.1. Particulate velocities

MATLAB was used extensively in solving, simulating and analyzing the above functions. Eq. (12) is converted into the form in Eq. (19):

$$d_z v/dt^2 = -\mathbf{g}\left(1 - \sin\theta/1+\kappa\right) d\varepsilon/dt. \tag{19}$$

Simulation of Eq. (19) with the boundary conditions of ε set to 1 and 0 gives the instantaneous velocity $\mathbf{v}(t)$ of the solids, spherical particles are assumed, $\kappa = 0.4$ at 15°, and the results show that the particles velocities are described by a linear function of time, $\mathbf{v}(t) = 7.988t$as shown in Fig. 4. The results were compared to that of a freefalling particle ($v = gt$) and plotted along the side. The freefalling particle does not reach terminal velocity within the simulation time (~6 seconds), it can be deduced that its velocity is higher due to the absence of retarding forces, while those in the simulation exercise are slower.

3.2. Determination of a screening constant and the rate of separation

MATLAB function $D_p = 0 + 3$ *rand ([1,100])) was used to generate a set of uniformly distributed random particle sizes up to the maximum particle diameter, see Table 1 (Appendix A). Integrating the rate equation from $M = M_T$; $M = M_u$ and $v = 0$; $v = v$;

$$\int_{M_u}^{M_T} \frac{1}{M} dm = \tau\left(A/D_p\right) \int_0^v dv \tag{20}$$

$$ln\ M_T = ln\ M_u + \tau\left(A/D_p\right) v, \tag{21}$$

where M_T is the total starting mass of the feed while M_u is the mass of the undersize. Particle velocities can be obtained by integrating Eq. (13) with respect to the runtime, T (Table 1), the mass of the undersize (rate of separation) at any given time is equal to the rate at which the mass of the feed reduces and can be approximated by curve-fitting of Eq. (21) for 100 linearly spaced values of starting masses M_T, corresponding to 100 virtual experiments.

MATLAB was used to for the curve-fitting of Eq. (21); the plot of $ln\ M_T$ $vs(Av/D\_p)$ on a log–log scale (Fig. 5) gives the screening constant τ as the slope. The y-intercept gives the increase in total mass of the undersize at any given time, which corresponds to the rate of separation.

An overall screening constant of 1.183×10^{-5} was obtained and the rate of screening (instantaneous increase in the mass of the undersize) was found to be 54.2 g/s (at 100% efficiency) upon further computation of slope and y-intercept respectively from Fig. 5 (see details of Eq. (C.1) on Appendix E). It is noteworthy that the rate of screening may differ at any given position of the cone surface due to the difference in the aperture sizes and the nature of particle sizes.

4. Experimental Verifications

It is well recognized that computational simulations alone is not sufficient to provide all information about a system. The above simulations were complemented through experimentation, with the aim of verifying whether the simulation results obtained were consistent to those obtained experimentally. The following sections describe the design, experimental setup procedures and the results obtained.

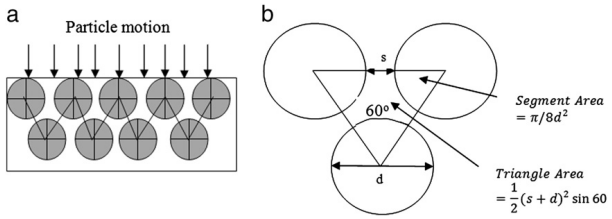

Fig. 2. (a): Illustration of particle motion over the screen. (b): Geometry of the open area.

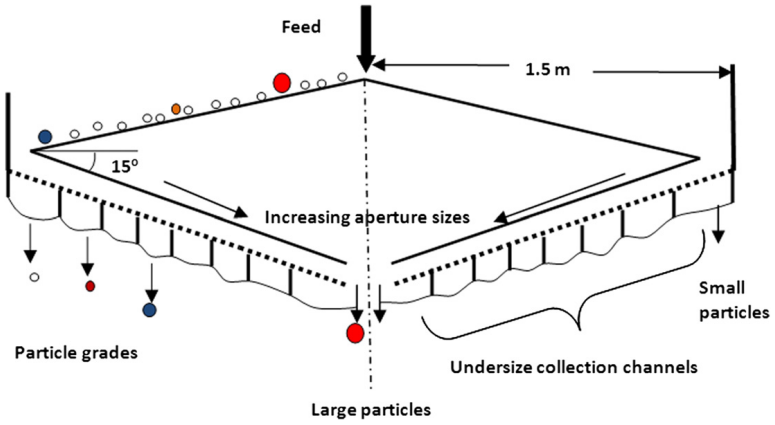

Fig. 3. Side view of the proposed solid–solid separator.

4.1. Design

For experimental verification, we designed a prototype screen of equivalent slant surface area (0.3 by 0.7 m) as that of the cone used in the simulation exercise (R = 0.2541 m). Due to practical limitations, a flat screen was used as a representative of a part of the modified Reichert cone separator. The four sieves were fabricated, with increasing aperture sizes 1, 2, 3, and 4 mm, drilled with laser precisely at an

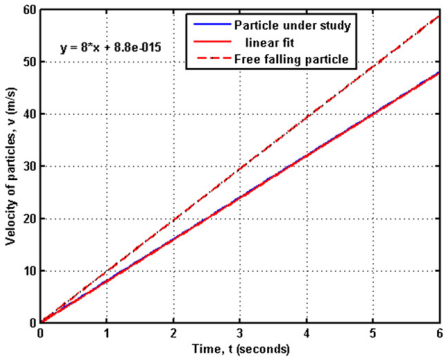

Fig. 4. Simulated particle velocities as a function of time compared to a freefalling particle.

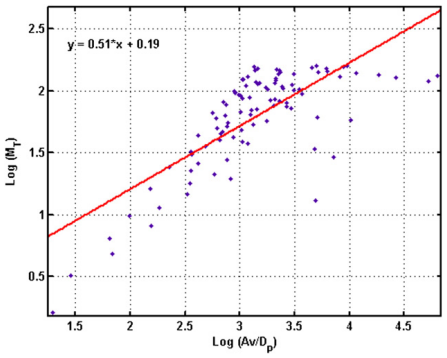

Fig. 5. Screening rate and constant determination by log-log graphing.

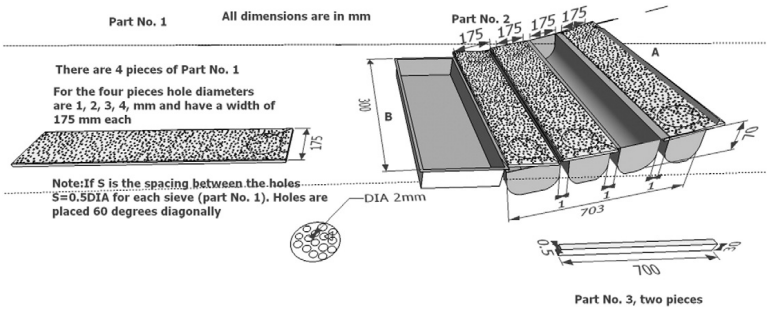

Fig. 6. The dimensioned prototype fabricated and used for experimental verification.

angle of 60°, and half a diameter apart, as discussed in Section 2.5.3 above. The resulting effective holed area was 40.31% of the total as earlier determined in Eq. (19). Fig. 6 shows a dimensioned prototype designed for the study.

4.2. Apparatus required and experimental setup

For this experiment the following apparatus were required: a stopwatch, porcelain bowl, electronic weighing balance, 16, 100 cc beakers, and four samples of 100 g glass beads of diameters 0.75, 1, 2 and 3 mm respectively. The four samples of glass beads were uniformly mixed in a porcelain bowl. 16 samples of the mixture were weighed to the beakers, with masses increasing at an interval of 10 g, from 10 up to 160 g. The prototype device was hinged at 15° from the horizontal, with the smallest sieve (1 mm) highest and the largest (4 mm) lowest. Each of the 16 mixture samples at a time were carefully distributed at the width of the starting point, A (top-most, smallest sieve) in Fig. 6, before allowing the particles to roll down the sieves. For all the samples, the stopwatch was started upon discharge and stopped roughly when the last particle hit the oversize collection box at point B. The following measurements were taken and recorded: Sample mass M_T, mass of the undersize collected on the 1, 2, 3 and 4 mm sieves (M_1, M_2, M_3, M_4 and oversize M_o), and runtime, t. The following values were calculated directly from the collected data: total undersize masses (M_u), separation efficiency, η computed as the ratio of total mass of undersize M_u, to the sample mass M_T, epsilon, ε computed as the ratio of mass of oversized collected at point B to the total sample M_T, and the mass of unseparated particles, M_{un} calculated by subtracting the sum of undersized and oversized from the total sample mass, M_T (Appendix B). Direct values of dv/dt were calculated from Eq. (10) by substituting M_T and ε and integrated over the runtime, t of each mass sample to get the average particle velocities **v**. These particle velocities were then plotted against the entire time column, T from which the first derivative yielded average particle acceleration comparable to the simulation result in Eq. (13). The total mass of the undersize M_u versus T was plotted and the first derivative computed to get the rate of separation, which was compared to the rate achieved in the simulated results in Section 3.2. To assess the rate of separation per particle size, the masses of undersized particles collected from each sieve (M_1, M_2, M_3, and M_4) were plotted against the aperture diameters and compared to that of simulation study (Appendix D) (Fig. 11).

4.3. Experimental results

The values measured, recorded and calculated in Section 4.2 (6–8) above were analyzed and presented in Figs. 7 and 8.

5. Discussion

As could be expected, smaller particles were separated and at a higher rate than the larger ones in the simulation study. This can be seen on the response surface representation of the simulated variations in the mass of undersize and particle diameters with time (Appendix F) (Fig. 12) and the plotted rates with particle diameters (Appendix C) (Fig. 10). The total masses collected from each sieve were plotted against the aperture diameters on the prototype experiment, which also showed that smaller particles were collected a higher rate (Appendix D).

The acceleration of particles down the inclined screens was found to be consistent in both simulated results and those from the experiment. In both cases this value was found to be approximately 8.0 m/s^2. It is important to note that acceleration is dependent on the surface characteristics of both the screen and the particles. Particles used in the experiment were round glass beads, assuming almost perfect spheres as those used during simulation ($\kappa = 2/5$). The rate of

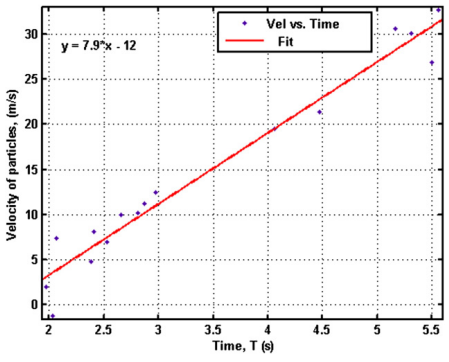

Fig. 7. Particle velocities as a function of time in the prototype experiment.

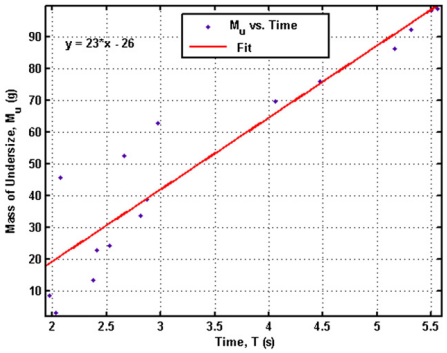

Fig. 8. Total mass of particles collected from the prototype as a function of time.

separation is quite low for the first few seconds e.g. the separation process was delayed for about 0.62 s and1.13 s for simulations and experiments respectively. This can be explained as the particles orient themselves on the screen, acquire momentum and the effective screening area increase.

In the simulation study, the total starting masses (M_T) were assumed to be completely separated by the end of the runtime so that $M_u = M_T$, as per the integration of the rate in Eq. (20). This is an ideal condition. Theoretically, the industrial screening efficiencies have been known to range between 60 and 85% [14]. Owing to this notion, coupled with the assumptions made in Section 2.2, the lumped efficiency of the simulation study was taken to be minimal at 60%.

Secondly, in simulation study only the boundary conditions of ε were known i.e. 1 at the beginning and 0 at the end. In the experiment however, this values were measurable and were greatly affected by the extra masses of M_{un} for each runtime, that was not accounted for during simulation study. Other assumptions made in simulation studies were that acceleration due to gravity was exactly 9.8 m/s^2 and particles are perfectly spherical and thus would easily roll down, which may not have been the case in the experiment (Fig. 8).

In the experiment, it was found out that there is a mass not taken into account: the mass which is unseparated either because they move with a momentum too high, and 'fly off' out of the equipment or are too low and get stuck blocking the screens, and also those that move with too high velocities, only to be collected as 'oversize' even though the aperture diameters were larger than the particles themselves. These can be addressed by extending the screening lengths with more sieves, optimizing the angle of inclination and covering the screening surface to avoid loss of mass. In the experimentation therefore, the mass balance equivalence of Eq. (5) is as shown in Eq. (22);

$$M_T = m_g + m_i + m_{un}, \tag{22}$$

Particles can get stuck on the screens, causing sieve blockage. Some of the particle sizes that were generated in the simulation study were quite small; fine particles have a tendency to acquire charges and agglomerate to form lumps. This also happens with hygroscopic particulates, which form lumps presenting a challenge in separation, as they tend block the apertures. Larger particles formed by agglomeration can also become separated in unintended stages. Indeed in the experiment, sieve blockage was evident (Fig. 9), and was partly attributed to the inconsistence in the achieved results with those under simulation. Sieve blockage is also high for transitional particle sizes almost equal to aperture sizes, which might have been the case here. Maintenance of the equipment is therefore expected to be a challenge. The screen surface requires clearing after every operation. This can be done by using pressurized fluid (e.g. water or air). However, it is important to ensure that the screen surface is sufficiently dry before any input of material. System specific efficiencies may be computed by measuring the mass fraction of the undersize [15] to the feed throughput. It would then be calculated as;

$$\eta = {}^{M_u}\!/_{M_T} \tag{23}$$

where M_T and M_u are the masses into and out of the separation process, respectively, at any given time.

6. Conclusion

A theoretical description of the motion of particles down the inclined screens was done. A mathematical model for approximating the screening rate was also formulated and tested under computer-generated particulate sizes of uniform distribution. Finally, an approach for the dimensioning of the screening unit was developed, with specific emphasis on the height to diameter ratio (aspect ratio). Based on these dimensions, an equivalent prototype screen was designed and used to verify the extent of consistence of simulated results to those achieved experimentally (Figs. 7–9).

A change in momentum of a heap of dry particulates controllably released on a perforated inclined surface is enough to cause sufficient separation of particles. The rates of separation achieved depend heavily on the momentum, screening area, and particle sizes and shapes. It is difficult to separately quantify the effects of mass and velocities on screening since a larger mass becomes more complex to separate, as it tend to create a thicker layer while a smaller mass correspondingly reduces the total rate of separation. At high velocities, particles move too fast to 'fall' while low velocities imply a reduction in the overall rate of separation, excessively long residence times and increased probability for sieve blockage.

From an equal effective screening area and same input masses M_T, a theoretical mean separation rate of 32.52 g/s was achieved (at 60%

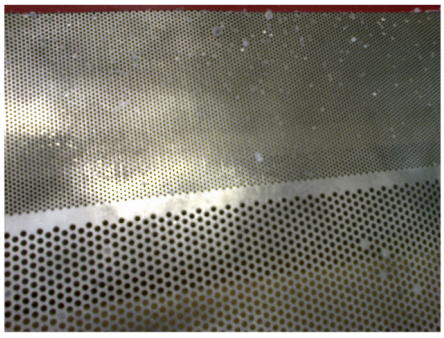

Fig. 9. Showing a section of the screen (1 and 2 mm sieves) blocked by the glass beads during experimentation.

efficiency) in the simulation study, while 23 g/s was achieved in the experiment (~0.708 times). The rates of separation achieved in simulation and experimental verification differed due to assumptions of perfect conditions during simulations, which gives ideal theoretical results. In our simulations it was assumed that only one layer of particles would be allowed to undergo separation at any given time, thus reducing particle interaction both laterally and longitudinally. Even though these assumptions simplified the complexity of simulation, they tend to limit the operation of the equipment during experimentation. With other modern computational techniques however, several particle layers interaction can be taken into account thereby gaining a deeper understanding of the dynamics in a particulate system. This study therefore serves to open up opportunities for future research with parallel tools e.g. Discrete Element Methods (DEM) simulation and extended DEM simulation (XDEM) etc., which factor in a wider range of particle interaction characteristics, both in continuous and discrete motions.

In the experimental study it was shown that efficiency η, was increasing with a reduction in $\boldsymbol{\varepsilon}$ as seen on the results in Table 2 (Appendix B), where a maximum of 66.4% efficiency was achieved. Upon successful development based on the simulation and experimental tests, the Reichert cone separator can therefore be applied across many industries that deal with dry particulates of minimal density variations, and expected to increase the overall energy efficiency in the target industry. The external energies needed to vibrate the mesh screens can then be optimized, depending on the type and size of industry in which the equipment is used.

List of symbols

A	Free area of the screen, m^2
a	Particulate acceleration, m/s^2
D_{ap}	Diameter of apertures, m
D	Diameter of the cone, m
D_p	Particulate diameter, m
g	Gravitational acceleration, m/s^2
H	Height of the cone, m
I_c	Moment of inertia of the particle, $g/m/s^2$
j	Third derivative of position, m/s^3 (Jerk)
L	Slant height of the cone, m
M	Mass of individual particles, g
m_g	Gravitational mass, g
m_i	Inertial mass, g
M_o	Mass of oversize particles, g
M_T	Batch wise starting masses of particulates to be separated per experiment, g
M_u	Mass of undersize, g
M_{un}	Mass of unseparated particles, g
$M_{1...4}$	Masses of particles collected on 1 mm, 2 mm, 3 mm and 4 mm sieves respectively, g
P	Momentum, g-m/s
R	Radius of individual particles, m
T	The entire matrix with elements of t, s
t	Runtime taken by the mass, M_T to be separated, s
v	Particulate velocities, m/s
v_0	Initial velocity of particles, m/s
Y	Product of mass with jerk, $g\text{-}m/s^3$ (Yank)
$\propto\_c$	Linear acceleration of the centre of mass of the particulate, m/s^2
ε	Fraction of material remaining on the screen at any instance, dimensionless
η	Separation efficiency, dimensionless
κ	Constant of moment of inertia, dimensionless
θ	Tilt angle of the screens, radians
τ	Screening rate constant, s^2/m
μ	Coefficient of static friction between screen surface and particulate, dimensionless

Appendix A

Table 1
Table of the data used in the simulation study.

Run	M_T (g)	Dp (mm)	T (s)	vel (m/s)
1	1.000	2.858	0.050	0.000
2	2.606	2.112	0.110	0.480
3	4.212	2.862	0.170	0.960
4	5.818	1.794	0.230	1.440
5	7.424	2.522	0.290	1.920
6	9.030	1.328	0.351	2.401
7	10.636	2.510	0.411	2.881
8	12.242	1.556	0.471	3.361
9	13.848	0.067	0.531	3.841
10	15.455	1.128	0.591	4.321
11	17.061	2.696	0.651	4.801
12	18.667	1.287	0.711	5.281
13	20.273	0.599	0.771	5.761
14	21.879	0.909	0.831	6.241
15	23.485	1.615	0.891	6.721
16	25.091	2.731	0.952	7.202
17	26.697	1.576	1.012	7.682
18	28.303	0.920	1.072	8.162
19	29.909	0.103	1.132	8.642
20	31.515	2.146	1.192	9.122
21	33.121	2.306	1.252	9.602
22	34.727	0.179	1.312	10.082
23	36.333	1.881	1.372	10.562
24	37.939	0.796	1.432	11.042
25	39.545	0.937	1.492	11.522
26	41.152	1.568	1.553	12.003
27	42.758	1.226	1.613	12.483
28	44.364	2.679	1.673	12.963
29	45.970	1.721	1.733	13.443
30	47.576	1.704	1.793	13.923
31	49.182	1.184	1.853	14.403
32	50.788	2.075	1.913	14.883
33	52.394	1.708	1.973	15.363
34	54.000	1.030	2.033	15.843
35	55.606	1.785	2.093	16.323
36	57.212	0.822	2.154	16.804
37	58.818	0.144	2.214	17.284
38	60.424	2.514	2.274	17.764
39	62.030	0.308	2.334	18.244
40	63.636	2.185	2.394	18.724
41	65.242	1.321	2.454	19.204
42	66.848	2.992	2.514	19.684
43	68.455	1.687	2.574	20.164
44	70.061	1.398	2.634	20.644
45	71.667	1.257	2.694	21.125
46	73.273	0.635	2.755	21.605
47	74.879	0.707	2.815	22.085
48	76.485	0.942	2.875	22.565
49	78.091	2.610	2.935	23.045
50	79.697	0.756	2.995	23.525
51	81.303	2.909	3.055	24.005
52	82.909	0.910	3.115	24.485
53	84.515	1.122	3.175	24.965
54	86.121	1.045	3.235	25.445
55	87.727	2.103	3.295	25.926
56	89.333	1.843	3.356	26.406
57	90.939	2.277	3.416	26.886
58	92.545	2.397	3.476	27.366
59	94.152	0.647	3.536	27.846
60	95.758	2.681	3.596	28.326
61	97.364	2.699	3.656	28.806
62	98.970	2.817	3.716	29.286
63	100.576	0.822	3.776	29.766
64	102.182	1.431	3.836	30.246
65	103.788	0.761	3.896	30.727
66	105.394	1.086	3.957	31.207
67	107.000	1.581	4.017	31.687
68	108.606	1.143	4.077	32.167
69	110.212	2.470	4.137	32.647
70	111.818	0.943	4.197	33.127

Table 1 (*continued*)

Run	M_T (g)	Dp (mm)	T (s)	vel (m/s)
71	113.424	1.990	4.257	33.607
72	115.030	1.942	4.317	34.087
73	116.636	1.411	4.377	34.567
74	118.242	2.154	4.437	35.048
75	119.848	0.057	4.497	35.528
76	121.455	1.436	4.558	36.008
77	123.061	2.968	4.618	36.488
78	124.667	2.932	4.678	36.968
79	126.273	1.494	4.738	37.448
80	127.879	0.123	4.798	37.928
81	129.485	0.401	4.858	38.408
82	131.091	2.805	4.918	38.888
83	132.697	0.053	4.978	39.368
84	134.303	0.183	5.038	39.849
85	135.909	1.522	5.098	40.329
86	137.515	1.131	5.159	40.809
87	139.121	0.308	5.219	41.289
88	140.727	1.516	5.279	41.769
89	142.333	0.689	5.339	42.249
90	143.939	0.581	5.399	42.729
91	145.545	1.622	5.459	43.209
92	147.152	2.732	5.519	43.689
93	148.758	1.743	5.579	44.169
94	150.364	0.615	5.639	44.650
95	151.970	2.652	5.699	45.130
96	153.576	0.857	5.760	45.610
97	155.182	0.445	5.820	46.090
98	156.788	2.927	5.880	46.570
99	158.394	0.804	5.940	47.050
100	160.000	0.430	6.000	47.530

Appendix C

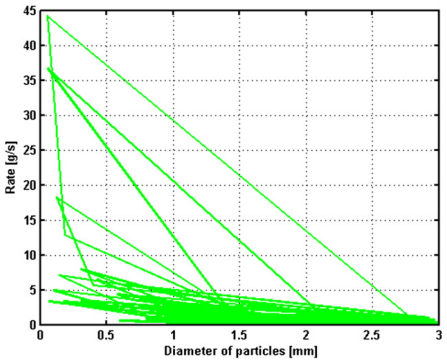

Fig. 10. Summary of interrelations between rate and particle sizes in the simulation study.

Appendix B

Table 2
A table of results obtained from the prototype screening experiment.

			Mass collected from												
Run	T (s)	MT (g)	1 mm	2 mm	3 mm	4 mm	Mu	Mo	n	ε	M	Mi	Mg	dv/dt	Vel
1	2.030	10	1.844	0.480	0.460	0.443	3.227	6.404	0.323	0.640	0.369	6.168	3.463	−0.623	−1.265
2	1.970	20	4.996	1.110	1.181	1.305	8.592	10.850	0.430	0.543	0.558	10.547	8.895	1.001	1.972
3	2.380	30	8.000	1.600	1.940	1.900	13.440	14.440	0.448	0.481	2.120	13.420	14.460	2.016	4.797
4	2.410	40	16.247	2.122	2.264	2.439	23.072	16.030	0.577	0.401	0.898	15.670	23.432	3.352	8.079
5	2.530	50	16.650	2.810	2.180	2.650	24.290	21.830	0.486	0.437	3.880	20.136	25.984	2.758	6.977
6	2.810	60	22.900	3.240	3.860	3.710	33.710	23.100	0.562	0.385	3.190	21.872	34.938	3.614	10.154
7	2.870	70	27.800	4.230	3.160	3.650	38.840	25.760	0.555	0.368	5.400	23.773	40.827	3.896	11.180
8	2.070	80	31.330	5.260	4.640	4.510	45.740	31.150	0.572	0.389	3.110	29.939	46.951	3.541	7.330
9	2.660	90	35.800	8.220	3.870	4.690	52.580	33.950	0.584	0.377	3.470	32.641	53.889	3.743	9.955
10	2.970	100	43.140	9.560	4.730	5.396	62.826	35.040	0.628	0.350	2.134	34.292	63.574	4.187	12.437
11	4.060	110	43.500	14.400	6.010	5.960	69.870	34.460	0.635	0.313	5.670	32.684	71.646	4.803	19.502
12	4.470	120	47.050	13.850	8.710	6.576	76.186	37.740	0.635	0.315	6.074	35.830	78.096	4.783	21.380
13	5.160	130	59.390	12.860	7.450	6.581	86.281	31.870	0.664	0.245	11.849	28.965	89.186	5.933	30.616
14	5.310	140	65.420	12.980	7.515	6.440	92.355	36.600	0.660	0.261	11.045	33.713	95.242	5.663	30.072
15	5.500	150	65.820	15.050	8.587	8.805	98.262	46.180	0.655	0.308	5.558	44.469	99.973	4.893	26.912
16	5.560	160	70.790	14.150	6.750	7.280	98.970	39.680	0.619	0.248	21.350	34.385	104.265	5.886	32.727

Appendix D

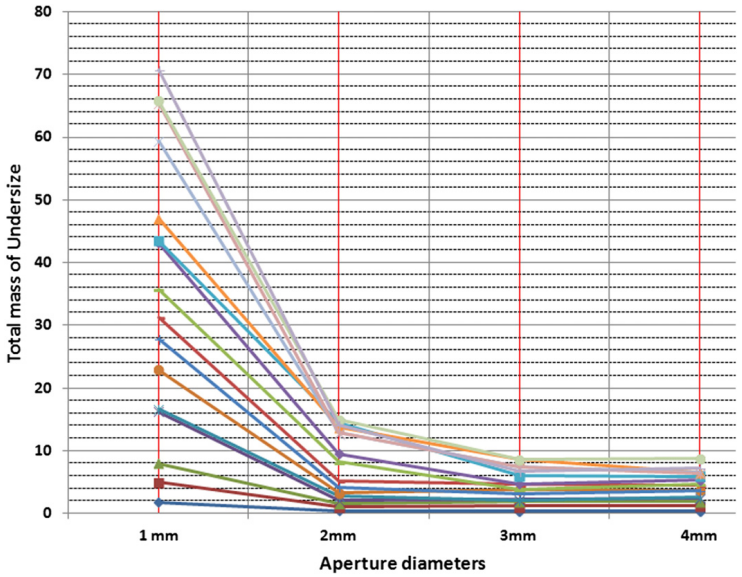

Fig. 11. Total masses collected from each sieve plotted against the aperture diameters.

Appendix E

Computation of slope and rate constant on logarithmic scales:

$$\log y = cx + \log k$$

In this case,

$$y = M_T, x = log\left(\frac{Av}{D_p}\right) c = \tau \text{ and } k = M_u \qquad slope = \frac{\Delta(\log y)}{\Delta x} \tag{C.1}$$

Appendix F

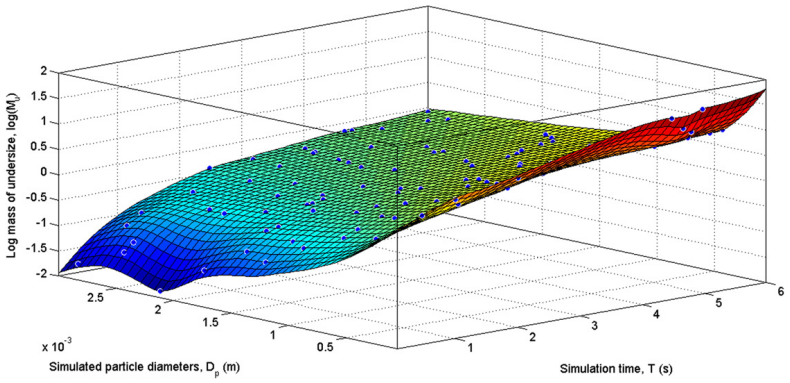

Fig. 12. Response surface representation of the variation in screening rate and particle sizes with time during simulation.

References

[1] J.C. Williams, M.A. Rahman, Prediction of the performance of continuous mixer for particulate solids using residence time distributions, Part I – theoretical, Powder Technology 5 (1972) 87–92.
[2] T. Akiyama, K. Yamamuro, S. Okutsu, A solid–solid extraction, Powder Technology 110 (2000) 190–195.
[3] MathWorks, MATLAB version 7.14.0.739 (R2012a), The MathWorks Inc., Natick, Massachusetts, 2012.
[4] J.B. Marion, Classical Dynamics of Particle Systems, Newtonian Mechanics, 2nd ed. Academic Press Inc., London, 1970.
[5] H.E. Cohen, Ullman's Encyclopaedia of Industrial Chemistry VB2-Unit Operations I, 5th ed. Wiley, Weinheim, 2000.
[6] N. Beloglazov, B. Zemlyakov, A method of calculating the efficiency of screening of minerals, Journal of Mining Science 8 (1982) 213–216.
[7] V. Grozubinskya, E. Sultanovitch, J.L. Israel, Efficiency of solid particle screening as a function of screen slot size, particle size, and duration of screening, the theoretical approach, International Journal of Mineral Processing 52 (1998) 261–272.
[8] F. Rioual, E. Piron, E. Tisjkens, Rolling and sliding dynamics in centrifugal spreading, Applied Physics Letters 90 (2007), (021918 - 021918–3).
[9] R.A. Serway, Physics for Scientists and Engineers, Rolling Motion of a Rigid Object, 6th ed. Thomson Brooks Inc., California, 2004.
[10] J. Drzymala, Mineral Processing, Foundations of Theory and Practice of Minerallurgy Part II- Characterization of Mineralurgical Processes, Jan Drzymala, Wroclaw, 2007.
[11] J. Li, C. Webb, S.S. Pandiella, G.M. Campbell, Discrete particle motion on sieves — a numerical study using DEM simulation, Powder Technology 133 (2003) 190–202.
[12] ISO, Vibration and Shock, ISO 2041-Vocabulary, International Organization for Standardization, Geneva, 1990.
[13] M.D. Bath, A.J. Duncan, E.R. Rudolph, Some factors influencing gold recovery by gravity concentration, Journal of South Africa Institute of Mining and Metallurgy (1973) 363–384.
[14] A. Gupta, D.S. Yan, Mineral Processing Design and Operation — An Introduction, Screening, 1st ed. Elsevier B.V., Oxford UK, 2006.
[15] Y.S. Chen, S.S. Hsiau, H.Y. Lee, Y.P. Chyou, C.J. Hsu, Size separation of particulates in a trommel screen system, Chemical Engineering Process 49 (2010) 1214–1221.

Publication II

Rotich N., Tuunila R., and Louhi-Kultanen M.

Empirical study on the effects of screen inclination and feed loading on size classification of solids by gravity

Reprinted from
Minerals Engineering
Vol. 70, pp. 162–169, 2015.

Minerals Engineering 70 (2015) 162–169

Contents lists available at ScienceDirect

Minerals Engineering

journal homepage: www.elsevier.com/locate/mineng

Empirical study on the effects of screen inclination and feed loading on size classification of solids by gravity

N. Rotich *, R. Tuunila, M. Louhi-Kultanen

Department of Chemical Technology, Lappeenranta University of Technology, P.O. Box 20, FI-53851 Lappeenranta, Finland

ARTICLE INFO

Article history:
Received 26 April 2014
Accepted 17 September 2014
Available online 11 October 2014

Keywords:
Solids-screening
Gravity-classification
Screening
Deck inclination

ABSTRACT

This study explored the insights into the theory of dry solids classification, in particular the classical dynamics aspects related to the mass loading of particles, deck inclination of the screen, and resulting measures of flowability. Prototype screening equipment was fabricated and experiments were carried out with ideal rounded mono-shaped glass beads. The overall performance of the prototype was assessed in relation to two screen design variables, the tilt angle of inclination and the mass throughput of the feed, which affects particles flow. Mathematical models relating to the classification process were developed, simulated and compared to the results obtained from the experiments. Important parameter ranges within which equipment may be operated with minimal malfunctioning were approximated from the models. Screen loading, bulk flow velocity, and screen inclination angles determine flowability of powders and particles in gravity classification; these parameters were used in this study to assess how well the particles flowed over the screens. A close correlation was found between theory, simulation models and the experimental results, which facilitated development of empirical models that may be used to predict and estimate the classification rates, efficiencies and flowability for such systems. Dense screen loading improved the classification rates, but hampered flowability, and consequently the efficiency. Increase in deck inclinations improved flowability and efficiency, but only to a certain optimum point after which it led to excessive overflow.

1. Introduction

Mineral ores and their gangue are usually sorted into grades of various sizes to maximize recovery of the primary product during concentration. Gravity classification which has been in use for many years is a very important process mostly in mining and other related industries. To realize the full potential of a production plant, cost effective strategies such as gravity classification must be exhausted before resorting to more energy intensive options (which may not necessarily be more efficient). Thus, detail understanding of the process is necessary. This research is built upon the models developed in an earlier work in which it was proposed that the rate of particles classification is proportional to the rate of change in momentum (P), and the screen area, and inversely proportional to the particles diameters. Successful development of the approach would enable gravity-based systems e.g. deck screens, to be applied not only in the minerals industry but across process industry as a whole (Rotich et al., 2013). Knowledge of process flow conditions together with information about the flow properties of materials over different equipment surfaces will enable process engineers to optimize material handling operations by utilizing approximate empirical models for instance, to predict material flows. Possible applications also exist in other areas such as, coal beneficiation or biomass classification during pre/post combustion, municipal solid waste management, food cereals processing, pharmaceutical, agricultural products and farm inputs, crystals classifications, and many other related industries. In applying such systems, the main factors to consider are flowability (of material on equipment), deck screen inclination, angle of repose and mass throughputs or loading per total projected area of screen.

Flowability is the ability of granular solids and powders to flow (Datta, 2012). It is important to note that flowability is not an inherent material property, but rather a combination of the physical properties of a material (particles) that affect its flow on another material (equipment used for handling, storing or processing). It follows, therefore, that consideration must be given to both the material and the equipment. Consequently, flowability has been defined more accurately as "the ability of the powder to flow in a desired manner in/on a specific piece of equipment" (Xiaowei et al., 2012).

* Corresponding author.

http://dx.doi.org/10.1016/j.mineng.2014.09.012
0892-6875/

Nomenclature

A	effective (free) screening area, m^2	R	classification rate, g s^{-1}
a	distance from the center of mass to the rotational axis, m	t	simulation run/elapsed time, s
D_{ap}	diameter of apertures, m	T	runtime taken by the mass, M_T to be separated, s
D_p	particulate diameter, m	$\bar{v}$	bulk particulate velocity, m s^{-1}
g	gravitational acceleration, 9.81 m s^{-2}	v_{rel}	relative velocity of undersize to the oversize
m	mass of individual particles, g	$\emptyset$	Waddell sphericity index, dimensionless
I	moment of inertia of the particle, expressed here as a function of sphericity, kg m^{-1} s^{-2}	η	classification efficiency, dimensionless
$M_{1..4}$	masses of particles collected on 1 mm, 2 mm, 3 mm and 4 mm sieves respectively, g	θ	tilt angle of the screens, °
M_T	batch masses, g	Ψ	mass loading coefficient, dimensionless
M_{un}	mass of un-separated particles, g	α_c	linear acceleration of the center of mass of the particulate, m s^{-2}
m_o	mass of oversize particles, g	α	angle of repose
m_u	mass of undersize, g	ε	fraction of oversize to total batch mass, dimensionless
M_{T_S}	simulation batch mass, g	κ	constant of moment of inertia for near spherical particles, dimensionless
M_{U_S}	simulation undersize mass, g	τ	screening rate constant, s m^{-2}
P	momentum, kg m s^{-1}	μ	coefficient of kinetic friction between screen surface and particulate, dimensionless

Another equally influential factor affecting screening is the angle of repose (α). By definition, the angle of repose is the angle between the horizontal and the slope of a heap of granular material dropped from some designated elevation (Ganesan et al., 2008). Screen inclination and/or mechanical agitation (such as vibration) are employed to enhance the flowability of the material and to improve the screening efficiency (Li et al., 2003), by modifying the angle of repose. Often as not, gravitational force is sufficient to cause necessary flow, when the right operating conditions are met.

Reducing inclination of the surface on which the particles are poured has the same effect as increasing the angle of repose; a situation that can better be visualized by considering the Carney funnel Fig. 1. In general, excellent flowability is achieved at low angles of repose (Ganesan et al., 2008; Bodhmage, 2006) or at higher inclinations, as can also be seen from the Carr classification of flowability by angle of repose. If the surface is not horizontal, h would be diminished, as the particles will flow down, and so the angle of repose is as seen in Fig. 1, and therefore higher flowability is achieved (Möller et al., 2002). Angle of repose, α can be estimated from the following Eq. (1).

$$\alpha = \tan^{-1}(h/r) \tag{1}$$

where h is the vertical height of the heap, and r is the radius of the heap formed and α is the angle of repose.

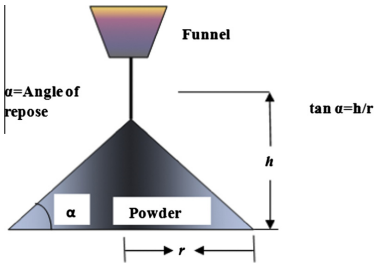

Fig. 1. Carney funnel used in measuring the angle of repose of particles less than 5 mm size, adapted from Datta (2012).

According to (Möller et al., 2002), glass beads of sizes ranging from 53 to 75 μm have α of 34 ± 1°, while relatively larger beads of sizes ranging from 0.5 to 0.75 mm have α of 22 ± 2°.

The models formulated in this study are a combination of phenomenological and numerical models based on Newtonian classical mechanics. The extent of difficulty to develop specific models is understood as an enormous and complex exercise. Certain bulk solid properties might be a reason why solid classification, old as it is, has not been fully understood to date (Chen et al., 2010; Li et al., 2003; Liu, 2009; Wang and Tong, 2011; Kruggel-Emden and Elskamp, 2014). Different materials have different properties and are thus unique and difficult to fully characterize, hampering the development of specific models for each of the materials. Models approximating system behavior are thus valuable for estimation and informed decision-making.

In this paper, we present experimental results on the effects of screen inclination on solids classification carried out on the prototype designed in Rotich et al. (2013); we also fine-tune the original models to reflect the realities of the experimental results. The formulated particle velocity models were solved by linear simulation, and found to behave similar to a linear time-varying system. Further trials however revealed that even though the motion of solid particulates along the inclined sieves may be linear, governing equations might not necessarily be linear functions of time but rather higher order nonlinear system that can be solved implicitly as ordinary differential equations (ODE).

It was concluded in Rotich et al. (2013) that there was no generation or degeneration of particulates, $dm/dt \approx 0$ during the classification process. However, upon further experimentation, it became apparent that some particles either got attached to and blinded the screens or flew off and hence could not be quantified as properly belonging to the undersize or oversize groups, which were the only groups covered by the model. It is important to note that these 'changes' in mass do not necessarily contradict the validation of the models, since there is no net increase or decrease in the mass of each particulate, but rather a temporary displacement from the two groups.

The objective of the current work is first to explore further insights into the theory of dry solids classification both individually and in bulk, especially the classical mechanics aspects involved. Secondly, the study aims to improve the operation of solids screening by refining and simulating the models developed earlier. This improved knowledge would help in identifying important

operating parameters and their corresponding ranges such that equipment may be operated with maximum efficiency and minimal disruption.

1.1. Classical dynamics of dry solids classification

1.1.1. Individual particle model

Important particle characteristics that determine the performance of most solid classification equipment are: (1) moisture content - bone dry particles are easy to classify; (2) Waddell sphericity index ($\emptyset$) – particles with $\emptyset \sim 1$ are easy to classify; (3) particle roughness coefficient (n) – this value affects particle motion and inter-particle locking; and (4) the second moment of area or moment of inertia (I) – particles with low moments of inertia need little force to change their rotation and velocity, thus they are easier to classify than those with high values of I. The scope of this work will be confined to moments of inertia and sphericity, which are quite easily understood and can be modeled physically.

The moments of inertia are characterized for most particles, e.g. conical, disk-shape, cylindrical shell, ring-like, spherical solids and shells, by a dimensionless parameter κ, relating the moment of inertia to the center of mass m of the particle and the shortest distance a from the rotational axis ($\kappa = \frac{I}{ma^2}$). There is a difference in classification of solids, e.g. uniformly filled spherical particles (with $\kappa \sim 2/5$), and particles that are less spherical or non-uniformly filled; conical particles have $\kappa \sim 3/10$, cylindrical $\kappa \sim 1$, while spherical shells have $\kappa \sim 2/3$, all revolved around the shortest distance from the axis of rotation of the particle. It is important to note that the moment of inertia of the particles is not simply a constant dependent on mass and some distance in the rotational axis, but is also dependent on how round/curved the particle is, in addition to how uniformly the matter is distributed within the particle. The acceleration of the center of mass of curved particles (α_c), is given Eq. (1) (Rotich et al., 2013);

$$\alpha_c = \frac{g \sin\theta}{1+\kappa} \tag{2}$$

Since all matter possesses mass and consequently moments of inertia, $\kappa \neq 0$ and thus only after knowing the nature of motion of the object, e.g., sliding, rolling and translation, or free falling, can it be affirmed whether α_c in Eq. (1) is dependent on κ. Knowing that the particle acceleration is related to the moment of inertia, and therefore shape, we can define an arbitrary symbolic function I, with $\emptyset$, m and a as explanatory variables, and search for an expression for to describe the changes in the moments of inertia with sphericity, $\frac{dI}{d\emptyset}$

$$I = f(\emptyset, m, a) \tag{3}$$

From (Eq. (3)) it can be shown that for particles with constant mass, m and distance, α from the rotational axis, and for specific particles whose moment of inertia can be expressed in the form $I = \kappa m a^2$. We can write the differentials for the moments of inertia as:

$$\delta I = \frac{\partial I}{\partial \emptyset}\delta\emptyset + \frac{\partial I}{\partial m}\delta m + \frac{\partial I}{\partial a}\delta a$$

$$\delta m = \delta a \rightarrow 0$$

$$\delta I = \frac{\partial I}{\partial \emptyset}\delta\emptyset$$

$$\frac{dI}{d\emptyset} = \frac{\partial I}{\partial \emptyset}\frac{d\emptyset}{d\emptyset}$$

Therefore, it can be shown that for such particles, the moment of inertia is a function of sphericity.

$$I = f(\emptyset) \tag{4}$$

The mathematical implication of Eq. (4) is that even though I as a parameter may never equal zero, its dependency on $\emptyset$ may be zero in some instances. The linear acceleration of the center of mass, α_c in Eq. (2), can then be expressed as a function of sphericity, inclination, and an additional retarding frictional force between the particle and the screen surface. The frictional force acting on a rigid rolling object on a horizontal rigid surface was revised and elaborated by Hierrezuelo and Carnero (1995), taking into consideration translation (slipping). In the case under study here, where surface inclination is involved, a resolved kinetic frictional force is considered responsible for retardation.

$$\alpha_c(\theta, f(\emptyset), \mu) = \frac{1}{1+\frac{f(\emptyset)}{ma^2}}[g\sin\theta - \mu g\cos\ \theta] \tag{5}$$

Limits can then be imposed on Eq. (5): for totally irregular particles e.g. flat particles, $\emptyset$ gets small values approaching zero, whereas spherical particles have typical values approximately equal to unity (Folk, 1980). It is therefore evident that the acceleration, and consequently velocity, of a particle on an inclined surface can also be computed as a function of its shape. The effect of screen inclination on classification has been discussed quite extensively (Wills and Napier-Munn, 2006; Wang and Tong, 2011). However, it has been shown less often in explicit numerical terms. At low inclinations ($\theta \approx 0°$), even though the horizontal projection of apertures is wide enough, the particles are almost completely immobile, and the only force acting on the particle is its own weight ($\sin\theta \approx \theta$), and static friction since $\cos 0° \approx 1$. Similarly, at critically high inclinations ($\theta \approx 90°$), the horizontal projection of the apertures diminishes, particle acceleration, and consequently velocity, is extremely high and becomes less of a function of inertia, i.e. $f(\emptyset) \approx 0$, and the coefficient of friction μ, thus assuming the usual form of free falling objects ($\sin 90° \approx 1$, $\cos 90° \approx 0$). In both low and high inclinations, the rolling velocity is nearly zero. Generally, for round particles, ($a \approx r$), at median inclinations, both coefficient of kinetic friction and moments of inertia plays an important role in classification, and the particle acceleration can be estimated using Eq. (5).

However, for totally irregular (flat) particles at median inclinations (with infinitely large values of a), the process is governed by simple sliding dynamics, obtained by taking the limits of Eq. (5) as α tends to infinity:

$$\lim_{a\rightarrow\infty}\alpha_c[\theta, f(\emptyset), \mu] = \frac{1}{1+\frac{f(\emptyset)}{ma^2}}[g\sin\theta - \mu g\cos\ \theta] \tag{6}$$

$$\alpha_c(\theta, \mu) = g\sin\theta - \mu g\cos\ \theta \tag{7}$$

When above surface kinematics set in as shown in Eq. (6), the particle tends to "ride" over the screen apertures as described in Wills and Napier-Munn (2006), which negatively affects screening processes. Particle motion can then be described using Eq. (7), which presents acceleration of sliding objects on any inclined surface. At the earliest opportunity the particle finds a free area on the sieve cloth, large enough to go through, three things happen:

i. The direction of motion of the particle changes.
ii. The particle falls at uniform motion towards the gravity field to the collection region.
iii. The friction force disappears at this area with zero shear force (Hierrezuelo and Carnero, 1995).

1.1.2. Empirical model for estimation solids bulk velocity

When bulk solids are involved, other bulk properties come into play e.g. feed loads and particle flow velocities, which are considered since they affect classification to a large extent. Consider for

instance, a mass of dry granular particles, M_T controllably released from a feeder e.g. hopper or silo, onto an inclined sieve with increasing aperture sizes downwards, with channels below each sieve width to tap the falling undersize grades. For such a system the principle of relativity holds, so that the reduction in the oversize mass (m_i) and increase in undersize mass (m_u) are equal at any given time (Rotich et al., 2013).

$$m_i = M_T\varepsilon \tag{8}$$

$$m_u = M_T[1-\varepsilon] \tag{9}$$

where m_i is the oversize mass of the particles that proceed to the next screen (tailings) at any given time, while m_u is the mass fraction representing particles falling through the apertures. Both m_i and m_u are functions of time as is the mass fraction of tailings ε. The rate of reduction in the overflow is by relativity, proportional to the increase in the underflow, and the overall change in momentum can be described for a system of particles with variable masses, using Newton's second law (Plastino and Muzzio, 1992).

$$F = \frac{d}{dt}(P) = \frac{d}{dt}(m\bar{v}) \tag{10}$$

where P is the linear momentum. For a system that has a total batch mass m and varying bulk velocity of tailings $\bar{v}$, Newton's second law for a system initially at rest, can be written as follows:

$$F_{ext} = m_i\frac{d\bar{v}}{dt} + v_{rel}\frac{dm_u}{dt} \tag{11}$$

In Eq. (10), F_{ext} is the sum of all external contact forces applied, and $v_{rel}\frac{dm_u}{dt}$ is the sum of all body or field forces applied, e.g., electrical, magnetic or gravitational fields. For the particular system under study, the force balance equation can therefore be obtained from the mass fractions in Eqs. (5) and (6), in which the falling particles moving with relative velocity are accelerated by a 'thrust' of $v_{rel}\frac{dm_u}{dt}$. v_{rel} is the relative velocity of the exiting underflow, m_u with respect to that of overflow m_i. As the underflow increases in mass, the overflow becomes 'separated' more mobile and decongested and gains sudden increase in falling probability, due to larger (and optimally placed) apertures, and therefore more increase in the underflow. This phenomenon was also observed by Li et al. (2003), discussing the applicability of first order law to determine classification intensities.

The net force can also be expressed in the form:

$$m_i\left(\frac{d\bar{v}}{dt}\right) = -v_{rel}\frac{dm_u}{dt} + F_{ext} \tag{12}$$

$$\frac{dm_g}{dt} = -\frac{dm_i}{dt} \tag{13}$$

$$v_{rel} = \bar{v} - \mu g t\cos\ \theta \tag{14}$$

$$F_{ext} = \mu m_i g\cos\ \theta - \mu\varepsilon m_i g\cos\ \theta \tag{15}$$

In the case in Eq. (12), the only external force causing relative motion is gravity and related friction force acting in the opposite direction (Eq. (15)). Here, $\frac{d\bar{v}}{dt}$ is the resultant bulk acceleration of the particles in the opposite direction to m_i. As we are tracking this mass (m_i), which varies with time, the instantaneous changes in the bulk velocity with time t, and mass fraction ε can be expressed by substituting Eqs. (13)–(15) in (12):

$$v_{rel}\frac{dm_i}{m_i} = \mu g\cos\ \theta\left(\frac{m_i}{M_T} - 1\right)dt \tag{16}$$

Integrating Eq. (16) results in with initial and final conditions t_o and t, $m(t_o) = M_T$, $\bar{v}(t_o) = \bar{v}$, and with negligible air resistance reduces to a nonlinear implicit form:

$$v_{rel}\log\left(\frac{m_i}{M_T}\right) = \mu g t\cos\ \theta\left[\left(\frac{m_i}{M_T} - 1\right) - \log\left(\frac{m_i}{M_T}\right)\right] \tag{17}$$

The bulk velocity, $\bar{v}$ of particles on such a screen with reducing overflow and increasing underflow can then be computed by substituting Eqs. (8), (17) in Eq. (14):

$$\bar{v}(t,\varepsilon) = v_0 + \frac{\mu g t\cos\ \theta[(\varepsilon-1) - \log(\varepsilon)]}{\log(\varepsilon)} \tag{18}$$

Noting the relationship between overflow, ε and classification efficiency, η:

$$\eta = 1 - \varepsilon \tag{19}$$

Eq. (19) can then be substituted in Eq. (18) to get bulk particles velocity as a function of classification efficiency.

$$\bar{v}(t,\eta) = u_0 - \frac{\mu g t\cos\ \theta[\eta + \log(1-\eta)]}{\log(1-\eta)} \tag{20}$$

1.1.3. Rates of classification

The rate of classification has been used for decades to assess the speed at which solid classification occurs. It quantifies the time component of the classification process, precisely how long it takes a certain amount of solids to be separated. There are numerous methodologies for quantifying classification rates. For the screening system under study, the constant of classification varies with the change in momentum of the particles, and was determined mathematically by following the procedures described in Rotich et al. (2013), with the velocity vector obtained in Eq. (18).

$$\log\ m_i = \log M_T - \tau(A/D_p)\bar{v}(t) \tag{21}$$

Also expressed in exponential form as:

$$m_i = M_T e^{-\tau(A/D_p)\bar{v}} \tag{22}$$

where m_i the mass of oversized particles, M_T is the total batch mass, τ is the classification constant, A the effective (holed) area of the screen, D_p the diameters of the particles, and $\bar{v}$ is a matrix of bulk velocities determined from Eq. (19). An important observation from Eqs. (21), (22) is that the rate and efficiency increases as long as there is a positive change in the bulk velocity.

2. Methodology

2.1. Experimental setup

Glass beads particles of mass, M_T ranging from 10 to 160 g (16 batches), and known particle sizes (0.75, 1, 2, 3 mm), were released from an elevation to an inclined sieve with increasing (known) aperture sizes downwards, D_{ap} (1–4 mm), with channels below each sieve to collect the undersize. In this experiment, the same methodology as in Rotich et al. (2013) was followed, with the exception that in the current study the process was repeated for six deck angles of inclinations (20°, 15°, 14°, 12.5°, 10°, 5°) for each batch (M_T) of glass beads. The aim was to assess the effect of different inclinations and changes in feed throughputs on flowability (velocity), classification rates and efficiencies.

The following measurements were taken and recorded: sample mass M_T, mass of the undersize collected on the 1, 2, 3 and 4 mm sieves (m_1, m_2, m_3, m_4 and oversize M_i), and elapsed time t. The following values were calculated directly from the collected data: total undersize masses (M_u), classification efficiency η, computed as the ratio of total mass of undersize M_u to the batch mass M_T, epsilon ε, computed as the ratio of mass of collected oversized particles to the total sample M_T, and the mass of un-separated (unaccounted for) particles, M_{un} calculated by subtracting the sum of undersized and oversized particles from the total sample mass,

Table 1
Results recorded for experiment performed at an inclination of 12.5°.

MT (g)	Ψ	Mass of Undersize Mu (g), the subscript indicates to aperture size (mm)										
		M1 (g)	M2 (g)	M3 (g)	M4 (g)	Mu (g)	Time (s)	R (g/s)	Mi (g)	ε	η	ν
10	0.0625	3.3845	0.9525	0.2675	0.4715	5.076	2.605	1.94856	4.924	0.4924	0.5076	0
20	0.125	6.998	2.08	0.678	0.99	10.746	2.72	3.950735	9.254	0.4627	0.5373	0.412869
30	0.1875	10.6	2.85	1.095	1.575	16.12	3.1625	5.097233	13.88	0.462667	0.537333	0.825727
40	0.25	15.2735	3.436	1.307	2.032	22.0485	3.2675	6.747819	17.9515	0.448788	0.551213	1.231891
50	0.3125	16.325	4.38	1.315	2.2375	24.2575	3.3625	7.214126	25.7425	0.51485	0.48515	1.684171
60	0.375	21.3	4.8825	2.18	2.7675	31.13	3.52375	8.834338	28.87	0.481167	0.518833	2.079005
70	0.4375	24.1625	5.3775	1.755	2.8125	34.1075	3.7575	9.077179	35.8925	0.51275	0.48725	2.524318
80	0.5	26.565	5.5925	2.52	2.8175	37.495	3.62375	10.34702	42.505	0.531313	0.468688	2.964905
90	0.5625	30.2375	7.1975	2.1475	3.27	42.8525	3.8775	11.05158	47.1475	0.523861	0.476139	3.379384
100	0.625	33.0325	7.4925	2.54	3.673	46.738	3.82625	12.21509	53.262	0.53262	0.46738	3.813808
110	0.6875	35.1875	9.8375	3.18	3.7425	51.9475	4.635	11.20766	58.0525	0.52775	0.47225	4.230161
120	0.75	35.9125	10.1	4.58	4.1755	54.768	4.655	11.76541	65.232	0.5436	0.4564	4.679581
130	0.8125	43.5325	8.505	3.9125	3.828	59.778	5.12125	11.67254	70.222	0.540169	0.459831	5.098789
140	0.875	46.6225	8.6775	3.945	3.9075	63.1525	5.12375	12.32545	76.8475	0.548911	0.451089	5.540794
150	0.9375	46.91	9.8375	4.531	4.9775	66.256	5.23875	12.64729	83.744	0.558293	0.441707	5.986663
160	1	49.42	9.025	3.525	4.2275	66.1975	5.01875	13.19004	93.8025	0.586266	0.413734	6.476303

M_T (Rotich et al., 2013). The normalized loading coefficient of the screen, Ψ, was calculated by taking ratios of the batch masses to the largest mass.

To our best knowledge, no universal method has been developed for estimation of bulk solids flow velocities over a perforated inclined surface, involving reduction in overflow and/or increase in underflow masses with time. Before attempting direct measurements, which would require more sophisticated instrument, we approximated bulk velocity $\bar{v}$ by substituting ε, θ, and μ from the empirical model in Eq. (19). The classification constant, τ is related to the bulk velocity vector $\bar{v}$ and was obtained by linearizing Eq. (22).

Simulation was carried out by solving Eqns. (20)–(22) for the flow velocities, classification rates and efficiencies, and compared with the results obtained from the experiments. For simulation, a constant value of $\tau \approx 8.315 \times 10^{-3}$ s m^{-2} was obtained, which did not seem to change significantly, for different masses and inclinations. The constant was then used to solve for the rates of classification and efficiencies. Response surface plots with MATLAB (Mathworks, 2013), were used to visualize particles bulk velocities, classification rates, and efficiencies as a function of inclination, and loadings for both the simulation and experiments. Table 1 shows a sample record sheet of results obtained at an inclination of 12.5°.

3. Results

3.1. Experimental results

3.1.1. Bulk flow velocities

Bulk velocities have been used here, directly to measure flowability of dry solid particles. In this experiment we obtained the bulk flow by solving Eq. (18), for the following parameters (see Fig. 2):

μ, total batch mass,
ε, ratio of overflow to total mass of the batch measured,
θ = 5°, 10°, 12.5°, 14°, 15°, and 20°,
NB: κ, is not applicable when dealing with bulk, hence not used.

3.1.2. Classification rates

The classification rates were obtained by calculating the mass of the undersize (M_u) per unit time (T). A response surface plot for the rates against the mass throughput and inclination angles is shown in Fig. 3. Classification rates increased with increase loading $0 < \Psi < 0.7$; highest rates were found near the domains $15° \leqslant \theta \leqslant 18°$ and $0.47 \leqslant \Psi \leqslant 0.77$. It is possible that an optimum screen performance can be found. However, care must be taken not to confuse optimal regions with the stratified regions with high rates described by Wills and Napier-Munn; a stratified region tends to be formed when a high feed rate is used.

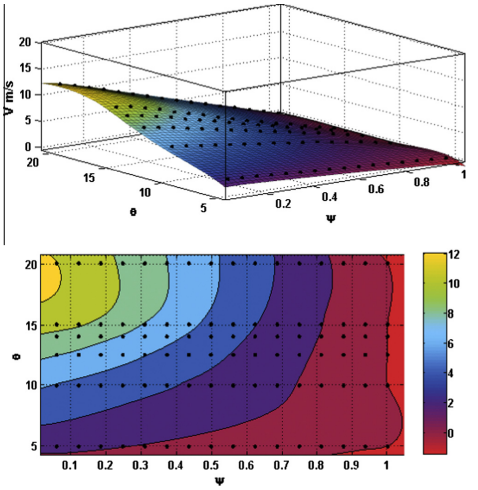

Fig. 2. Surface/contour plots of experimental bulk overflow velocity with mass fractions and inclinations.

3.1.3. Classification efficiencies

The classification efficiencies were obtained from the ratios of the mass of the undersize to that of the initial starting batch masses. There were multiple solutions for relatively high efficiencies near 12.5° and 17.5°. In general, higher efficiencies were obtained by reducing the loading and increasing the deck inclination. The results are shown in the response surface plot in Fig. 4.

3.2. Simulation results

3.2.1. Simulated particle velocities

The first step in simulating results is solving for particle velocities in Eq. (19), followed by solving for the classification constant

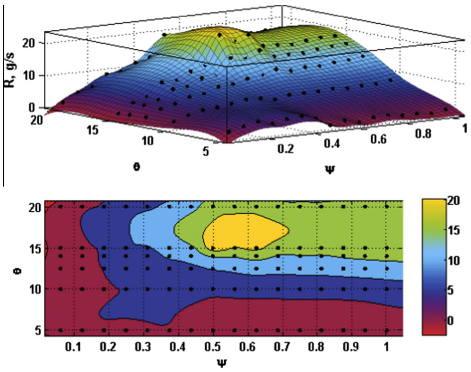

Fig. 3. Surface/contour plots of experimental particle classification rates, R with mass fractions, Ψ and inclinations, θ.

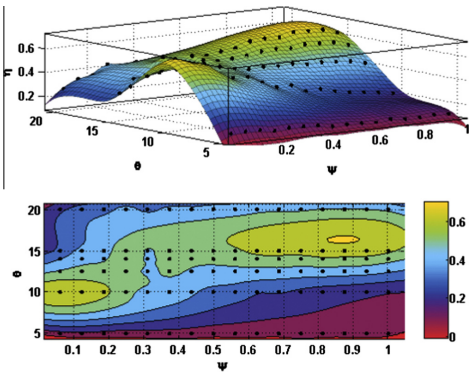

Fig. 4. Surface/contour plots of experimental particle classification efficiencies with mass loading and inclinations.

(τ). The constant was calculated by curve-fitting Eq. (18) (at 95% confidence level). The simulation process then proceeds by using the rate equation of Eq. (18) to solve for the mass of undersize per unit of simulation time for known parameter ranges of particle diameters, effective projected area of the screen, and each of the masses of the glass beads. Mass loading coefficient, Ψ, was calculated as a normalized parameter, taking the ratio of the batch masses to the largest mass. As expected, simulation test showed that less dense loading facilitated smooth flow of particles, while flowability increased with screen inclination. The surface contour plot of the mass throughput loading as a function of inclination and bulk velocities as a response variable is shown in Fig. 5. The following variables and parameters were used in the simulation:

t, residence time,
M_{U_s}, simulation undersize masses,
Ψ, mass loading coefficient,
ε, m/M_{T_s}, $0 \leqslant \varepsilon \leqslant 1$,
μ, coefficient of kinetic friction, 0.127 being theoretically that of between glass and steel surface,
D_p, simulated particle diameters (0.75, 1, 2, 3 mm) sizes,

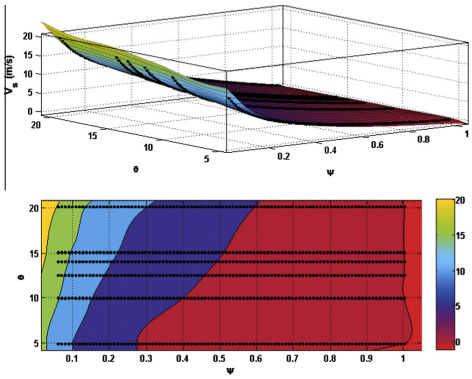

Fig. 5. Surface/contour plots of simulated bulk overflow velocities with mass fractions and inclinations.

τ, screening rate constant,
$\theta = 5°, 10°, 12.5°, 14°, 15°, 20°$.

3.2.2. Classification rates

The particles bulk velocity obtained from Eq. (19) was used to solve Eq. 23 for the undersize mass per unit of simulation time. Results show that the classification rates did not respond to changes in the loads and inclination between the domain $0 < \Psi < 0.4$. However, it increased steadily with additional increase in masses afterwards as is supposed to be from Eq. (18). Further increase in inclination beyond 15° between in the domain $0.6 < \Psi < 0.87$ led to subsequent drop in the rates. Fig. 6 depicts surface and contour plots of the simulation results for the rate of classification with loading and inclinations.

3.2.3. Classification efficiencies

Classification efficiency is an important element in determining how effective and reliable a system is. For this study, classification efficiencies were obtained by calculating the ratios of the mass of undersize to that of the batch masses in the simulation model.

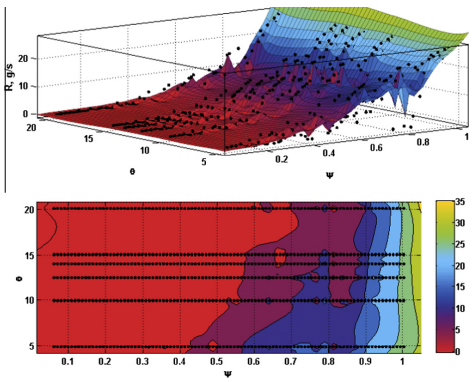

Fig. 6. Surface/contour plots of simulated particle classification rates, R with mass loading, Ψ and inclinations, θ.

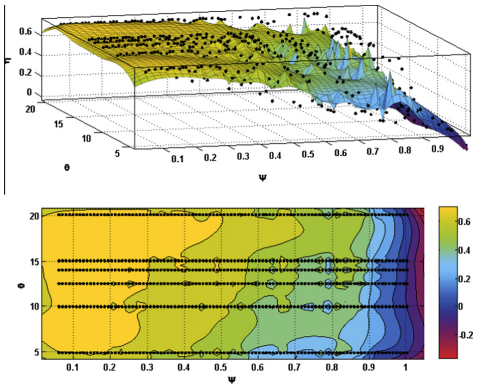

Fig. 7. Surface/contour plots of simulated particle classification efficiencies with mass fractions (Ψ) and inclinations (θ).

The response surface plot for the efficiencies versus throughputs and inclinations is shown in Fig. 7.

4. Discussion

There was a strong correlation between the simulated and experimental results. However, the simulated results tended to have wider and more flexible operating ranges of both inclinations and throughputs; the experimental results were narrower. Fewer solutions were obtained for the experiments compared to the simulation. These variations are likely due to the fact that the simulated results were obtained from 100 simulation points, almost 6 times more than the number of physical experiments, hence providing a greater possibility of finding solutions within the studied loading and inclination ranges. Simulation tests showed that screening was more efficient with lower loadings ($\Psi < 0.4$); changes in inclinations did not seem to have a significant effect on the efficiencies both for higher loadings ($\Psi > 0.9$) and lower loading coefficients ($0 < \Psi < 0.3$). Efficiencies reduced steadily with increase in screen loading in the domain ($0.3 < \Psi < 0.9$).

Based on the experiments, loading of up to $\Psi = 0.77$ was achievable without any malfunctioning; in the simulation, a maximum of $\Psi = 1$ was calculated, but loadings of up to $\Psi = 0.9$ seemed to be achievable without significant issues. There were excellent flows and high classification rates, but relatively low classification efficiencies at high angles (15–20°). It should be noted that the simulated data assumes 100% classification efficiency, which brings discrepancies like those obtained by (Li et al., 2003) with the model having high feed throughputs compared with experimental data. Industrial units barely go beyond 85% efficiencies, with most ranging between 65% and 85% (Gupta and Yan, 2006). Thus, correction factors must be set to restrain the simulated results. This can be done by equating the simulation response, i.e., efficiency or classification rate, to a known theoretical value as was done by Rotich et al. (2013). For this case, 85% of maximum loading ($\Psi \sim 1$) was taken and compared to the maximum experimental value ($\Psi = 0.77$).

At higher inclinations of 15–20°, relatively larger particles (2–3 mm size) seem to separate quite well to the undersize, though not as well as small particles at the same inclinations. At low angles (<5°), a significant amount of smaller particles (0.75–1 mm) were separated to the undersize, although with very poor flows, while most of the larger particles seemed to stagnate

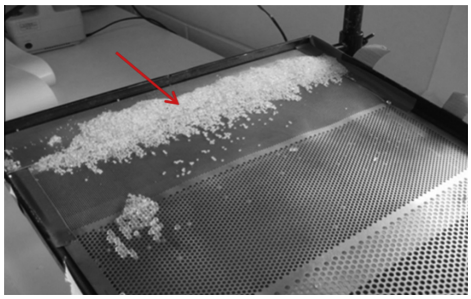

Fig. 8. Screen positioned at inclination, θ of slightly less than 5° and masse loading, Ψ higher than 0.5.

blinding the screens (Fig. 8). For these groups of particles at low inclinations, we attribute the results to the onset of bulk solid properties, especially those related to flowability, e.g., compressibility, bulk density, angle of repose, specific energy, permeability, and shear stress, as discussed in Ganesan et al. (2008), Bumiller et al. (2002), and the effects of other forces that the model does not take into consideration, e.g., inter-particle friction, Van Der Waals, surface tension and electrostatic forces.

Even though the initial formulation of the problem discussed in this study assumed that the particles were dry, the repose angle sufficiently low, and only one layer of particles rolled down at a time (Rotich et al., 2013), these assumptions seem to have been overridden for low angles of inclinations followed by unmatched increase in solids loading.

In the current study, a further increase in the angle of inclination (>15°) seemed to cause a reduction in the underflow and an increase in the overflow (low classification efficiencies). This can be attributed to too high bulk velocity and a virtual reduction of the projected area of the apertures, relative to the motion and interactions of the screen surface with particles, and thereby a reduced probability to report to the underflow (Li et al., 2003; Wills and Napier-Munn, 2006). The qualitative nature of the grades required is to a large extent determined by the inclination. To get a simple fractionation of particles, for example, in the manner that screens are currently used to separate shredded municipal solid waste into two grades, say, a finer and a coarser grade (also called scalping), steeper inclinations (~40°) may be used. However, for multiple grades, the process requires a longer residence time and more space to flow (Wills and Napier-Munn, 2006). The models formulated in this study are therefore functional only within certain confines of the angle of inclinations, particle shapes, and sizes and the quality grades required.

5. Conclusion

The paper aims to improve the understanding of gravity solids classification through the formulation of mathematical models based on both experiments and theoretical approaches. These models were used to quantify the extent of mechanical classification of glass beads by size.

Dense screen loading improved the classification rates, but hampered flowability, and consequently the classification efficiency. On the other hand, increase in deck inclinations improved flowability and efficiency, but only to a certain optimum point after which it led to excess overflow and low classification efficiencies. Higher the rates are achieved at the expense of low efficiencies.

Based on the results presented in the paper, an optimum performance point seems to exist between the loadings and deck angle of inclination, where best performance can be achieved. It follows that a balance may be struck between the two operating parameters (θ and Ψ), to obtain optimal point(s). Efforts for future research should therefore focus on optimization of the system. Possible optimization strategies may be as simple as *extrema* calculus, n-factorial design, or other common optimization techniques. Optimization objectives can be set as classification capacities (rates) and efficiencies, and constraints set as mass loading at different inclinations. Such optimization may help to reduce the gap between simulated and experimental results, and also it may provide additional information for consideration during systems design process.

Acknowledgments

The authors wish to acknowledge the Finnish Cultural Foundation (SKR-05131803) and the Finnish Science Foundation for Economics and Technology (KAUTE-201300353) for funding this research. Special thanks go to the laboratory manager at the LUT's Department of Chemical Technology, Mr. Markku Maijanen, for his help in fabricating the prototype system used in the experiments. Finally acknowledgements to Ms. Minna Laitinen for her important work on the experiments relating to this work.

References

Bodhmage, A., 2006. Correlation between Physical Properties and Flowability Indicators for Fine Powders, M.Sc. thesis, Department of Chemical Engineering, University of Saskatchewan, Saskatoon, Canada.

Bumiller, M., Carson, J., & Prescott, J., 2002. A preliminary investigation concerning the effect of particle shape on a powder's flow properties. In: World congress on particle technology 4 (WCOPT4), July 21st–25th, Sydney, Australia.

Chen, Y.S., Hsiau, S.S., Lee, H.Y., Chyou, Y.P., Hsu, C.J., 2010. Size classification of particulates in a trommel screen system. Chem. Eng. Process. 49 (11), 1214–1221.

Datta, B.K., 2012. Raw materials: their production and characteristics. In: PHI Powder Metallurgy: An Advanced Technique of Processing Engineering Materials. PHI Private Learning Limited, New Delhi, pp. 8–63.

Folk, R.L., 1980. Properties of sedimentary rocks. In: Petrology of Sedimentary Rocks. Hemphill Pub. Co., Austin, TX, USA, pp. 3–10.

Ganesan, V., Rosentrater, K.A., Muthukumarappan, K., 2008. Flowability and handling characteristics of bulk solids and powders – a review with implications for DDGS. Biosyst. Eng. 101, 425–435.

Gupta, A., Yan, D.S., 2006. Mineral Processing Design and Operation – An Introduction, Screening, first ed. Elsevier B.V, Oxford UK.

Hierrezuelo, J., Carnero, C., 1995. Sliding and rolling: the physics of a rolling ball. Phys. Educ. 30 (3), 177.

Kruggel-Emden, H., Elskamp, F., 2014. Modeling of screening processes with the discrete element method involving non-spherical particles. Chem. Eng. Technol. 37 (5), 847–856.

Li, J., Webb, C., Pandiella, S.S., Campbell, G.M., 2003. Discrete particle motion on sieves – a numerical study using DEM simulation. Powder Technol. 133, 190–202.

Liu, K., 2009. Some factors affecting sieving performance and efficiency. Powder Technol. 193 (2), 208–213.

MathWorks, 2013. MATLAB version 7.14.0.739 (R2013a). The MathWorks Inc., Natick, Massachusetts.

Möller, L., Kuhlman, K., Marshall, J., Towner, M., 2002. The snoopy angle experiment: calibration of an instrument to determine the angle of repose of Martian dust. Lunar Planet. Sci. XXXIII. Abstract #2015.

Plastino, A.R., Muzzio, J.C., 1992. On the use and abuse of Newton's second law for variable mass problems. Celest. Mech. Dyn. Astr. 53, 227–232.

Rotich, N., Tuunila, R., Louhi-Kultanen, M., 2013. Modeling and simulation of gravitational solid–solid classification for optimum performance. Powder Technol. 239, 337–347.

Wang, G., Tong, X., 2011. Screening efficiency and screen length of a linear vibrating screen using DEM 3D simulation. Min. Sci. Technol. (China) 21 (3), 451–455.

Wills, B.A., Napier-Munn, T., 2006. Industrial screening. In: Mineral Processing Technology: An Introduction to the Practical Aspects of Ore Treatment and Minerals Recovery. Elsevier Science & Technology Books, Oxford, pp. 186–203.

Xiaowei, F., Huck, D., Makein, L., Armstrong, B., Willen, U., Freeman, T., 2012. Effect of particle shape and size on flow properties of lactose powders. Particuology 10 (2), 203–208.

Publication III

Rotich N., Tuunila R., Elkamel A., and Louhi-Kultanen M.

Nonlinear optimization of gravity solids classification based on the feed and deck angles: a law of mass action approach

Reprinted from
Powder Technology,
Vol. 291, pp. 140–146, 2016.

Powder Technology 291 (2016) 140–146

Contents lists available at ScienceDirect

Powder Technology

journal homepage: www.elsevier.com/locate/powtec

Nonlinear optimization of gravity solids classification based on the feed and deck angles: a law of mass action approach

Nicolus Rotich [a,*], Ritva Tuunila [a], Ali Elkamel [b], Marjatta Louhi-Kultanen [a]

[a] Lappeenranta University of Technology (LUT), School of Engineering Sciences, P.O Box 20, FI-53851 Lappeenranta, South Karelia, FI
[b] University of Waterloo, Chemical Engineering, 200 University avenue west, Waterloo, ON N2L 3G1, CA

ARTICLE INFO

Article history:
Received 27 March 2015
Received in revised form 19 October 2015
Accepted 3 November 2015
Available online 22 December 2015

Keywords:
Gravity-classification
Mineral particles
Modeling

ABSTRACT

Deck screen design parameters e.g. material of construction, deck angle of inclination, the feed throughputs, and physicochemical properties of the particles, are critical factors to consider in solids classification. Two significant and easily manipulated parameters that greatly affect screen performance are the feed rate and design geometry configuration. In this work we apply statistical analysis of variance (ANOVA) and nonlinear least squares optimization with parameter estimation concepts, first, to assess the significance of the two factors and, second to formulate flow prediction models that optimize the feed rate and classification efficiency. Experiments were conducted on a prototype screen of 556.28 cm^2 effective area, (1380 cm^2 total area). For glass beads of sizes 0.75, 1, 2, and 3 mm, with 16 feed batches of 10 g to 160 g, and six inclination angles 5, 10, 12.5, 15, 17.5, and 20°, a maximum efficiency of 66.7% was achieved with a screen loading of 86.5 g, and an inclination angle of 17.5°. These results were then subjected to nonlinear least squares optimization, which showed that a maximum efficiency of 93.2% can be achieved at batch loading as low as 36 g. There was a favorable performance at the range of angles $12.5 \le \theta \le 17.5°$, but poor performance outside this range. The screening efficiency did not respond significantly to changes in screen loading, although loading had a significant effect on the screening capacity. Confirmation tests conducted at selected optimum parameters achieved a maximum efficiency of 72% (at 12.5° with 49.6 g batch load), and a maximum rate of 27 g/s at 17.5° with 104 g.

1. Introduction

Solids–solids separation is the process of segregating particles in terms of desired criteria or properties tied to the solids, using an applied force. The properties of the separated particles are dictated by downstream unit operations or end use. In general, the fundamental aim of classification is to separate the behavior of the solids into definite regimes of class patterns [1–2].

To underscore the significance of bulk solids classification in mineral processing for instance, research over the last decade has pointed out that the most energy intensive stage is comminution [3–4]. However, the exact root cause emanates from insufficient classification. Poor classification results in the transfer of excessive barren load to the grinding circuits, which end up consuming prohibitive energies (of 30–70% of the overall consumption), during comminution among other processes [4]. This thus makes classification a significant stage at which a large part of the profiting is determined. It is during classification, that the quality and quantity of the mineral, as well as downstream expenses are compromised [5].

In general, particles classification by screening has a long and exceptional history, with some research citing that it is probably the oldest [6]. It constitutes a large part of particles' classification in most mining, food industries, pharmaceuticals, coal and biomass industries, as well as many other chemical and processing plants.

When dealing with particles classification, a number of factors determine the extent of both capacity and efficiency that can be achieved. Although it is commonly presumed that if a process has been in use for many years, its controlling factors and optimum operating parameters will have been found, this unfortunately is not the case with gravity separation. The reasons being: (i) There are countless materials on earth, each with its own unique properties; (ii) the materials are not treated individually, but as bulk matter with diverse properties; and (iii) the material handling equipment also introduces complexities because of the varied materials and configurations used. The complex of interrelated factors thus makes a supposedly simple process highly complicated. Here is an example where this complexity can be found: in powder material science, flowability can be easily defined as "the ability of granular solids and powders to flow" [7], and the definition is comprehensible and valid. However, when the powder has (inevitably) come into contact with some material handling equipment e.g. hoppers, mesh screens, conveyors etc., the definition becomes inadequate, and instead a more accurate definition has to been coined

* Corresponding author.
E-mail address: nicolus.rotich@student.lut.fi (N. Rotich).

http://dx.doi.org/10.1016/j.powtec.2015.11.007
0032-5910/

"the ability of the powder to flow in a desired manner in a specific piece of equipment" [8]. The former definition while accurate, is somewhat incomplete; the later attempts to expand the definition by including the idea that flowability is never an inherent property on its own, but a compounded concept used to describe the motion of particles over others or an equipment surface.

Solid separators, e.g. deck screens, spiral concentrators, and Reichert cones, are some of the many types of materials handling equipment in use, and such equipment requires immense compromise as regards design and day to day operations. Bearing in mind the numerous materials constituting the bulk properties of solids, the critical factors to consider when using gravity force for solids separation can be classified into intrinsic, extrinsic, and other factors.

1. Intrinsic factors: These factors are easily manipulated by adjusting the mechanical design, e.g., overall configuration of the screen, feed rate, deck angle of inclination, aperture sizes, screen material, feed throughputs, and mesh size.

2. Extrinsic factors: These factors are seldom varied by the user, either because it is not possible, or because manipulating them negatively affects the overall product quality. Such extrinsic factors are: particle sizes, moisture content, shape, densities, purity, relative motion of particles to that of the screen surface, the physicochemical properties of the solids etc.

3. Others: This group of factors accounts for those unknown or known factors that demand great effort in their determination or manipulation, either qualitatively or quantitatively. Examples include the many factors linked to hydro, thermo, electro or even aerodynamic variables.

The number and diversity of the different factors involved underscore the difficulty of identifying an optimal combination of design and operating parameter values. However, it is possible to fit a mathematical function to most of the processes and thus try to understand the whole as a combination of its parts. The chief limitation of most models today is they are based on capacity, rather than the efficiency. For instance the screen is designed based on the amount of material presented to the screen rather than the yield. Realistic models base the design of screens on the actual amount of particles transmitted to the underflow. An example of such a model was formulated by V. Karra back in 1979. The Karra model while it is still useful in designing current processes, it can further be improved by extending it to quantify both undersized and oversize, together with the material loses involved [9]. The current study is primarily based on the law of mass action, which provides a systematic attempt to quantify the three quantities of materials by simultaneously solving a set of state equations (ODEs) that describes the process.

Material throughput and screen deck inclination are particularly significant and easily manipulated operational parameters that affect both the screening capacity (rate) and efficiency. Operating with a large feed throughput makes the screen susceptible to blinding, gives poor flowability and causes an overall reduction in the underflow. Low feed rates, while they increase the efficiency as observed in [10], extends the processing times, resulting in long residence times, affecting the economics of production. On the other hand, low deck angles are good for optimizing the efficiency in terms of separation effectiveness but adversely affect flowability on the screen, and thereby significantly reducing the rate of separation. High deck inclinations deprive the particles of the ability to report to the underflow, the projected screen area becomes narrower; and the flow velocities increase, making the particles ride over the apertures, instead of passing through [2,10].

The objective of this research paper is to conduct a mass balance around a lab scale screen for different sizes and batch masses of glass bead samples, M_o, and measure their undersizes, M_u, overflows, M_o, overflow fractions, ε and efficiencies η, at six different deck angles of inclination. The measured results are then formulated into an analysis of variance optimization (ANOVA) strategy, taking the angles as treatments, and the 16 glass beads samples as blocks, each with their values as factors. The results are then used to construct ANOVA tables and boxplots with MATLAB [11]. Decisions are then be made regarding the significance of each factor (based on the null hypothesis) and to what extent the factors can be enhanced. The second process involves formulation of nonlinear models based on the Guldberg–Waage law of mass action. The so developed models are then tested for flow prediction before subjecting them to nonlinear least squares optimization. Finally, we take confirmation tests at selected optimal parameters and draw conclusions.

2. Methodology

The numeric data used for this research paper were adapted from [12]. Ideal spherical glass beads of mass (M_o) and mixed known sizes (0.75, 1, 2, 3 mm) were released from an elevation to an inclined multi-sized prototype linear screen, with increasing (1, 2, 3, 4 mm) circular-aperture sizes downwards. Channels were used below each sieve to collect the undersized particles used for this study. The prototype screen measured 30 cm × 46 cm, i.e. approximately 1380 cm^2 in total area. The circular apertures were arranged in a 60° equilateral triangular pattern and spaced at a half-diameter apart. This by default scales the effective perforation to a maximum of 40.31% of the total screen plate area as observed in 2013 [13]. In this case it reduced the effective area to 556.28 cm^2 (Fig. 1). The batch screening process was repeated for six angles θ), (20°, 17.5°, 15°, 12.5°, 10°, and 5°, for each batch (M_o) of glass beads. For all the experiments, the screening time lasted for 2–3 s from batch mass release. The aim was to assess the effect of varied inclination and increases in feed throughputs on the degree of separation rates and efficiencies. The following measurements were taken and recorded: Sample mass; F, mass of the undersized collected on the 1, 2, 3 and 4 mm sieves (m_1, m_2, m_3, m_4); oversize, M_o; and runtime, t. The following values were calculated directly from the collected data: total undersized mass (M_u); separation efficiency, η computed as the ratio of total mass of undersized M_u to the batch mass F; overflow fraction, ε computed as the ratio of mass of oversize collected to the total sample F; and the mass of material loss, L un-separated or (unaccounted), calculated by subtracting the sum of undersized and oversize from the total sample mass, F. The rates of separation, R were obtained by calculating the mass of the undersized per unit time of separation. Loading coefficient, Ψ is a normalized parameter corresponding to the ratio of the load in grams to the overall largest feed mass used 160 g. [2]. The results of the variations in feed rates and efficiencies with inclinations were then tabulated in Tables 1 and 2.

Using the results as design matrices, analysis of variance (ANOVA) was carried out to assess the significance of the changes in inclinations and the feed quantities on the classification rates and efficiencies. Based on the analysis, the null hypothesis may then be accepted or rejected.

2.1. Analysis of variance (ANOVA)

Analyses of Variance constitute a very important tool in statistical quality control and optimization in engineering. Its main application is to provide guided decision making by comparing the variations caused by certain changes in the factors affecting the process, without making assumptions of pre-existing conditions. It is based on the null hypothesis that a certain group of factors do not have significant effect on the resulting observation.

In this case, for both increase in feed batch masses and inclinations, the null hypothesis is that the two have no effect on the rates and efficiencies observed in Tables 1 and 2. The probability, P of the occurrence of the hypothesis is then calculated and used to make necessary decisions regarding the factors assessed. We will construct two-way ANOVA tables for the feed rates and efficiencies for Tables 3 and 4.

2.2. Formulation of nonlinear unconstrained optimization strategy

The final stage is to formulate an optimization strategy to determine which deck angles and feed rates are sufficient to operate the screening process at optimum performance. The optimization is done keeping in

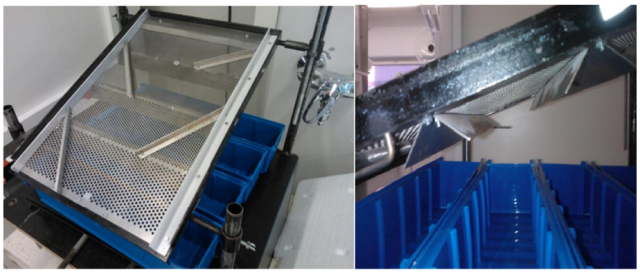

Fig. 1. Plan and side view of the prototype deck screen used for the experiments.

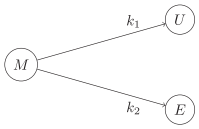

mind that very high throughputs are detrimental to the efficiencies, as high deck angles; while low inclinations do not provide sufficient force to cause adequate classification. Nonlinear least squares regression (NLSR) was chosen for this study, since the overflows need to be minimized, while maximizing underflows.

The total batch mass, M_o is the sum of the underflow, M_u, and the overflows, M_ε, at any given time, so that the system follows the principle of conservation of mass. Efficiency and overflow can be expressed with the following equations:

$$\begin{aligned} U &= M_u(\Psi,\theta,t) \\ E &= M_\varepsilon(\Psi,\theta,t) \\ L &= M_o - \{M_\varepsilon(\Psi,\theta,t) + M_u(\Psi,\theta,t)\}. \end{aligned} \tag{1}$$

The overflow can also be expressed as a function of stage efficiency, making it possible to compute the overflow fraction with the function:

$$\varepsilon(\Psi,\theta,t) = 1 - \eta(\Psi,\theta,t). \tag{2}$$

The implication of Eq. (2) is that the amount of the underflow fraction η at any given time can be optimized by minimizing the overflow fraction ε. It is ideally desired that the feed into the system equals exiting the system. The above description allows Eq. (1) to be written into a set of state equations describing the rates at which the undersized, oversize and the material losses are generated.

$$\begin{aligned} \frac{dU}{dt} &= k_1 M \\ \frac{dE}{dt} &= k_2 M \\ \frac{dL}{dt} &= (-k_1 - k_2) M \end{aligned} \tag{3}$$

Coincidentally, this set of equations (in (3)) resembles those used by Guldberg–Waage over a century ago to describe the formation of the desired E and undesired product U, such that k_1 and k_2 represent the parallel reaction activity constants. In this case however, they represent unique constants that change with time, t, deck inclination θ, reduction in the original batch of solid particles, M_o, and all the factors that affects the screening process. This method is deemed accurate since it does not necessarily imply by deduction that the undersized fraction is the subtraction of oversized from unity, like many models do.

We then model the process using the analogy of a parallel first order chemical reaction, yielding the desired product; undersized, U, and an undesired by-product; oversize E for every successful mesh size. The law of mass action is well explicated in [14].

The most important outcome for using the above analogy is, it immediately transforms the process into an optimization scheme. Eq.(3) constitutes objectives by themselves, meaning approximate functions $E(t)$, $U(t)$ and $M(t)$ can be found to estimate U, E and M respectively. Phenomenologically, the total mass is reducing with time, hence the decay function is assumed. This is a gray box model since population functions have been used before, to estimate the particles' separation rates [2].

$$\begin{aligned} U &= e^{k_1 t} - residuals \\ E &= M\left(1 - e^{-k_2 t}\right) - residuals \\ L &= \left(e^{k_1 t} - Me^{-k_2 t}\right) - residuals \end{aligned} \tag{4}$$

Overdetermined Eq. (4) as estimated by nonlinear least squares, as exponential functions, obtaining the coefficients (with 95% confidence

Table 1
Recorded underflow with increasing load (Ψ) and inclinations (θ).

Angle(θ)	Feed loading coefficient (Ψ)															
	0.1	0.13	0.19	0.25	0.3	0.35	0.4	0.5	0.56	0.69	0.7	0.80	0.84	0. 9	0.94	1.00
5	1.6	3.4	5.0	6.0	8.0	9.5	10.5	10.3	12.1	12.9	13.4	16.5	16.2	17.4	20.0	20.2
10	6.9	12.9	18.8	21.0	24.2	28.6	29.4	29.3	33.1	30.7	34.0	33.4	33.3	34.0	34.3	33.4
12.5	5.1	10.7	16.1	22.0	24.3	31.1	34.1	37.5	42.9	46.7	51.9	54.8	59.8	63.2	66.3	66.2
15	4.0	9.5	14.5	22.7	24.3	32.7	36.9	42.4	48.7	56.4	62.7	67.6	75.7	80.7	85.5	85.9
17.5	3.2	8.6	13.4	23.1	24.3	33.7	38.8	45.7	52.6	62.8	69.9	76.2	86.3	92.4	98.3	99.0
20	6.4	10.9	14.4	16.0	21.8	23.1	25.8	31.2	34.0	35.0	34.5	37.7	31.9	36.6	46.2	39.7

Table 2
Recorded classification efficiencies with increasing load (Ψ) and inclinations (θ).

Angle(θ)	Feed loading coefficient (Ψ)															
	0.1	0.13	0.19	0.25	0.3	0.35	0.4	0.5	0.56	0.69	0.7	0.80	0.84	0. 9	0.94	1.00
5	0.16	0.17	0.17	0.15	0.16	0.16	0.15	0.13	0.13	0.13	0.12	0.14	0.12	0.12	0.13	0.13
10	0.66	0.65	0.63	0.53	0.48	0.48	0.42	0.37	0.37	0.31	0.31	0.28	0.26	0.24	0.23	0.21
12.5	0.51	0.54	0.54	0.55	0.49	0.52	0.49	0.47	0.48	0.47	0.47	0.46	0.46	0.45	0.44	0.41
15	0.4	0.47	0.48	0.57	0.49	0.54	0.53	0.53	0.54	0.56	0.57	0.56	0.58	0.58	0.57	0.54
17.5	0.32	0.43	0.45	0.58	0.49	0.56	0.55	0.57	0.58	0.63	0.64	0.63	0.66	0.66	0.66	0.62
20	0.27	0.34	0.35	0.43	0.37	0.43	0.41	0.44	0.44	0.47	0.48	0.48	0.51	0.5	0.5	0.48

bounds). The problem set may now be written in the standard least square optimization connotation as shown in Eq. (5).

$$\begin{aligned} &\min_{k_1} f(\Psi,\theta) = \left[\sum_{i=1}^{16}\left(e^{k_1 t} - U\right)^2\right] \\ &\min_{k_2} f(\Psi,\theta) = \left[\sum_{i=1}^{16}\left(M\left(1-e^{k_2 t}\right) - E\right)^2\right] \\ &\text{subject to } k_1 > 0 \text{ and } k_2 < 0 \end{aligned} \tag{5}$$

Where parameters k_i are estimated coefficients which minimize the residuals and can be used to solve the system of ordinary differential equations in Eq. (3). The optimal sets of parameters are those that result in component E, having a value as low as possible, and U having a value as high as possible, meaning a system within the constraints $k_1 \gg k_2$ and $k_2 < 0$. These parameters are explored in this study by adjusting the screen deck angle and the amount of batch masses of solids in each of the 16 experiments. Successful manipulation of these quantities may enable optimization by process control, where best performance of the solids classification system may be achieved, following the recent empirical studies presented in [2].

3. Results

3.1. The significance of increased feed and inclinations on the classification rates

Table 3 shows a two-way analysis of variance (ANOVA) conducted to gage the significance of varying feed and deck-screen inclination on the rates at which classification occurs.

3.2. Assessing the significance of feed increase and inclinations on the classification efficiency

Table 4 shows a two-way analysis of variance (ANOVA) on the significance of variations in the feed and deck-screen inclination on the extent of particle classification in %.

Generally, nonlinear least square solutions are of the form:

$$Y_i = \text{Model-residuals} \quad (\text{errors}).$$

In which Y_i is the response data supplied for model approximation. Since the computer program returns the residuals, the model results can easily be computed by subtracting the errors from the supplied initial data (Y_i). The optimal parameter values for the batch mass, M_o, inclination, θ, k_1, k_2 and the resulting efficiency, η, in Eq. (4) were approximated to the following matrix:

$$\begin{bmatrix} M_o \\ \theta \\ k_1 \\ k_2 \\ \eta \end{bmatrix} = \begin{bmatrix} 36 \\ 12.5 \\ 3.38 \\ 0.23 \\ 0.93 \end{bmatrix}.$$

Table 3
ANOVA table showing the significance of increased feed and inclination on classification rates.

Source	Sum Square	Deg. of freedom	Mean square	F-Density	Prob >f
Angles	1588.9	5	317.78	39.67	8.9×10^{-20}
Feed	1017.76	15	67.85	8.47	6.5×10^{-11}
Error	600.78	75	8.01		
Total	3207.43	95			

4. Confirmation test

Confirmation tests were conducted on the new selected optimum parameters (randomly picked values from the highest contours on Fig. 3). The selected points and confirmation test results are shown in Table 5.

5. Discussion

Tables 3 and 4 were generated from two-way ANOVA results carried out for Tables 1 and 2. The values of f in column six of Table 3 are less than 0.001. The results suggest that we reject the null hypothesis; namely, that variations in inclination and feed rate have no significant effect on the rate of classification. Similarly, f values in Table 4 suggest otherwise. For inclination, $f < 0.001$, while for the load $f > 0.001$,

Table 4
ANOVA table showing the significance of increased feed and inclination on classification efficiency.

Source	Sum Square	Deg. of freedom	Mean square	F-Density	Prob >f
Angles	1.83	5	0.37	44.71	4.2×10^{-21}
Feed	0.03	15	0.002	0.23	0.9988
Error	0.615	75	0.0082		
Total	2.48	95			

Table 5
Table of confirmation results at optimized parameters (adapted from [12]).

Loading (Ψ)	Angle (θ)	Rates (g/s)	Efficiency(η)
.5	20	19.82	62.5
.31	12.5	14.3	72.1
.625	20	20.07	57.9
.5	15	18	68.5
.55	17.5	23.68	71.6
.65	17.5	26.9	63.4

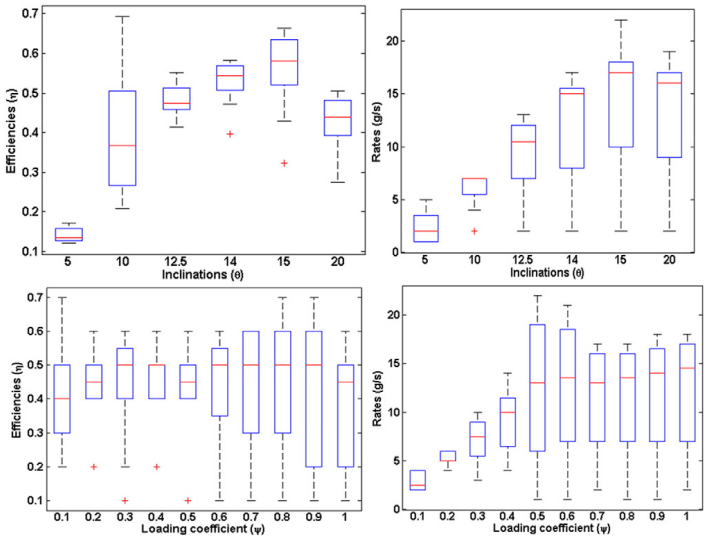

Fig. 2. ANOVA boxplots of the significance of feed and inclinations on efficiencies and rates.

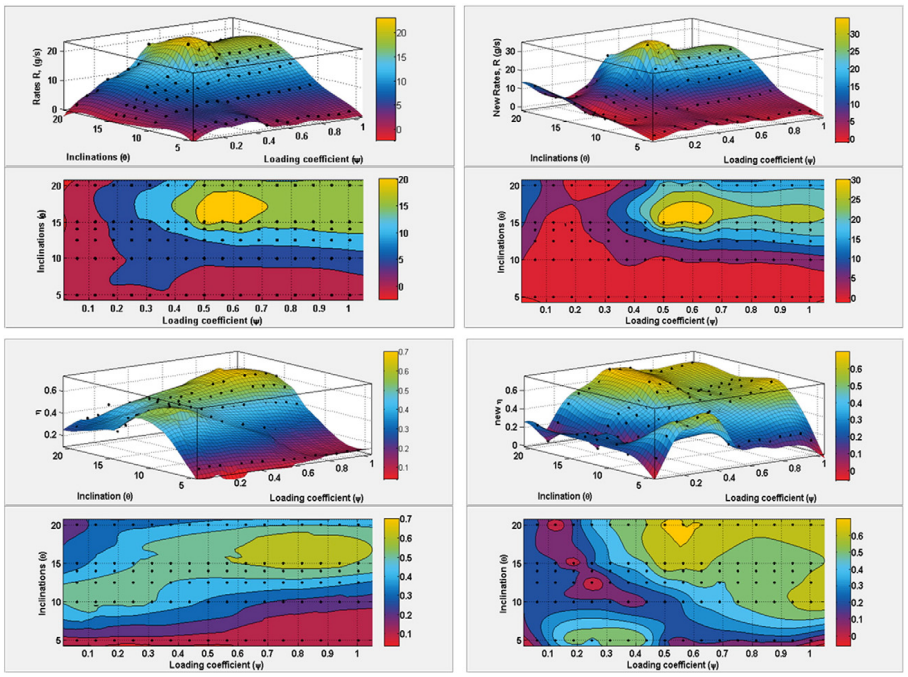

Fig. 3. Summary response surface and contour plots for rates and efficiencies (left) before and (right) after optimization (adapted from [12]).

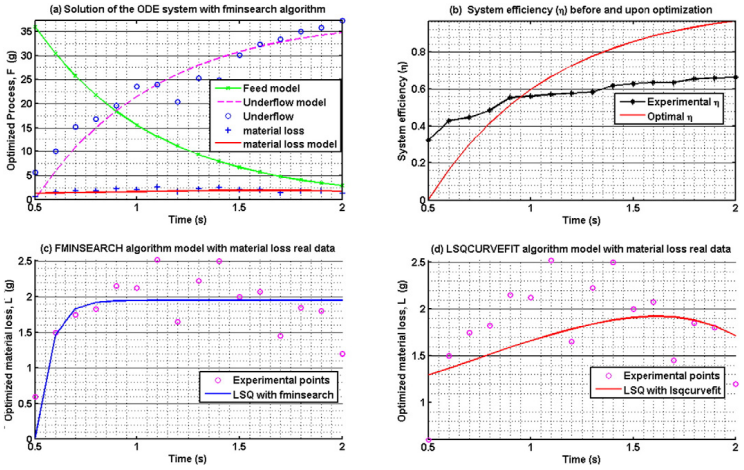

Fig. 4. Summary of the solution of the ODEs system Eq. (3) and LSQ fitting at selected optimal parameters.

implying that we should partially judge the null hypothesis and say, while changes in the load might not have a significant effect on the classification efficiency, deck angle variations do affect the system significantly.

The same information is conveyed by the ANOVA box plots in Fig. 2. Additional information that can be extracted from the boxplots is that even though feed rates do not seem to have a significant effect on the efficiencies, lower loads ($\Psi < 0.6$), have some positive effect on the efficiencies, while high inclinations ($\theta < 10$), have some negative effect. Classification throughput seems to increase proportionally with both loading and inclination for the first few batches (up to $\Psi = 0.65$ and 17.5°). Further increases in Ψ and θ causes a decrease in both classification capacity and efficiency.

The nonlinear models in Eq. (4) were chosen based on previous knowledge of system behavior, i.e. that the reduction in overflow particles is proportional to the increase in the underflow and follows decay functions of exponential nature [13]. Fig. 4 a) shows the solution of the ODE system Eq. (3), describing the feed, overflow and underflows, b) compares the classification efficiencies before and after optimization, and c) and d) compares the two optimization algorithms LSQCURVEFIT and FMINSEARCH used to build the overflow model. It can be seen that the screen performance has been enhanced by selecting the right operating conditions, with the system efficiency being improved by 5.5%. The operating ranges of θ and Ψ have also been determined clearly, especially for the case of efficiencies ($0.49 \le \Psi \le 0.63$). For the loads, the loading factor Ψ did not shift much but shrank, making it easier to determine the optimum loading point ($0.5 \le \Psi \le 0.65$). In all the cases, inclination between the ranges $12.5^{\circ} \le \theta \le 17.5^{\circ}$ was found to be favorable. Exceptionally high efficiencies but relatively low capacities (about 14.3 g/s) were found near the domain $0.2 \le \Psi \le 0.4$ and $\sim 10 - 12.5^{\circ}$. Upon successful development of these models they can be applied for equipment calibration. For specific bulk material properties, this process can be replicated to determine optimal operating inclination and feed rates in order to achieve a specified target efficiency and capacity. Equipment designers can also use these schemes if they have information on the bulk solid the equipment is intended for. They would then easily carryout trials, varying the two aspects studied in the present work, before fixing them (inclination) and/or recommending the feed rates accordingly.

6. Conclusion

The study covered most critical issues related to gravity classification, its importance, and in research and development progress. With the help of statistical analysis (ANOVA), the significance of two key parameters, feed rate Ψ and deck inclination, θ were assessed relative to each other and the experimental data fitted to computational models to yield optimization schemes. Upon optimization the classification rates were enhanced by up to 23.18% and the efficiencies were improved by 5.5% when the correct deck inclination and optimal feeds batch masses were chosen. Inclination angle seems to be a versatile and robust factor that can be manipulated to influence both separation rates and efficiencies. The load seems to be equally significant to the classification efficiency and critical to the rates too. The theoretically obtained optima of classification rate 31.45 g/s and efficiency (93.2%) were not achieved due to possible inefficiencies in the measurement methods applied. Secondly, only two aspects out of many design considerations were studied: deck inclination, and the feed rate. Therefore further investigation is required on the relative importance of other factors in defining the system's efficiency. Finally, this method, like many, is semi-empirical and only applicable upon carrying out trials on an equipment. It therefore opens up opportunities for future research work aiming at coming up with standard design considerations that optimizes bulk solid separation, taking into account not only mechanical, but also process engineering aspects of bulk solid separators.

7. Acknowledgments

The Authors wish to acknowledge the Finnish Science Foundation for Economics and Technology, KAUTE grant No. 201300353 for supporting this research. Special thanks go to Mr. Markku Maijanen, for fabricating the prototype equipment. We also acknowledge Ms. Minna Laitinen, and Mr. Henri Vainio for their invaluable help with the experiments, which contributed to the success of this work.

Nomenclature

a, b, c, d	Model coefficients
E	Overow, g
ε	Fraction of oversize to total batch mass, dimensionless
f	Statistical probability distribution, dimensionless

k_1	Constant related to increase in underflow
k_2	Constant related to increase overflow
L	Material loss, g
M_o	Batchwise mass, g
$M\varepsilon$	Mass of oversize particles, g
M_u	Mass of undersized, g
$m_{1..4}$	Masses of particles collected on 1, 2, 3 and 4 mm screens, g
R	Classification rate, g/s
t	Runtime taken by the batch mass, s
U	Undersized, g
Y_i	Design matrix with the results expected from the model
η	Separation efficiency, dimensionless
θ	Deck angle of the screens, degrees
ψ	Normalized loading coefficient, dimensionless

Appendix A. Supplementary Data

Supplementary data to this article can be found online at http://dx.doi.org/10.1016/j.powtec.2015.11.007.

References

[1] S. Savage, R. Pfeffer, Z. Zhao, Solids transport, separation and classification, Powder Technol. 88 (3) (1996) 323–333, http://dx.doi.org/10.1016/S0032-5910(96)03137-3.
[2] N. Rotich, R. Tuunila, M. Louhi-Kultanen, Empirical study on the effects of screen inclination and feed loading on size classification of solids by gravity, Miner. Eng. 70 (2015) 162–169, http://dx.doi.org/10.1016/j.mineng.2014.09.012.
[3] T. Napier-Munn, Is progress in energy-efficient comminution doomed?, Miner. Eng. http://dx.doi.org/10.1016/j.mineng.2014.06.009
[4] S. Nadolski, B. Klein, A. Kumar, Z. Davaanyam, An energy benchmarking model for mineral comminution, Miner. Eng. 65 (2014) 178–186, http://dx.doi.org/10.1016/j.mineng.2014.05.026.
[5] L. Albuquerque, J. Wheeler, S. Valine, B. Ganahl, G. Barrios, Application of high frequency screens in closing grinding circuits, Int. Miner. Process. Semin. Gecamin Vol. 5 (2008) 257–265.
[6] J. Li, C. Webb, S. Pandiella, G. Campbell, A numerical simulation of separation of crop seeds by screening-effect of particle bed depth, Food Bioprod. Process. 80 (2) (2002) 109–117, http://dx.doi.org/10.1205/09603080252938744.
[7] V. Ganesan, K. Rosentrater, K. Muthukumarappan, Flowability and handling characteristics of bulk solids and powders — a review with implications for ddgs, Biosyst. Eng. 101 (2008) 425–435, http://dx.doi.org/10.1016/j.biosystemseng.2008.09.008.
[8] M. Bumiller, J.C.J. Prescott, A Preliminary Investigation Concerning the Effect of Particle Shape on a Powder's Flow Properties, in: World Congress on Particle Technology 4 (WCOPT4) July 21–25th, 2002, Australia, Montana State University, Sydney, 2002.
[9] R.P. King, Modeling and Simulation of Mineral Processing Systems, Elsevier, 2012.
[10] B.A. Wills, F.A. James, Mineral Processing Technology: An Introduction to the Practical Aspects of Ore Treatment and Minerals Recovery, eighth ed. Elsevier Science & Technology, 2016http://dx.doi.org/10.1016/B978-0-08-097053-0.00001-7.
[11] MathWorks, MATLAB Version 7.14.0.739 R2013a, MathWorks Inc., Natick, Massachusetts, 2013.
[12] N. Rotich, R. Tuunila, M. Louhi-Kultanen, Nonlinear optimization of gravity separation, feed and deck angles with response surface methodology, Proceedings of the XXVII International Mineral Processing Congress — IMPC, 2014.
[13] N. Rotich, R. Tuunila, M. Louhi-Kultanen, Modeling and simulation of gravitational solid–solid separation for optimum performance, Powder Technol. 239 (2013) 337–347, http://dx.doi.org/10.1016/j.powtec.2013.01.056.
[14] M.E. Davis, R.J. Davis, Fundalmentals of Chelmical Reaction Engineering, McGraw-Hill Higher Education, 2003.

Publication IV

Rotich N., Tuunila R., Elkamel A., and Louhi-Kultanen M.

Dynamic Population Balance and Flow Models for Granular Solids in a Linear Vibrating Screen

Reprinted from
AIChE Journal,
Vol. 62, No.11, pp. 3889–3898, 2016.

AIChE

Dynamic Population Balance and Flow Models for Granular Solids in a Linear Vibrating Screen

Nicolus Rotich
Lappeenranta University of Technology (LUT), School of Engineering Sciences, P.O. Box 20 FI-53851, Lappeenranta, South Karelia, FI

University of Waterloo, Chemical Engineering, 200 university avenue west, Waterloo, ON, CA N2L 3G1

Ritva Tuunila
Lappeenranta University of Technology (LUT), School of Engineering Sciences, P.O. Box 20 FI-53851, Lappeenranta, South Karelia, FI

Ali Elkamel
University of Waterloo, Chemical Engineering, 200 university avenue west, Waterloo, ON, CA N2L 3G1

Marjatta Louhi-Kultanen
Lappeenranta University of Technology (LUT), School of Engineering Sciences, P.O. Box 20 FI-53851, Lappeenranta, South Karelia, FI

DOI 10.1002/aic.15318
Published online in Wiley Online Library (wileyonlinelibrary.com)

Vibrating screens are a widely applied form of particle separations. In spite of this significance, their understanding is still an obstacle. Three approaches were used to characterize the flow of granular material in a linear vibrating screen. The statistical model, mass action, and kinetic model based on conservation of momentum were derived. Experiments were then conducted on a multi-sized prototype screen and glass beads of sizes 0.75, 1, 2, 3 mm. Deck inclinations were varied over 7.5,12.5, and 17.5°, and frequencies over 7, 15, and 20 Hz. A total of 72 feed batches and a constant power of 50 W was used. The experimental data was then used to validate the models. The three models provided accurate flow prediction over the screens. Additionally, the kinetic model also provided a basis for optimal design of the screening unit operation, by allowing manipulation of seven design variables to obtain a 95–100% efficient vibrating screen. © 2016 American Institute of Chemical Engineers *AIChE J*, 00: 000–000, 2016
Keywords: separation techniques, particle/count/measurements, numerical solutions, mathematical modeling, solids processing

Introduction

Research over the last decade has pointed out that the most energy intensive unit operation in industries dealing with solid particulates, is comminution. In the mining industry for instance, Napier-Munn and Nadolski,[1,2] respectively, have discussed this topic extensively. However, a contributing root cause which is less often discussed is the inefficiency component resulting from poor particles' classification. Insufficient classification in mining for instance, results in the transfer of excessive barren loads to the grinding circuits, which end up consuming prohibitive energies (30–70% of the overall consumption), during comminution among other processes.[2] This is also true for many industries dealing with solid particulates, e.g., fertilizer plants in which precise and clean cut is required. Clean cut is the most significant consideration when evaluating classification equipment in that, even the most efficient classifier will pass a proportion of oversized and/or retain a proportion of undersized material.[3] In these processes, any particles' sizes outside the required range implies added costs of re-manufacturing, involving grinding (for the upper cut-off diameter), and size enlargement through agglomeration or granulation for the lower cut-off diameter. This fact thus makes classification a significant stage at which a large part of the profiting is determined. It is during classification, that the quality and quantity of the final product, as well as downstream expenses are compromised.[4]

Vibrating screens have an exceptional, and long history in particles' classification, with some research stating that it is probably the oldest.[5,6] They play an important role, first before comminution, to reject excessive coarse material, e.g., earth and rock from the finer gangue in the mines, and second, to grade the products on final processing.

The salient challenge with linear vibrating screening is the general lack of insightful understanding on the topic, and therefore lack of optimal designs. This aspect has been

Correspondence concerning this article should be addressed to N. Rotich at Nicolus.Rotich@Student.lut.fi.

observed by many researchers within the last decade, even though linear screens have been in use for well over a century.[4–8] Big steps have however been made on building empirical models that have successfully guided screening operations in the industry. A prominent example of empirical model currently used by most screen designers is the modified version of that developed by the Vibrating Screen Manufacturers Association (VSMA), discussed in Refs. 9 and 10. A number of these models were also systematically examined, simulated, and digitally packaged by R. P. King in Ref. 3. Design of these units have for long relied on empiricism due to lack of analytical models. The reasons for resorting to empirical studies and exploratory statistics is due to in-numerous factors relating to solids classification. These factors are grouped into three: intrinsic, extrinsic and others discussed in Ref. 11, and are extremely difficult to quantify the effect of each variable independently. Even though empiricism has evolved since the 17th and 18th centuries, empirical models lack universality in their applicability. For instance, some screening charts and formulae have in the past produced results deviating by up to a factor of 3.[5] To understand particle technology, including vibrating screens, one needs to be keen on some important factors that require high inter-disciplinary approaches, as discussed by Zhu et al. in Ref. 7.

Conversely, there has been a lot of activity recently on the applications of computer-aided techniques in this area of chemical engineering.[12] With the advent of powerful computer algorithms, the computation time has greatly been reduced through discretization of the particulate systems, even though the algorithms do not necessarily eliminate the error in totality. Algorithms such as discrete element method, computational fluid dynamics, finite element modeling and post-processing, among others, have been applied specifically to model linear vibrating screens over the last few years.[5,7,11,13] A detailed theoretical development and review of the discrete particle simulation systems has been discussed in Refs. 7, 14. Of course the use of computer models have their undeniable flaws. The question on applicability and shortcomings of modeling and simulation is increasingly becoming more of a philosophical and/or epistemic aspect, rather than that of core engineering discipline.[15]

The current study is primarily intended to systematically identify (in the *system identification* sense) the screening process. We have done this by combining the mathematics involved, with familiar chemical reaction kinetics to achieve a holistic and unified understanding of granular particles classification.

Theoretical Models Development

A statistical approach to physical separation by screening

With some known statistical data and linear algebra, a particulate system can be characterized statistically to achieve a generalized model. To build such a model, we consider a group of particles, U_o discharged from a hopper to a series of n shaking screens or stages with different (increasing) aperture diameters, A_{di}. The number of particles falling through to the fines in each of the n screen sections at a time interval, t_i is represented by, D_i, while those proceeding to the next separation stage are given as intermediate products, U_i, where i represents the current stage number. With statistical inference, a generalization for the intermediate particle count or overflow at each separation stage can be expressed algebraically as shown in Eq. 1 below:

$$\begin{aligned} U &= U_o, \\ U_1 &= U_o - D_1, \\ U_2 &= U_o - (D_1 + D_2), \\ U_i &= U_o - \sum_{i=1}^{n} D_i(t_i) \end{aligned} \tag{1}$$

Equation 1 can be normalized by dividing through by the total number of particles, U_o. Such normalization enables direct measurement of the extent of separation achieved or efficiency, η and the overflow, ε of the screening unit. Eq. 1 is therefore transformed to the form in Eq. 2 below.

$$\frac{U_i}{U_o} = \frac{U_o - \sum_{i=1}^{n} D_i(t_i)}{U_o} \quad \text{or} \quad \varepsilon_i = 1 - \eta_i \tag{2}$$

Where ε_i is the oversized and η_i, undersized fraction, at section i. At the end of the separation, $i = n$, it is expected that no particle leaves without falling to the fines, i.e., $U_n = 0$. With least squares optimization (LSQ), U_n can forcefully be driven to zero, so that the cumulative particle count of D_i roughly equals the original number of particles, U_o. This is done by taking the residual particles count E_i as an objective function (or error) that needs to be minimized as shown in Eq. 3. This process was followed in the recent paper involving optimization of gravity classification.[11]

$$f(t_i) = \sum_{i=1}^{n} E^2 \quad \text{Where } E = E(t_i) = U_o - \sum_{i=1}^{n} D_i(t_i) \tag{3}$$

$E(t_i)$, is the error function, representing the number of particles which neither collect to the fines, nor proceed as U_i. Once the problem has been converted into underdetermined LSQ optimization scheme as shown in Eq. 3, it can then be easily solved. The most common solution of such problems is by finding an approximate function that minimizes the residuals, E_i. Linear models, $\hat{Y}(\alpha)$ of the forms shown in Eq. 4 for instance, have been used widely in describing most engineering systems, and they have proven accurate. Computing the first derivative of the error function, $f(t_n)$ in Eq. 3, and setting it to zero, yields Eq. 5 at a constant slope, or the minimum value of E_i.

$$\hat{Y}(\alpha) = \sum_{i=1}^{n} D_i(\alpha) \simeq \beta_0 + \sum_{i=1}^{h} \beta_i \alpha_i(t) \tag{4}$$

$$\frac{df}{d\beta_i} = 2\sum_{i=1}^{n} \left[U_o - \left(\beta_0 + \sum_{i=1}^{h} \beta_i \alpha_i(t) \right) \right](-1) \quad \left(\mathbf{t^T t}\right)\hat{\beta} = \mathbf{t^T} U_o \tag{5}$$

Where $\hat{\beta}$ are the optimal coefficients of the function, $D(\alpha)$, obtained by solving the *normal* Eq. 5. In most cases the particulate systems are continuous functions of time, and the solution can also be obtained by converting the Riemann infinite sum in Eq. 1 into a set of definite integrals of the forms in Eq. 6.

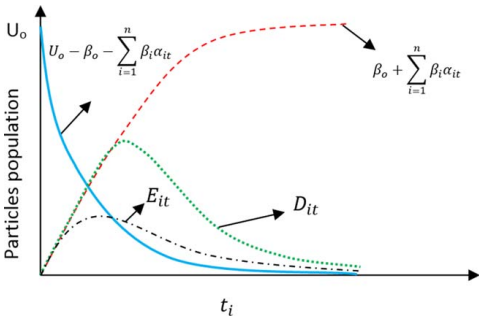

Figure 1. An illustration of a typical particle screening model.

[Color figure can be viewed in the online issue, which is available at wileyonlinelibrary.com.]

$$U(t_i) \quad = U_o - \frac{i}{h} \int_0^{\alpha_{th}} \sum_{i=1}^{h} \beta_i \alpha_i(t) \tag{6}$$

The existence of residual particles contributes to system inefficiency. To optimize, the term, $E(t_i)$ can be monitored by continuously checking the difference in Eq. 3, to ensure that it is minimal at any given time.

Simultaneous solutions of Eqs. 2, 3, and 6 yield a typical population balance equation (PBE), in which U_o decays exponentially, as the undersized grows with a cumulative distribution function. The undersized, $D(t_i)$ takes a temporary growth before dying out as shown on Figure 1 and the difference E_i also minimal for efficient system. If the material flow is perfect (i.e., the yield is 100%), then at any given time, the sum total of the undersized with the oversized gives the total amount of particles as shown in Eq. 1. To represent such an ideal system, the line $E_i(t_i)$ is eliminated, and the rates of undersized, $D_i(t_i)$ exactly equals the reduction in the oversized material, $U_i(t_i)$. In real systems, however, due to imperfections, particles often cling to the surface and at worst blind the screen, preventing more particles from falling through to the underflow.[16] This situation constitutes the overall inefficiency of the screening process quantified by E_i.

A law of mass action approach to screening

Many attempts in the past to describe the performance of screening processes kinetically have ended up adopting either probabilistic or empirical approaches.[3,17,18] However, a recent study seems to have found another intuitive method that enables dynamic quantification of not only the oversized and undersized particles simultaneously, but also estimates the intermediate amounts between the initial feed and the overflow product at any given time.[19]

By *Physical separation* we refer to an *inert* system in which mass is conserved, and obeys the law of conservation of mass. Even though there are no chemical reactions involved, we use the analogy of an extended Guldberg-Waage network of nested irreversible parallel chemical reactions as shown in Figure 2. Where U_o is the batch number or mass as before, U_i is the proceeding overflows, while D_i is the undersized particles falling through to the underflow. k_is are empirical constants related to the screening process factors discussed in Ref. 11, and *not* the usual reaction kinetics constants.

Formulation of the screening system as shown in Figure 2 allows for *decomposition* of U_o into its components of underflow, D_is, intermediate products, U_is, and oversized, U as shown in the set of state equations in Eq. 7 below.

$$\left.\begin{aligned} \frac{dU}{dt} &= -(k_1 + k_2)U \\ \frac{dD}{dt} &= k_1 U + k_3 U_1 + k_5 U_2 \\ \frac{dU_1}{dt} &= k_2 U - k_3 U_1 - k_4 U_1 \\ \frac{dU_2}{dt} &= k_4 U_1 - k_5 U_2 - k_6 U_2 \\ \frac{dU_3}{dt} &= k_6 U_2 \end{aligned}\right\} \tag{7}$$

The system in Eq. 4 is coincidentally identical to a Guldberg-Waage network of irreversible chemical reactions discussed in Ref. 20. The uniqueness of this modified scheme is in the combination of both parallel and consecutive reaction pathways in one system. A typical solutions of a parallel reaction yields the desired product, D and a side or intermediate product, E, and also gives the dynamics of the original reagents, U_o. The results from above system of equations in Eq. 7 are exactly same as that of the statistical model discussed in the previous section, and the model can generally be represented again as shown in Figure 3.

Just as in parallel chemical reactions, this model may also be employed to calculate the system efficiency. By taking the ratios of derived constants, system specific performance, η_n for n separation stages can be estimated through Eq. 8. This gives the same results as seen earlier (in Eq. 2).

$$\eta_n = \frac{\sum_{j=1}^{n} |k_{(2j-1)}|}{\sum_{j=1}^{n} k_j} \tag{8}$$

A classical dynamics approach to screening

While the two models discussed in sections "A statistical approach to physical separation by screening" and "A Law of mass action approach to screening" may accurately predict the material flow within the classification unit, they do not provide mechanistic details which are not only helpful in determining the energy requirements by the system, but also the optimal engineering design of the unit operation.

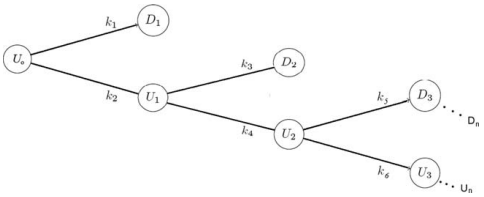

Figure 2. A screening model analogy of Guldberg-Waage nested parallel reactions.

Within the past years, little work has been done that considers industrial screening as a *variable mass system* in which mass and momentum are conserved. In classical mechanics, variable mass systems have historically been reserved for celestial mechanics, and the most practical it has gotten is in the physics laboratories and applied mathematics courses, e.g., the leaking oscillator experiments. Even though some physicists had started to take a keen interest on this aspect as early as 2008,[21,22] they are yet to be applied on some key ground-based industrial systems.

Industrial screening as a variable mass system has been explored to some extent over the last two years, both through computational modeling, and by and experimental studies.[11,23,24] The advantages of introducing variable mass equations to screening is that the particles' velocity is determined more accurately, and the rate of separation can be determined relative to it, Eq. 9–12.

With reference to section "A statistical approach to physical separation by screening," for completeness on the description of the model screen, it was further given that the screen is made of a material which exerts a coefficient of friction μ_k on the particles, and the deck is inclined at an angle of θ° to the horizontal. It has a net perforated area, a, out of the total screen area of A, and the mean particles' diameter is denoted by D_p. The mass fraction of particles proceeding down the screen is denoted by ε, while undersized falling through is represented by the fraction η, of the total mass, U_o.

Variable mass systems are described by Newton's second law in the form of Eq. 9.

$$\frac{dU}{dt}+\frac{U}{u}\frac{dv}{dt}=\frac{F}{u} \tag{9}$$

Where U is the mass of the system. In a similar way to chemical reaction kinetics and continuum models e.g. Navier Stokes', it was shown that the rate of particles' screening may also be determined at equilibrium, when the net sum of external forces acting on the system, F in Eq. 9 is zero.[23] This allows the rate of particles classification to be described by Eq. 10.

$$\begin{gathered}\frac{dU}{dt}-bU\frac{dv}{dt}=0\\ \text{where}\\ b=\tau\frac{a}{D_p}\end{gathered} \tag{10}$$

Assuming that the movement of particles on the screen and to the underflow contribute to the change in the x-axis momentum, Newton's second law for variable masses can then be written by substituting the rate Eq. 10, as shown in Eq. 11 below (details in Appendix).

$$\begin{gathered}v=\frac{Ft}{U}+u\ln\varepsilon\\ F=F_{net}+k_s z+Ug\sin\theta-Ug\mu_k\cos\theta\end{gathered} \tag{11}$$

Where u is the relative velocity with respect to the velocity v of the continuing mass, εU_o, and the velocity of the x-axis component of the falling particle mass, ηU_o. k_s is the stiffness constant related to the vibration mechanics of the screen, g is the gravity field acceleration, z, screen displacement from equilibrium, and F_{net} is the resultant force on the system. The relative velocity is assumed to be constant since the system is at equilibrium. For a constant value of b, and v obtained from

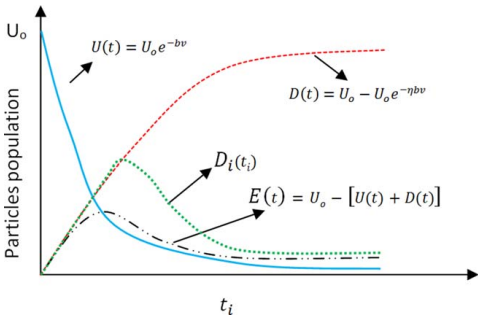

Figure 3. An illustration of the general solution of parallel chemical reaction paths.

[Color figure can be viewed in the online issue, which is available at wileyonlinelibrary.com.]

Eq. 11. Integrating Eq. 10 from 0 to v, corresponding to U_o to $U(t)$ gives:

$$\begin{gathered}\int_{U_o}^{U(t)}\frac{dU}{U}=-b\int_0^v dv\\ \ln\left(\frac{U(t)}{U_o}\right)=-bv\end{gathered} \tag{12}$$

This relation can also be written in exponential form as:

$$\begin{gathered}U(t)=U_o e^{-bv}\\ \varepsilon=e^{-bv}\end{gathered} \tag{13}$$

$$\text{Where } \varepsilon=\frac{U(t)}{U_o} \text{ is the oversized fraction}$$

Since b is present in both Eqs. 10 and 13, they are solved iteratively. The screen efficiency function can also be derived from Eq. 13, which gives the efficiency of transfer of particles of size D_p to the underflow.

$$\eta(v)=1-e^{-bv\left(t,\theta,\mu_k,\varepsilon,F,a,D_p\right)} \tag{14}$$

Equation 14 therefore combines up to seven factors affecting the screening process. It also gives a clear relationships of the overall effects of the manipulating factors. For instance, it can be concluded qualitatively from Eq. 14, that higher velocities are necessary to raise the screening efficiency. However, too high velocities are associated with higher vibration energy costs, but at the same time high velocities without sufficient free area, a will still lead to excessive overflow. Therefore a compromise must be made by adjusting the other variables accordingly. Equation 14 is comparable to the Rosin-Rammler empirical model (1933).

The equations governing conservation of mass and momentum in this model can then be written based on Eq. 12 so that the original notation of the batch mass, U_o, underflow, $D(t_i)$, cumulative underflow, $D(t)$, oversized, $U(t)$ and the intermediate product $E(t)$ can be expressed as shown in Eq. 15:

$$\begin{gathered}D(t)=U_o-U_o\left(1-e^{-bv}\right)\\ E(t)=U_o-[U(t)+D(t)]\end{gathered} \tag{15}$$

This model provides for optimal design considerations for particles classification. For instance, an efficient design can be

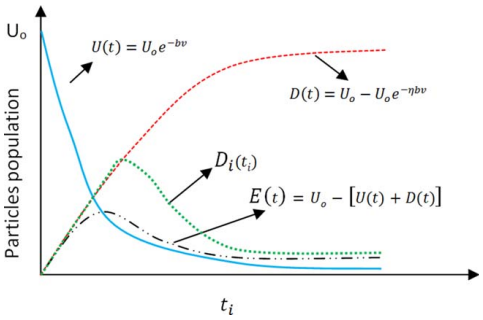

Figure 4. The solution of mass and momentum conservation dynamic state equations of a vibrating screens.

[Color figure can be viewed in the online issue, which is available at wileyonlinelibrary.com.]

obtained by constraining bv to yield a desired efficiency. Equation 14 has a value of $\eta \simeq 99\%$ when the product bv is set to ~4.5, with $b \geq 0$. A summary plot of individual equations in (15) also produces similar results as previous models as seen in Figure 4.

Experimental Setup and Design

Materials and methods

For models verification, 72 screening experiments were conducted on a multi-sized prototype single degree vibrating screen, with aperture sizes 1, 2, 3, 4 mm. The particles were rounded glass beads of sizes 0.75, 1, 2, and 3 mm, a mean particle diameter of $D_p = 1.875$ mm and a mixed particle size distribution. Deck inclinations, θ were varied over three angles (7.5,12.5, and 17.5°), and vibration frequencies, f varied over 7, 15, and 20 Hz, running a total of 8 feed batch masses, U_o of 10−80 g at an interval of 10 g with a constant power of 50 W. The prototype screen had a total area of 1380 cm^2 and effective (holed) area of 556.28 cm^2, (40.31%). On average it took 2−2.5 s for complete classification of each batch. Figure 5 shows the schematic of the prototype screen used for experimental validation.

Experimental design and analysis of variance

Owing to the large amount of data, the following sections constitute factorial design, and analysis of variance (ANOVA), to assess the significance of the three manipulated variables and their interactions, and to ensure statistical significance. Table 1 shows a coded, randomized, matrix table used to setup the three-factor two level factorial designs for these experiments.

The contrasts calculated in Table 1 are then used to estimate the sum of squares, variable coefficients in the model, and their combined effects on the response variable. Table 2 shows calculated model coefficients based on the squared sum and effects.

Models Validation

Each of the three models were tested by comparing the results with experimental runs. In general, the data sets

Figure 5. A schematic of the prototype screen used for experimental validation, 1. Multi-sized sieve plate, 2. 100 W tumbler motor, 3. FC-MTY4 IP54 motor frequency controller, 4. Underflow collection troughs.

[Color figure can be viewed in the online issue, which is available at wileyonlinelibrary.com.]

Table 1. Coded Matrix Table for Three-Factor Two Level Factorial Design

Run.	θ	U_o	f	θU_o	θf	U_{of}	$\theta U_o f$	D_i
1	−1	−1	−1	1	1	1	−1	4.3
2	1	−1	−1	−1	−1	1	1	6
3	−1	1	−1	−1	1	−1	1	34.7
4	1	1	−1	1	−1	−1	−1	47.9
5	−1	−1	1	1	−1	−1	1	7.4
6	1	−1	1	−1	1	−1	−1	6.3
7	−1	1	1	−1	−1	1	−1	59.3
8	1	1	1	1	1	1	1	50.3
Cont.	4.7	168.8	30.4	3.7	−24.9	23.6	−19.4	186.3

Table 2. Table for Estimation of Model Coefficients

α	θ	U_o	f	θU_o	θf	U_{of}	$\theta U_o f$
Contrasts	4.7	168.2	30.4	3.7	−24.9	23.6	−19.36
Sum of squares (SS)	2.8	3535.4	115.5	1.7	77.4	69.8	46.8
Model coefficients (β_i)	0.6	21	3.8	0.46	−3.1	3	−2.4
Effects	1.2	42.04	7.6	0.92	−6.2	5.9	−4.8

Table 3. ANOVA Table with Predictions

Var.(α)	SS	Df	MS	f_o	p	30% sig.	Y(D_i)	$\hat{Y}$	Resid. (R)	Rel.% err
Θ	44.7	1	44.7	0.067	79.8	No	4.3	4.5	0.13	3.0
U_o	56565	1	56565	83.9	0.0	Yes	6	5.9	−0.13	−2.19
f	1845	1	1845	2.7	10.3	Yes	34.7	35.7	1	3
θU_o	27	1	27	0.04	84.2	No	47.9	46.9	1	−2.19
θf	1239	1	1239	1.84	18	Yes	7.4	7.5	0.13	1.77
U_{of}	1116	1	1116	1.7	20.3	Yes	6.3	6.2	−0.13	−2.09
$\theta U_o f$	749	1	749	1.1	29.6	Yes	59.3	60.3	1	1.8
Dev. Sq	17762	72	β_0=	27.03			50.3	49.3	1	−2.09

followed the models well, with relative errors less than ±3% for the statistical model, Table 3.

The statistical model

The validation of this model is shown in Table 3. Based on these results, the accumulated underflow, D, total batch run, U_o and the model of residuals were plotted (Figure 6), against the results of the model. In this case the cumulative underflow was estimated to be in the form, $\hat{Y}$ in Eq. 16.

$$\hat{Y}=27.03+21U_o+3.8f-3.1\theta f+3.0U_o f-2.4\theta U_o f \qquad (16)$$

ANOVA and Prediction Bounds. It is always wise to check the statistical significance of the variables so as to reduce bulkiness of the model and cut down the experimental burden. This was done by conducting ANOVA in Table 3. ANOVA table shows that indeed not all variables assessed are significant. Inclination on its own does not affect the process significantly, but in conjunction with the vibration effect. Both coefficients β_1 and β_4 are left out, and the model is therefore reduced to Eq. 17 below.

$$\hat{Y}(\alpha)=\beta_o+\sum_{i=1}^{6}\beta_i\alpha_i$$

$$\text{Where } \beta_0=27.03;\beta_1=\beta_4\simeq 0 \qquad (17)$$

$$\text{and } \beta_2=21;\beta_3=3.8;$$

$$\beta_5=-3.1;\beta_6=3.0;\beta_7=-2.4;$$

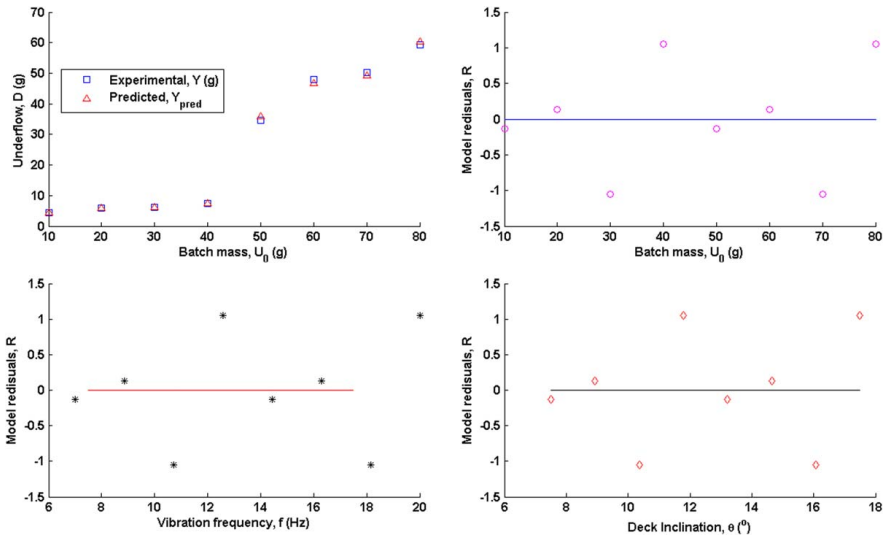

Figure 6. A graphical representation of the results, effects, with the model residuals.

[Color figure can be viewed in the online issue, which is available at wileyonlinelibrary.com.]

Table 4. Results of Eight Batches Separated at an Angle of 12.5° with a Vibration Frequency of 20 Hz

Expt.	U_o	D_1	D_2	D_3	D_4	OF	AB	Time
1	10	4.43	2.55	0.83	0.65	0.445	1.11	1.94
2	20	8.375	4.485	1.385	0.97	0.705	3.97	1.955
3	30	13.68	6.165	1.755	1.22	0.895	6.275	2.14
4	40	20.05	6.27	2.18	1.8	0.905	8.615	2.22
5	50	24.395	7.705	2.48	2.53	1.375	11.34	2.19
6	60	27.32	8.99	3.75	3.0	1.9	14.865	2.155
7	70	33.605	10.76	3.905	3.46	2.09	15.925	2.24
8	80	37.07	11.475	4.14	3.59	1.895	21.595	2.26

Lastly, the residuals were graphed against each factor studied. Figure 6 visualizes the results of the statistical model analysis.

The mass action model

With the help of an optimization algorithm, the recorded underflow data, D_i in Table 4 was used to build and train a model that minimizes any deviations from the data. The optimization algorithm used here is *FMINSEARCH*, which is a built-in application in MATLAB software.[25] The optimal coefficients, ks obtained are then used to infer the cumulative mass $\sum D_i$, the reduction in U_o, and the intermediate products at any given time. Validation therefore involves solving the Guldberg-Waage set of ordinary differential equations in Eq. 7 using the optimal coefficients so obtained. The data chosen is the first row in Table 4 (in bold), which pertains to an initial batch mass, U_o of 10 g, frequency, 20 Hz, and amplitude 2.11 mm with deck inclination set to 12.5°. The optimization yields k constants in Eq. 18.

Table 5. Values that Satisfy the Design Eqs. 10–14

Input	Output
θ=0.22 rad	G = 0.4634 G
ε=0.0509	v = 1.5625 m/s
μ_k=0.127	η=0.9491
D_p=0.0017 mm	a = 0.0556 m^2
b = 1.9059 sm^{-1}	τ=0.0583 sm^{-2}

$$\begin{bmatrix} k_1 \\ k_2 \\ k_3 \\ k_4 \\ k_5 \\ k_6 \end{bmatrix} = \begin{bmatrix} 3.37 \\ 0.26 \\ -1.73 \\ 28.67 \\ -26 \\ 28.16 \end{bmatrix} \tag{18}$$

$$\eta = \frac{|k_1|+|k_3|+|k_5|}{|k_1|+|k_2|+|k_3|+|k_4|+|k_5|+|k_6|} = 94.91\%$$

The variable mass system model

The following steps are necessary to validate this model. The process is started by implicitly estimating the value of b in Eq. 12 as a function of ε at various values of material flow velocities, v. The parameter b is an allocation parameter relating screen surface to the particles sizes (see Eq. 9). Appropriate values of b and v are then chosen depending on the acceptable threshold limit value of the overflow ε. This

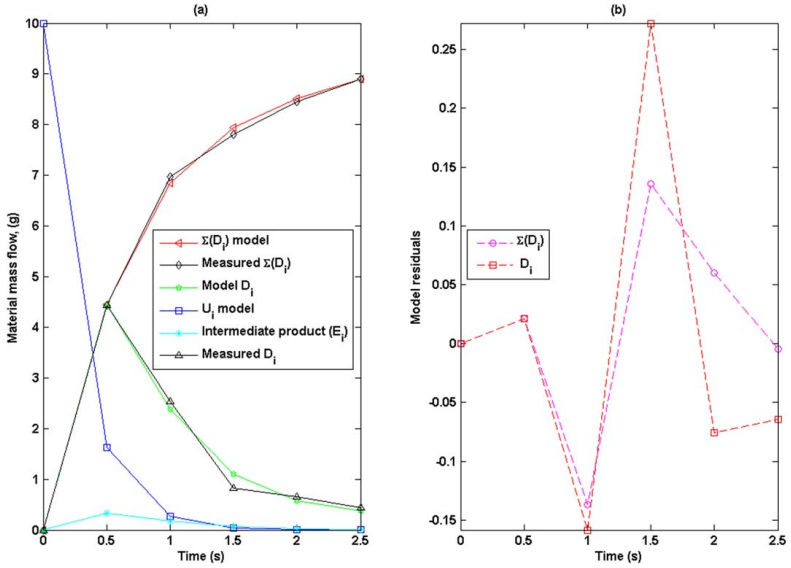

Figure 7. (a) The variable mass system model compared to the actual flow of material, (b) Corresponding model residuals.

[Color figure can be viewed in the online issue, which is available at wileyonlinelibrary.com.]

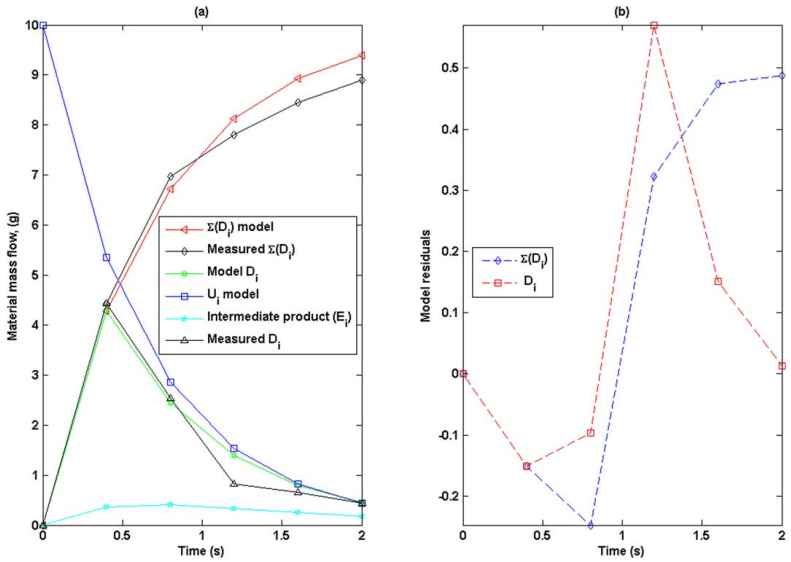

Figure 8. (a) The law of mass action model compared to actual flow of material, (b) Corresponding model residuals.

[Color figure can be viewed in the online issue, which is available at wileyonlinelibrary.com.]

estimation was done through pattern search optimization. For a particulate system with known mean diameter, D_p and/or available screen area, the rate constant is determined from Eq. 9 which is also solved implicitly with pattern search. The next step is to determine the vibration force needed to drive the particles at the predetermined velocity over the screen sections. This is done by solving for the vibration G-force as a function of kinetic friction coefficient, μ_k and inclination, θ. The last step is to verify whether the target efficiency has been achieved by re-calculating all the design Eqs. 9–13.

With this model, to achieve $\eta \simeq 94.91\%$ as of the experimental value, ε=5.09%, with the given particles' mean diameter, D_p=0.0017 mm, Table 5 shows the estimated values that satisfy the design equations Eqs. 9–13. $G=F/mg$ quantified as the vibration G-force, defined as the ratio of applied force to gravity.

For plot-able results on this model, the set of Eq. 14 are solved and compared to the actual data on Figure 7. Stage-wise particle collection according to this model is the *anti-cumulative* or backward loop count of the overall efficiency curve estimated as shown in Eq. 19.

$$\begin{gathered} n=StagesNumber; \\ \text{for } i=2:n; \\ D_i(i)=D_i x(i)-D_i x(i-1); \\ end \end{gathered} \tag{19}$$

Discussion

This work has provided a basis towards building of discrete statistical and continuum models for linear vibrating screens. Some advances have also been made by introducing a conservation of mass approach based on the law of mass action, that enables accurate quantification of the underflow and instantaneous overflow of particles on the screen simultaneously. The models have also been systematically formulated into unconstrained optimization strategies that were used to enhance particles' separation efficiency in all the three.

Both the statistical and mass action models are data-driven, with an implication that the user needs to have experimental results and related technical skills to replicate the model and use. Optimal results are then obtained by selecting among the set of experiments the one with correct settings with highest efficiency. In general, with a constant power of 50 W, optimal results were achieved with higher frequencies of (15−20 Hz), lower feed rates between 10−20 g as expected, and a median inclination of 12.5°.

Statistical ANOVA showed existence of an intricate relationship between the effects of screen loading, deck inclination and the vibration frequency, on the process. The most significant of all is the screen load, having a positive effect, followed by the vibration magnitude, seen from Eq. 16. Deck inclination on it's own, unexpectedly has no relative effect, but in combination with the rest of the factors. The p/f limits used in this study are 30% and 0.07, respectively. This information can also be seen from the p/f-values in Table 3. Factors with large p-values or low f_o values (θ and θU_o), are less significant. Even though the model suggests that increasing the screen load would improve the screening process, attention must also be focused on the negative effect of aperture blockage and low flowability when low deck inclinations and vibration frequencies are used.

While the first two models are sufficient in predicting the flow of material on the screen sections as seen in Figures 6 and 8, they do not provide tangible design information such as energy requirements, screen area needs, and overall

mechanical behavior of the system. The variable mass model however does provide for system designability besides the functional flow prediction.

Conclusion

Statistical, mass action, and a kinetic model have been derived based on statistical analysis and the physical laws governing mechanical separation and transport of solids. It was observed that even though empirical models are successful in predicting the flow of material to an accuracy of less than 3% relative error, they are specific to processes and equipment. They lack universality in providing tangible design information that can be applied across all unit operations. Kinetic models, conversely, makes it possible to come up with useful artifacts for process design and improvements through optimization. Based on Newtonian classical mechanics of the variable mass systems, the kinetic model uses targeted results as constraints to come up with design strategy. For instance, the input parameters for this model are: available screen area, target efficiency or threshold limit overflow allowed (in percentage), mean particles' diameter, and the surface coefficient of kinetic friction between the screen and granular material. With a well defined model that satisfies the design equations, important outputs such as travel velocity of material, deck inclination angle, and the required vibration force (in G-force) are obtained as outputs, and used during fabrication stages. These study therefore combines flow predictability provided by empirical models and optimal designability provided by kinetic models. The study also forms basis for process control uncertainty calculations with selected modern rigorous regimes, such as perturbation analysis in future. A continued development on the variable mass system could provide a direct correlation between the screening efficiencies and the energy used, which is a significant missing link at present.

Acknowledgments

The authors wish to acknowledge the financial support of The Alfred Kordelin—Gust. Kompan, and the Finnish Cultural Foundation (SKR) -Grant No. 05152027, for the grants which contributed to the success of this research and publication. We also wish to acknowledge Mr. Henri Vainio for conducting useful experiments which initiated this study.

Notation

$\mathbf{U_o}$ = material batch mass, g
$\mathbf{U(t)}$ = oversized at time t, g
$\mathbf{U_n}$ = overflow at n_{th} stage
$\mathbf{D(t)}$ = desired underflow, g
$\mathbf{E(t)}$ = intermediate product, g
$\mathbf{i}$ = i^{th} stage
$\mathbf{n}$ = number of stages
$\mathbf{A_{di}}$ = aperture size at i^{th} stage
$\mathbf{D_i}$ = underflow at i^{th} stage, g
$\mathbf{D_n}$ = underflow at n_{th} stage
$\mathbf{U_i}$ = oversized at i^{th} stage, g
ε = oversized fraction
$\varepsilon_{\mathbf{n}}$ = Last overflow fraction
$\varepsilon_{\mathbf{i}}$ = overflow fraction at i^{th} stage
η = underflow fraction
$\eta_{\mathbf{n}}$ = last underflow fraction
$\eta_{\mathbf{i}}$ = underflow fraction at i^{th} stage
$\mathbf{E_i}$ = intermediate product at i^{th} stage, g
β = approximate rate function for D_i
γ = approximate rate function for E_i
$\mathbf{h}$ = stage count in the function, β
$\mathbf{k_i s}$ = mass rate constants
$\mathbf{j}$ = constants (k) count in the mass action model
$\mathbf{a}$ = holed screen area, m^2
$\mathbf{A}$ = total screen area, m^2
$\mathbf{D_p}$ = particles' mean diameter, m
$\mathbf{m}$ = particles' mass, g
τ = variable mass rate constant, sm^{-2}
$\mathbf{v}$ = particles' average velocity, ms^{-1}
$\mathbf{k_s}$ = vibration stiffness constant, Nm^{-1}
$\mathbf{z}$ = Vibrating screen displacement, m
$\mathbf{F_{net}}$ = net force on the particles, N
$\mathbf{u}$ = particles' relative velocity, m
$\mathbf{b}$ = = screen allocation parameter, sm^{-2}
$\mu_{\mathbf{k}}$ = kinetic friction coefficient
$\mathbf{X}$ = the ratio $\frac{F}{m}$, ms^{-2}
θ = screen inclination, Rad

Literature Cited

1. Napier-Munn T. Is progress in energy-efficient comminution doomed? *Mineral Eng*. 2014;73:1–6.
2. Nadolski S, Klein B, Kumar A, Davaanyam Z. An energy benchmarking model for mineral comminution. *Mineral Eng*. 2014;65:178–186.
3. King RP. *Modeling and Simulation of Mineral Processing Systems*. Oxford, UK: Elsevier, 2012.
4. Albuquerque L, Wheeler J, Valine S, Ganahl B, Barrios G. Application of high frequency screens in closing grinding circuits. In Proceedings of the Vth international mineral processing seminar, procemin 2008, Santiago, Chile.
5. Li J, Webb C, Pandiella S, Campbell G. A numerical simulation of separation of crop seeds by screening-effect of particle bed depth. *Food Bioprod Process*. 2002;80(2):109–117.
6. Li Z, Tong X, Zhou B, Wang X. Modeling and parameter optimization for the design of vibrating screens. *Mineral Eng*. 2015;83:149–155.
7. Zhu H, Zhou Z, Yang R, Yu A. Discrete particle simulation of particulate systems: theoretical developments. *Chem Eng Sci*. 2007;62(13):3378–3396.
8. Wang G, Tong X. Screening efficiency and screen length of a linear vibrating screen using DEM 3 D simulation. *Min Sci Technol China*. 2011;21(3):451–455.
9. Olsen L, Carnes B. *Screen Capacity Calculation*. 86470 Franklin Blvd., Eugene, OR, 97405, Retrieved March 30, 2016, from VIBFEM: http://vibfem.com.au/resources/vibrating_screens_and_feeders/Screen_Capacity_Paper.pdf.
10. Schlemmer G. *Principles of Screening and Sizing*. San Antonio, TX: Quarry Academy, 2012.
11. Rotich N, Tuunila R, Louhi-Kultanen M. Nonlinear optimization of gravity separation, feed and deck angles with response surface methodology. In: *Proceedings of the XXVII International Mineral Processing Congress*. IMPC, Gecamin, 2014.
12. Saravacos GD, Kostaropoulos AE. *Handbook of Food Processing Equipment*. *Springer Science & Business Media*. Kluwer academic publishers: New York, 2002.
13. Li J, Webb C, Pandiella S, Campbell G. Discrete particle motion on sieves—a numerical study using the DEM simulation. *Powder Technol*. 2003;133(1):190–202.
14. Zhu H, Zhou Z, Yang R, Yu A. Discrete particle simulation of particulate systems: a review of major applications and findings. *Chem Eng Sci*. 2008;63(23):5728–5770.
15. Grim P, Rescher N. How modeling can go wrong. *Philos Technol*. 2013;26(1):75–80.
16. Wills BA, Napier-Munn T. *Wills' mineral processing technology: an introduction to the practical aspects of ore treatment and mineral recovery*. Oxford, UK: Butterworth-Heinemann, 2015.
17. Karra VK. Development of a model for predicting the screen performance of vibrating screens. *CIM Bullet*. 1979;168–171.
18. Subasinghe GKNS, Schaap W, Kelly EG. Modelling the screening process: a probabilistic approach. *Powder Technol*. 1989;59(1):37–44. Available from: http://www.sciencedirect.com/science/article/pii/0032591089800932.
19. Rotich N, Tuunila R, Elkamel A, Louhi-Kultanen M. Nonlinear optimization of gravity solids classification based on the feed and deck angles: a law of mass action approach. *Powder Technol*. 2016;291:140–146.
20. Davis ME, Davis RJ. Fundalmentals of chelmical reaction engineering. In: Jeans Z, Lorkovic M, editors. New York, NY: McGraw-Hill Higher Education, 2003.

21. Rodrigues H, Pinho MO, Portes D, Jr, Santiago AJ. Modelling the dynamics of bodies self-propelled by exponential mass exhaustion. *Europ J Phys*. 2008;29(3):527.
22. Rodrigues H, Panza N, Portes D, Jr, Soares A. A model of oscillator with variable mass. *Education* 2014;60(2014):31–38.
23. Rotich N, Tuunila R, Louhi-Kultanen M. Modeling and simulation of gravitational solid–solid separation for optimum performance. *Powder Technol*. 2013;239:337–347.
24. Rotich N, Tuunila R, Louhi-Kultanen M. Empirical study on the effects of screen inclination and feed loading on size classification of solids by gravity. *Mineral Eng*. 2015;70:162–169.
25. MathWorks. *MATLAB version 7.14.0.739 R2013a*. In: Inc M, editor. Natick, MA: MathWorks Inc., 2013.

Appendix A

This section is a supplement on derivation of the variable mass system model.

$$m\frac{dv}{dt}+u\frac{dm}{dt}=F+mg\sin\theta-\mu_k mg\cos\theta \tag{A1}$$

This is Newton's second law

$$\frac{dm}{dt}=-b\frac{dv}{dt} \text{ stating the rate Eq. 8} \tag{A2}$$

$$\frac{dv}{dt}=\frac{F}{m(1+ub)}+\frac{g\sin\theta}{1+ub}-\frac{\mu g\cos\theta}{1+ub} \tag{A3}$$

Substitute the rate equation in A1

$$b=-\ln(\varepsilon)/v \tag{A4}$$

$$\frac{F}{m}=X \tag{A5}$$

$$1G\simeq -9.81\frac{N}{kg} \tag{A6}$$

$u=v-v_f$ u is the relative velocity of the bulk solids front (A7)

$v_f=\mu_k g t\cos\theta$ is the velocity due to friction force (A8)

$$\frac{dv}{dt}=\frac{-X+g(\sin\theta-\mu_k\cos\theta)}{1+ub} \tag{A9}$$

$$v=\left\{\frac{-X\,t-g\,t\sin(\theta)+\mu_k\,g\,t\cos(\theta)+\mu_k\,g\,t\cos(\theta)\ln(\varepsilon)}{\ln(\varepsilon)-1}\right\}$$

integrating A10 to get v (A10)

$$\frac{dv}{dt}=\frac{-X-g[\sin\theta-\mu_k\cos\theta(1+\ln\varepsilon)]}{\ln\varepsilon-1}=0 \tag{A11}$$

$G(\theta,\mu_k)=\sin\theta-\mu_k\cos\theta[1+log(\varepsilon)]$ noting $F/mg=X/g=G$. (A12)

$$G(\theta,\mu_k)=\sin\theta-\mu_k\cos\theta[1+log(\varepsilon)] \tag{A13}$$

With a given ε find optimal G that gives a constant velocity, v. This value is then plugged onto Eq. 14 to solve for system efficiency, η.

Manuscript received Oct. 22, 2015, and revision received Mar. 30, 2016.

Publication V

Rotich N., Tuunila R., and Louhi-Kultanen M.

Nonlinear optimization of gravity separation, feed and deck angles with response surface methodology

Reprinted with permission from
IMPC Conference Proceedings Series
Proceedings of the XXVII International Mineral Processing Congress – IMPC 2014.
Santiago, Chile, 20.-24.10.2014,
Online 2014.

Nonlinear optimization of gravity separation, feed and deck angles with response surface methodology

Conference Paper · October 2014

DOI: 10.13140/RG.2.1.2535.1768

3 authors, including:

Nicolus Rotich
Lappeenranta University of Technology
15 PUBLICATIONS **16** CITATIONS
SEE PROFILE

Marjatta Louhi-Kultanen
Lappeenranta University of Technology
89 PUBLICATIONS **842** CITATIONS
SEE PROFILE

XXVII SANTIAGO • CHILE IMPC•2014 | 20 - 24 October 2014, Hotel Sheraton, Santiago, Chile
impc2014.org | impc@impc2014.org | +56 2 2652 1528

ABSTRACT 381

Nonlinear optimization of gravity separation, feed and deck angles with response surface methodology

Nicolus Rotich*, Ritva Tuunila & Marjatta Louhi-Kultanen
School of Engineering Sciences, Lappeenranta University of Technology
P.O Box 20 Lappeenranta, South Karelia, Finland

ABSTRACT

Most minerals, their ores, and gangue require sorting in order to maximize the recovery of the primary product during concentration. Gravity separation though old, is not obsolete and is continually playing an important role in mineral processing and many other industries, especially where plant energy efficiency is of concern. Screen designs e.g. material of construction, deck angle of inclination, the feed throughput, and physical as well as chemical properties of the particles, are critical factors to consider when using gravity for solid separation. Solids loading and screen geometry are significant, and easily manipulated operational parameters that affect both the screening rate and efficiency to a large extent. In this paper we applied nonlinear least squares optimization technique, and response surface methodology first, to assess the significance of the two factors, and secondly to select the best mathematical models that optimize both capacity and efficiency of the screening process. Initial experiments and confirmation tests were conducted on a prototype screen of 846.51cm^2 effective area, (2100 cm^2 total area). For glass beads of sizes 0.75-3mm, with feed loads of 10g up to 160g, and inclination angles from 5-20^o, a maximum efficiency of 66.7%, and a screening rate of 22g/s was achieved with a screen loading of 86.5g, and an inclination angle of 12.43^o. These results were then subjected to nonlinear least squares optimization, in which afterwards an optimum theoretical efficiency of 72% and screening rate of 31.2g/s were achieved at a loading of up to 104g. There was excellent performance at angles $12.5 \leq \theta \leq 17.5$, but poor at the angles outside this range. The screening efficiency did not seem to respond significantly to changes in screen loading. Confirmation tests conducted at selected optimum parameters achieved an efficiency of 72.1% (at 17.5^o with 88g load), and a rate of 27g/s at 16.5^o with 104g.

*Corresponding author: LUT School of Engineering Sciences, Lappeenranta University of Technology, Doctoral Student. Telephone: +358 40 50 14334, Email: Nicolus.Rotich@Student.Lut.fi

INTRODUCTION

Solids separation, screening and concentration (in mining), is the process of segregating of particles according to desired criteria or property tied to the solids, under some applied force. These properties are often dictated by downstream unit operations, or end use. In general, the fundamental aim of classification is to separate the behavior of the solids into definite regimes of class patterns (Savage, Pfeffer, & Zhao, 1996).

Gravity separation is an important unit in many industries dealing with solid particulate products (wet or dry). A part from mining, other industries such as construction, food, chemical process, pharmaceutical, agricultural and farm productions, require sorting of some kind in terms of size, density, shape or resilience, prior to further utilization or in final use . Often as not, separation by size is the most common, especially where the density variation between the solids in question is low (Rotich, Tuunila, & Louhi-Kultanen, 2013).

Gravity concentration converts the potential energy of a system into mechanical agitation that causes separation of the material to various classes. The use of this energy therefore, is renewable energy context, payoff when its potential is fully exploited. Some advantages associated with the use of gravity are:

1) It enables optimization of plant energy use e.g. by conducting a pre-concentration with gravity before powered agitation processes. In China for instance, most vanadium is discovered from Vanadium–titanium magnetite ore and stone coal, making its extraction expensive in terms of large ore tonnage mix, expended energy, chemical (acid) consumption and overall costs. Traditional extraction processes for extraction of Vanadium from its ore may involve methods such as direct acid leaching, roasting-acid/alkali leaching, calcified roasting carbonate leaching and low salt roasting-cyclic oxidation. In such cases, decarburization, followed by selective grinding and pre-concentration with gravity, makes it easier to reject up to 28.9% of the feed ore before the main extraction process. (Zhao et al. 2013).
2) It allows operations in remote places e.g. in mining when used for concentration in remote sites, especially where external energies are out of reach.
3) Some unique metals may dictate that only gravity concentration is necessary. A good example is the application in concentration of *cassiterite, chromite, wolframite* and *tantalum* among others which to date, use gravity as the only mode of concentration. In fact, the largest tonnages separated by gravity are in iron ore and coal industry (Burt, R. 1999).

When dealing with gravity separation, a number of factors determines the extent of separation (both capacity and efficiency). While it may seem obvious that if a process has been used for ages, its factors and optimum operating parameters have possibly been found, this unfortunately is not the case. The reasons being: 1) there are hundreds of thousands of materials on earth, each with unique properties; 2) we are not dealing with each of these materials singlehandedly, but as bulk matter with bulk properties; 3) the equipment used for handling also contributes a misunderstanding, as it is also made from its own unique material, dictated by other factors. It therefore forms a cocktail of intertwined factors, making a

supposedly simple process one of the most complex. Here is a quick example: in powder material science, when defining flowability, we can easily say "flowability is the ability of granular solids and powders to flow (Genesan et al. 2008)", and it makes sense. However, when the powder has now (inevitably) come in contact with some material handling equipment e.g. hoppers, mesh screens, conveyors etc., the prior definition becomes short of sufficiency, and instead a nearly accurate definition has been coined "the ability of the powder to flow in a desired manner in a specific piece of equipment" (Bumiller, Carson & Prescott, 2002). Therefore, the former definition is quite casual and seems to suit just the dictionary; the later attempts to give an idea of what flowability really encompass, and give it its engineering meaning.

Solid separators e.g. deck screens, spiral concentrators, Reichert cones etc., are some of the many materials handling equipment, which requires a compromise when it comes to design, and in their day to day operations. Bearing in mind the numerous materials constituting the bulk properties of solids, some critical factors to consider when using gravity force for solid separation, can be classified into intrinsic and extrinsic factors.

1) *Intrinsic factors*: are those which are easily manipulated by mechanical design e.g. Overall configuration of screen, feed rate, deck angle of inclination, aperture sizes, screen material, feed throughputs, mesh size etc.
2) *Extrinsic factors*: accounts for those which are hardly varied by the user either because it is not possible, or manipulating them affects the overall product quality (negatively). These are: particle sizes, moisture content, shape, densities, purity, relative motion of particles to that of screen surface, the physicochemical properties of the solids etc.
3) *Others*: this group of factors account for those unknown or known, but takes an extra effort to determine or manipulate them, either qualitatively or quantitatively. Examples are those linked to the hydro, thermo, electro or even aerodynamic variables

Looking at above factors, it just serves to remind the process engineer that striking an optimum balance of say design and operating parameters is next to impossibility. However, it is actually possible to fit some mathematical function to most processes, and try to understand them in parts.

Material throughput and screen deck inclination are significant and easily manipulated operational parameters that affect both the screening capacity (rate) and efficiency largely. Passing a large feed throughput makes the screen susceptible to "blinding" of the screen, poor flowability and overall reduction in the underflow. Too small feed throughputs, which even though it may increase the efficiency (as observed by Wills & Napier-Munn), makes the process now "tedious" and take long residence times, affecting the economics of production. On the other hand, too low deck angles are good in optimizing the efficiency, but also affect flowability on the screen and significantly reduce the rate of separation. Too high angles of inclinations deprive the particles of the ability to report to the underflow, as they tend to: 1.) "See" a narrow projected, effective screen area, 2.) The flow velocities tend to be too high, making the particles to "ride" over the apertures, instead of passing through. (Wills & Napier-Munn, 2006).

The objective of this research paper is to conduct lab scale gravity screening experiments on a prototype screen for different (sizes and batch masses) of glass beads samples (g), and measure their separation rates (g/s) and efficiencies (η), at six different deck angles of inclinations. The registered results would then be formulated into analysis of variance optimization (ANOVA) strategy, taking the angles as treatments, and

the 16 glass beads samples as blocks, each with their values as factors. The results are then used to construct ANOVA tables and boxplots with MATLAB (Mathworks, 2013). The decisions will then be made on the significance of each factor (based on the null hypothesis), what factors to enhance. The second process involves nonlinear least square optimization to improve the process. Finally, we take confirmation tests at selected optimized parameters then compare the results side by side, and draw necessary conclusions.

METHODOLOGY

Glass beads of mass F and mixed particle size distribution (0.5-3mm) were released from an elevation to an inclined sieve with increasing (known) aperture sizes downwards, with channels below each sieve width to collect the undersize. The process was repeated for six angles (θ), of inclinations (20°, 15°, 14°, 12.5°, 10°, 5°), for each batch (F) of glass beads. The aim was to assess the effect of varied inclinations and increases in feed throughputs on the degree of separation rates and efficiencies. The following measurements were taken and recorded: Sample mass F, mass of the undersize collected on the 1, 2, 3 and 4 mm sieves (m_1, m_2, m_3, m_4), oversize, M_o and runtime, T. The following values were calculated directly from the collected data: total undersize masses (M_u), separation efficiency, η computed as the ratio of total mass of undersize M_u to the batch mass F, epsilon, ε computed as the ratio of mass of oversized collected to the total sample F, and the mass of un-separated particles, M_n (unaccounted for), calculated by subtracting the sum of undersized and oversized from the total sample mass, F. The rates of separation, R were obtained by calculating the mass of the undersize per unit time of separation. Loading coefficient, Ψ is a normalized parameter corresponding to the ratio of load in grams to the overall largest feed mass used (160 g). (Rotich, Tuunila, & Louhi-Kultanen, 2013).

The results of both rates and efficiencies were then tabulated as shown in tables [1-2].

2.1 Table of inclinations, feed throughputs, and separation rates

Table 1: Observed rates of separation with increasing load (Ψ) and inclination angles (θ)

Angle(θ)	Feed loading coefficient (Ψ)															
	0.1	**0.13**	**0.2**	**0.25**	**0.3**	**0.8**	**0.4**	**0.5**	**0.6**	**0.6**	**0.7**	**0.8**	**0.8**	**0.9**	**0.94**	**1**
5	2.4	3.5	4.4	3.4	4.3	4.6	3.6	1.0	2.0	0.9	1.9	2.0	1.4	1.4	1.11	1.74
10	2.2	3.7	4.8	5.1	5.8	6.7	6.3	5.6	6.5	6.5	6.5	6.9	6.5	6.9	6.88	7.47
13	1.9	4.0	5.1	6.7	7.2	8.8	9.1	10.3	11.1	12.2	11.2	11.8	11.7	12.3	12.65	13.19
14	1.8	4.2	5.4	8.2	8.5	10.6	11.5	15.8	15.5	17.0	14.6	14.9	14.7	15.4	15.84	16.07
15	1.6	4.4	5.6	9.6	9.6	12.0	13.5	22.1	19.8	21.2	17.2	17.0	16.7	17.4	17.87	17.80
20	1.7	4.3	5.5	8.9	9.0	11.3	12.5	18.9	17.6	19.1	15.9	16.0	15.7	16.4	16.85	16.93

2.2 Table of inclinations, feed throughputs, and separation efficiencies

Table 2: Recorded efficiencies with increasing feed loading (Ψ) and inclination angles (θ)

Angle(θ)	Feed loading coefficient , F (Ψ)															
	0.1	**0.13**	**0.2**	**0.25**	**0.3**	**0. 8**	**0.4**	**0.5**	**0.6**	**0.6**	**0.7**	**0.8**	**0.8**	**0. 9**	**0.94**	**1.00**
5	0.16	0.17	0.17	0.15	0.16	0.16	0.15	0.13	0.13	0.13	0.12	0.14	0.12	0.12	0.13	0.13
10	0.69	0.65	0.63	0.53	0.48	0.48	0.42	0.37	0.37	0.31	0.31	0.28	0.26	0.24	0.23	0.21
13	0.51	0.54	0.54	0.55	0.49	0.52	0.49	0.47	0.48	0.47	0.47	0.46	0.46	0.45	0.44	0.41
14	0.40	0.47	0.48	0.57	0.49	0.54	0.53	0.53	0.54	0.56	0.57	0.56	0.58	0.58	0.57	0.54
15	0.32	0.43	0.45	0.58	0.49	0.56	0.55	0.57	0.58	0.63	0.64	0.63	0.66	0.66	0.66	0.62
20	0.27	0.34	0.35	0.43	0.37	0.43	0.41	0.44	0.44	0.47	0.48	0.48	0.51	0.50	0.50	0.48

Using the results as design matrices, we then carry out analysis of variance (ANOVA), to assess the significance of the changes in inclinations and the feed quantities on the separation rates and efficiencies. Based on the results, we reject or accept the null hypotheses, that variations in inclination angle and feed quantities have no effects on the rates and efficiencies of separation.

2.3 Analysis of Variance (ANOVA)

Analyses of Variance constitute a very important tool in statistical quality control and optimization in engineering discipline. Its main application is to provide guided decision making on various systems, by literary comparing the variation caused by certain changes in the factors affecting the process, without making assumptions of pre-existing conditions. It is based on the null hypothesis that a certain group of factors do not have significant effect on the resulting observation.

In this case, for both increase in mass and inclinations, the null hypothesis is that the two have no effect on the rates and efficiencies observed in tables [1-2]. The probability, P of the occurrence of the hypothesis is then calculated and used to make following decisions. We will construct two-way ANOVA tables for the rates and efficiencies tables [Tables 3-4].

2.4 Formulation of nonlinear unconstrained optimization strategy

The final stage is to formulate an optimization strategy to determine which deck angles and feed loads are sufficient to operate the screening process at optimum performance. This is done keeping in mind that too high throughputs are detrimental to the efficiencies; so do high deck angles, while low inclinations do not provide sufficient force to cause adequate separation. We chose nonlinear least squares regression for this study, since the overflows need to be minimized, while maximizing underflows.

The total batch mass, F at any given time is the sum of the underflow, Mu and the overflows, Mo so that the total mass balance, efficiency and overflows can be expressed with the following equations:

$$R = M_u(\Psi, \theta) \quad (1)$$

$$F = M_o(\Psi, \theta) + M_u(\Psi, \theta) \quad (2)$$

$$F\eta(\Psi, \theta) = M_u(\Psi, \theta) \quad (3)$$

$$\varepsilon F(\Psi, \theta) = M_o(\Psi, \theta) \quad (4)$$

Substituting equations (4) in (2) we get equation (5), relating ε to M_u, to yield the design matrix.

$$\varepsilon(\Psi,\theta) = 1 - \eta(\Psi,\theta) \quad (5)$$

The implication of Eq. (5) is that, the amount of the underflows (η) at any given time can be maximized by reducing the overflows (ε), it is ideally desired that the feed into the system equals that exiting the system, separated. We can therefore write the function in the form of Eq. (6)

$$\varepsilon(\Psi,\theta) = \frac{\varepsilon F(\Psi,\theta)}{F} \quad (6)$$

$$M_o(\Psi,\theta) = \varepsilon F(\Psi,\theta) \quad (7)$$

Eq. (6-7) thus constitutes objectives by themselves, meaning we can find functions $\hat{\varepsilon}(\Psi,\theta)$ and $\hat{M}_o(\Psi,\theta)$, to estimate $\varepsilon(\Psi,\theta)$ and $M_o(\Psi,\theta)$ respectively. Phenomenologically, the total mass is reducing with time, thus we assume the decay function. We have also used this type of functions before to estimate the separation rates (Rotich, Tuunila, & Louhi-Kultanen, 2013).

$$\hat{\varepsilon}(\theta) = K_1 e^{a_1\theta} - residual \quad (8)$$

$$\hat{M}_o(\theta) = K_2 e^{a_2\Psi} - residual \quad (9)$$

Over determined equations (8-9) were estimated by nonlinear least squares, as exponentials functions, obtaining the coefficients (with 95% confidence bounds). The problem set may now be written in the standard least square optimization notation as shown in Eq. (10-11), in which parameters, (K_1, a_1) which minimize the residuals, can be computed. The same analogy was used to approximate (K_2, a_2) for the rates, in eq. (11). The response surface plots for the optimized rates and efficiencies are presented in Fig. 2

$$\min_{K_1,a_1} R = \sum_{i=1}^{96}[\Psi K_1 e^{a_1\theta} - f(\Psi,\theta)]\text{^}2 \quad (10)$$

$$\min_{K_2,a_2} R = \sum_{i=1}^{96}[\Psi K_2 e^{a_2\Psi} - f(\Psi,\theta)M_o]\text{^}2 \quad (11)$$

RESULTS

3.1 The significance of increased feed and inclinations on the rates [TABLE 1]

Table 3: ANOVA table showing the significance of increased feed and inclination on separation rates

Source	Sum Square	Freedom deg.	Mean Square	F-density	Prob>f
Angles	1588.9	5	317.78	39.67	8.92×10^{-20}
Feed load	1017.76	15	67.85	8.47	6.46×10^{-11}
Error	600.78	75	8.01		
Total	3207.43	95			

3.2 Significance of feed increase and inclinations on the separation efficiencies [table 2]

Table 4: ANOVA table for the significance of increased feed and inclination on the efficiencies

Source	Sum Square	Freedom deg.	Mean Square	F-density	Prob>f
Angles	1.83379	5	0.36676	44.71	4.16×10^{-21}
Feed load	0.02788	15	0.00186	0.23	0.9988
Error	0.61523	75	0.0082		
Total	2.4769	95			

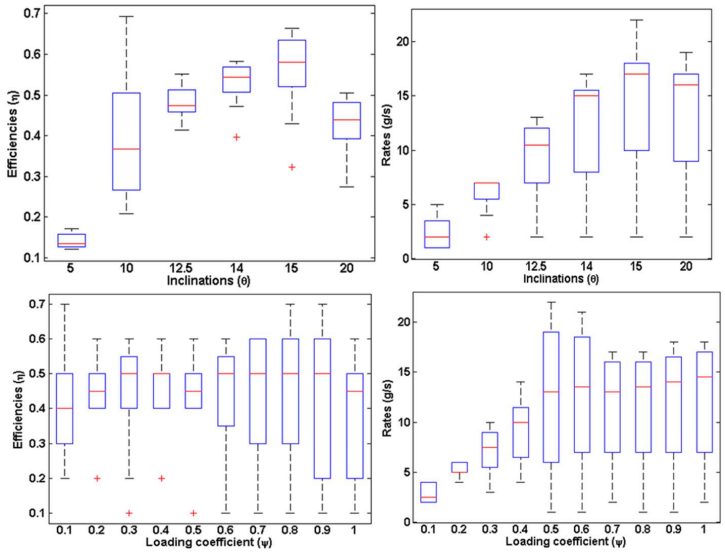

Figure 1: ANOVA boxplots of the significance of Feed and Inclinations on efficiencies and rates

Generally, nonlinear least square solutions are of the form:

Y_i=Model-residuals (errors)

In which Yi is the response data supplied for model approximation. If the computer program returns the residuals, the model result can easily be computed by subtracting the errors from the supplied initial data (Yi). The parameter values for *K* and *a* in eq. (8-9) were approximated as shown in the matrix in eq. (12):

$$\begin{bmatrix} K \\ a \end{bmatrix} = \begin{bmatrix} 11 & 8.054 \\ 0.0013 & 0.718 \end{bmatrix} \quad (12)$$

CONFIRMATION TESTES

Confirmation tests were conducted on the new selected optimum parameters (random points picked from highest points on Fig. 2 b). Confirmation test results are shown in Table 5.

Table 5: Table of confirmation results at optimized parameters

Loading (Ψ)	Angle (θ)	Rates (g/s)	Efficiency(Π)
0.5	18	19.82	62.5
0.31	12.5	14.3	71.6
0.625	19	20.07	57.9
0.5	15	18	68.5
0.55	17.5	23.68	72.1
0.65	16.5	26.9	63.4

3.3 Response surface plots of converged optimal solutions

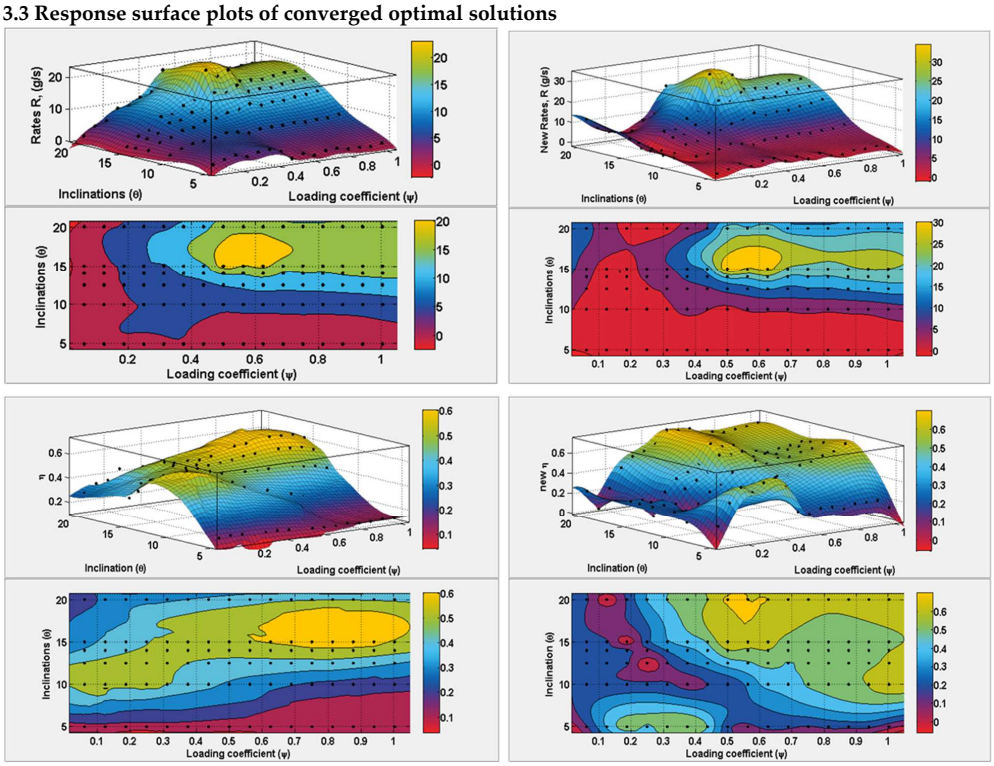

Figure 2: Summary response surface and contours for rates and efficiencies (a) before and (b) after optimization

DISCUSSION

TABLES [3-4] were generated from the ANOVA results for TABLES [1-2]. The values of *f* in column six of [TABLE 1] are less than 0.001. The results suggest that we reject the null hypothesis, that variations in inclinations and feed loads have no significant effect on the rate of separation. Similarly, *f* values in [TABLE 2] suggests otherwise. For inclination, $f<0.001$, while for the loads it is larger than 0.001, implying that we should partially judge the null hypothesis and say, while changes in the loads truly do not have a significant effect on the efficiencies, deck angle variations actually have some effects on the system. The same information is conveyed by ANOVA boxplots in Fig. 1. The additional information that can be extracted from boxplots is that, even though feed loads do not have a significant effect on the efficiencies, lower loads ($\Psi<0.6$), have a positive effect on the efficiencies, while inclinations ($\theta<12.5^{o}$), have a negative effect. Separation rates seems to increase proportionally with both loading and inclinations at the

beginning (up to Ψ=0.65 and 16.5°). Further increases in Ψ and θ causes a decrease in both separation rates and efficiencies.

Nonlinear models in eq. (7-8) were chosen based on previous knowledge of the system behavior, that the reduction in overflow particles is proportional to the increase in the underflow and follows decay functions of exponential nature. The models therefore seemed to have mimicked the system quite well, even though there were residuals, which constituted the error matrices. By comparing the data before and after optimization, it can be seen in [Fig. 2] that the rates have been enhanced by about 9g/s, while system efficiency has been increased by about 5.4%. The operating ranges of θ and Ψ have also been determined clearly, especially for the case of efficiencies ($0.49 \leq \Psi \leq 0.63$). For the rates, the loading factor Ψ did not shift much but shrunk, making it easier to determine optimum loading point ($0.5 \leq \Psi \leq 0.65$). In all the cases, inclination between the ranges $16^{o} \leq \theta \leq 19^{o}$ was found to be favorable. Some additional solutions of efficiencies were also found at $0.2 \leq \Psi \leq 0.4$ and ~6°

CONCLUSION

The study has covered most critical issues on gravity separation, its importance, and research & development progress. Main obstacles to the application of gravity separation have also been highlighted, especially those of design and operation. Even though gravity separation has been used for long, not all optimal design and operational parameters have been found. In this research, only two aspects out of hundreds of design considerations have been studied: the deck angle of inclination, and the feed loading.

With the help of computational techniques the experimental data was fitted to approximate models which were studied to assess their optimal ranges for the two parameters. In deed after optimization the process was improved considerably. The separation rates were improved by about 23% while the efficiencies were improved by about 5.5%. The inclination angle seems to be the most versatile and robust factor that can be manipulated to affect both rates and efficiencies. The loads seem to be less significant to the efficiencies of the system; while on the other hand seeming to be critical for the rates. The maximum rate of separation (31g/s) was not achieved due to possible inefficiencies in the measurement methods applied; this therefore calls for further investigation into the subject area in future.

ACKNOWLEDGEMENTS

Authors wish to acknowledge the Finnish Cultural Foundation, (SKR) and the Finnish Science Foundation for Economics and Technology, (KAUTE) for supporting this research. Special thanks go to Mr. Markku Maijanen, for fabricating the prototype equipment. We also acknowledge Ms. Minna Laitinen for carrying important experiments, which contributed to the success of this work.

NOMENCLATURE

M_o	Mass of oversize particles, g
F	Batchwise masses, g
f	Statistical probability distribution, dimensionless
M_u	Mass of undersize, g
M_n	Mass of un-separated particles, g
$m_{1...4}$	Masses of particles collected on 1 mm, 2 mm, 3 mm and 4 mm sieves respectively, g
T	Runtime taken by the mass, F to be separated, s
ε	Fraction of oversize to total batch mass, dimensionless
η	Separation efficiency, dimensionless
θ	Deck angle of the screens, degrees
R	Separation rate, g/s
Ψ	Normalized loading coefficient, dimensionless
Y_i	Design matrix with the results expected from the model

REFERENCES

Bumiller, M., Carson, J., & Prescott, J. 'A preliminary investigation concerning the effect of particle shape on a powder's flow properties', *World congress on particle technology* 4 (WCOPT4), July 21-25th, 2002, Sydney, Australia (viewed- January 23, 2014 URL- http://tinyurl.com/qhn5glx

Burt, R. (1999), 'The role of gravity concentration in modern processing plants', *Minerals Engineering*, vol. 12, no. 11, pp. 1291-1300.

Ganesan, V., Rosentrater, K. A., Muthukumarappan, K. (2008), 'Flowability and handling characteristics of bulk solids and powders – A review with implications for DDGS', *Biosystems Engineering*, vol. 101, pp. 425-435.

Rotich, N., Tuunila, R. & Louhi-Kultanen, M. (2013), 'Modeling and simulation of gravitational solid–solid separation for optimum performance', *Powder Technology*, vol. 239, pp. 337-347.

Savage, S., Pfeffer, R. & Zhao, Z.M. (1996), 'Solids transport, separation and classification', *Powder Technology*, vol. 88, no. 3, pp. 323-333.

Wills, B., & Napier-Munn, T. (2006), 'Mineral Processing Technology: An Introduction to the Practical Aspects of Ore Treatment and Minerals Recovery', Oxford: Elsevier Science & Technology

MathWorks, 'MATLAB version 7.14.0.739 R2013a (2013)', The MathWorks Inc., Natick, Massachusetts

Zhao, Y., Zhang, Y., Liu, T., Chen, T., Bian, Y. & Bao, S. (2013), 'Pre-concentration of vanadium from stone coal by gravity separation', *International Journal of Mineral Processing*, vol. 121, pp. 1-5

Other Publication(s)

Rotich N., Tuunila R., and Louhi-Kultanen M.
The fall and rise of gravity separation

Reprinted with permission from
Mining Magazine
Physical Separation.
Vol. 9, pp. 60–67, 2014.
Online 2014.

An FLSmidth Krebs hydrocyclone cluster

The fall and rise of gravity separation

In an independent look at gravity classification and separation over the past 20 years, a researcher with Lappeenranta University in Finland suggests gravity is back where it belongs in the mineral-processing R&D and application hierarchy – near the top. Richard Roberts reports

"Gravity separation... has not been fully developed and understood in terms of key parameters that determine its performance"

Nicolus Rotich's co-written "sustainability perspective" on gravity-based systems in mining is based on a review of the two decades book-ended by 1994 and 2014. It indicates that the pace of gravity classification and separation/concentration development, in the areas of application and research, has quickened again after becoming somewhat sluggish in the last quarter of the 20th century.

Environmental factors are playing a pivotal role in this revival, in mining and other industries, he says.

"Maximum recovery at minimum cost, coupled with high efficiencies, effectiveness and environmentally acceptable operating standards, are the main objectives during modern plant set-up," says Rotich and his co-authors Ritva Tuunila and Marjatta Louhi-Kultanen from the Lappeenranta University of Technology (LUT) Department of Chemical Technology.

"Sustainability is a new entrant to the competitiveness of industries. Many companies have had to re-think the use of gravity due to the high costs of flotation reagents, the relative simplicity of gravity separation, the fact that it creates less environmental pollution, and

efficiency, even for particulates at the range of 50µm.

"Gravity concentration is as good as a renewable source of energy, converting potential energy to mechanical agitation in size separation. Gravity separation enables the optimisation of plant energy in cases where it is used as a means of pre-concentration before subjecting the material to electrically powered processes. In remote places, gravity is also used in concentration where external energies are out of reach," continues Rotich.

"The low cost and environmentally friendly operation has led to the intense use of gravity for the recovery of gold. Moreover, we expect that limitations of discharge will be tightened by legislation in the future, further favouring gravity-separation processes over other methods."

Rotich says there is a "clear role [for] gravity separation in the present-day mining industry".

"[Despite] all misconceptions [about] the downfall of gravity separation, these methods have grown to see the light of day after all. Industrialists have realised that some processes such as concentration of some unique metal-bearing ores – for example, cassiterite, chromite, wolframite and tantalum, among others – use gravity as the only mode of concentration. [And] beneficiation of gold has long been accomplished with gravity-based separators such as spiral concentrators.

"In general, orebodies requiring thorough treatment are becoming increasingly complex," Rotich says.

"In China, for instance, most vanadium is discovered from vanadium-titanium magnetite ore and stone coal, making its extraction expensive in terms of large ore-tonnage mix, expended energy, chemical (acid) consumption and total costs. Traditional processes for the extraction of vanadium from ore may involve methods such as direct acid leaching, roasting-acid leaching, calcified roasting carbonate leaching, low salt roasting-cyclic oxidation and roasting-alkali leaching. In such cases, decarburisation, followed by selective grinding before pre-concentration with gravity, makes it easier to reject about 28.9% of the feed ore before the main extraction. ►

Spiral concentrators use gravity to concentrate ore, separating material by density in certain size ranges

Holman 8000 shaking-table installation

Copper recovery on a Wilfley 7000 water table; a GIW hydrocyclone

"Even today, most giant mineral-processing companies in Australia, South Africa, China, Chile, Russia and Peru still value gravity as one of the most competitive methods for concentrating minerals," Rotich adds.

"A multinational corporation in the mining sector reported [this year] that replacement of differential flotation with gravity separation in its operation enhanced concentration in a tin-recovery plant by 8-10%."

"Giant mineral-processing companies in Australia, South Africa, China, Chile, Russia and Peru still value gravity as one of the most competitive methods for concentrating minerals"

THE ROLE OF RESEARCH

A Moi University, Kenya, graduate in 2007 (bachelor of technology), Rotich worked in a government industrial-research institute for three years before moving to Lappeenranta University to attain a master of technology degree in environmental engineering. After securing that, he started on his doctor of science in chemical engineering degree last year, majoring in physical separation of solid particles.

"Physical separation is an old process, not only in mining but also in the energy sub-sectors – for example, beneficiation of coal," Rotich says. "More important are the recently developed sustainable biomass processing and refining systems [such as] the new combustion systems for generating steam, especially in Scandinavia, which require sizing of solids, be they domestic animal wastes or solid residues from forests. These were some of the fundamental reasons that drove me to investigate these processes.

"The mechanisms of solids separation, in particular, have a history of being poorly understood in academia [with more than 20 journal papers citing this], so this was one important aspect that will make the dissertation not only technological but also academic."

Rotich will present a paper based on his extensive investigation of modelling, experimental verifications and re-engineering of particle-classification systems, at a major international mineral-processing congress in mid-October in Santiago, Chile. The paper is focused on the optimisation of gravity-separation deck angles and feed throughput.

"We [previously] developed mathematical schemes for quantifying the rates and efficiencies for solid separation, and we are continuing the work now with empirical studies aiming to verify those models," he says.

Rotich explains that LUT, established in 1969, was among a handful of Finnish universities that gained international standing for practical R&D aimed at providing industry with real technical solutions. "Nowadays, LUT's strategic focus areas are green energy and technology, the creation of sustainable competitiveness and operation as a hub of international Russian relations," Rotich says.

The government collaborates with the universities to set priority areas that are geared towards benefiting the industry and society in general. The universities in turn implement strategic plans with the sole purpose of benefiting the environments around them. And they tend to be specialised, so that each university is known for a specific discipline strength.

BOOSTING GRAVITY SEPARATION

Rotich says that the fundamental aim of gravity classification is to separate material into definite regimes of behaviour class patterns. It generally promotes high operational efficiency in equipment, could improve material handling within process units, and ensures that the best-quality product goes to downstream processes (including final use). In mining, gravity separation helps to curb tendencies of over-grinding and high energy consumption.

Key mineral-processing gravity systems have undergone several metamorphic re-designs in recent times in order to fit to the current industry permutations, notes Rotich.

Yet not so long ago, gravity separation "became a neglected subject in academia, technical conferences and research in journal papers. It ended up being given a cold shoulder in most scientific forums, [with] gravity separation papers labelled among 'others' and always banished to the last afternoon [of conferences]", he says.

It was thought that young mineral-processing engineers would not be willing to specialise in gravity concentra-

Introducing the
ME FIT SYSTEM

An innovative concept for our mineral processing customers

The **ME FIT System** is a new concept developed by ME Elecmetal. It consists of integrating optimized mill liner and grinding media systems. The system is developed through the on going analysis of dynamic operating data by mineral processors and ME Elecmetal sales engineers. It takes advantage of the highest standards in manufacturing, quality, service, and logistics, along with the people that bring it all together. The end result: **Improved performance for SAG and ball mills.**

FIT is an acronym for Fully Integrated Technology.
ME Elecmetal combines mill liner and grinding media technology with the dynamics inside each mill.
The **ME FIT System** is part of ME Elecmetal's integrated solutions approach to product development and operational support which includes a range of services such as simulations and 3D scanning.

ME Elecmetal's almost 100 years of providing innovative solutions makes the **ME FIT System** possible. This unique value proposal to our market will provide positive results in operations, mill economics, service, logistics, environmental and safety areas.

OPTIMIZED MILL LINER + GRINDING MEDIA SYSTEM

ME FITSYSTEM

Learn more about how the ME FIT System can help to improve your milling operation at
www.me-elecmetal.com and **www.mefitsystem.com**

We Speak Mining

Proven Mining Solutions

Whether your process is above ground or below, conventional, surface or longwall, Baldor offers a seasoned team of mining pros that are second-to-none at helping you keep your operation up and running.

Our Industry Solutions specialists have decades of crushing, conveying and ventilation application experience…expertise gained from years of working with and listening to customers in-the-field and delivering products that get the job done.

Count on the Industry Solutions team to deliver the knowledge, solutions, products and performance you expect with the confidence of knowing they're with you every step of the way.

baldor.com **479-646-4711**

BALDOR®
A MEMBER OF THE ABB GROUP

tion. "These misconceptions almost led to a collapse in the continual development in theory and its practical applications," Rotich says.

"Gravity separation, old as it is, has not been fully developed and understood in terms of key parameters that determine its performance. The subject has been deficient, especially when it comes to the use of modern tools such as mathematical modelling and simulation, statistical and computational techniques which have allowed other fields to prosper stunningly in the last few years.

"Attention seems to have shifted [in this period], leading to a sharp increase in the number of publications in the area of gravity separation, with significant advances including the mathematical modelling and simulation aspect. Some researchers report new discoveries on methods/configurations of gravity separators that have resulted in the successful extraction of particles smaller than 0.5mm."

But Rotich says there remains a real need for more accurate methods of quantification and optimisation of the operating parameters of gravity separators.

He believes that increased interest in gravity separation is being driven partly by a deeper focus in the industry on more environmentally responsible solutions in response to increasingly weighty social, energy, water and cost challenges.

"The industry has to work within certain constraints, imposed not only by economies of scale, but also by adherence to factors of sustainability, such as the corporate, social and environmental responsibility concept among others," Rotich says.

"Cost and maximum recovery are no longer the only dicta in plant design. On the contrary, today's optimum plant design is determined by a cocktail of complex criteria composed of efficiency, effectiveness and environmental sustainability, together with the fact that maximum product recovery may not necessarily conform to optimal industry economics.

"In fact, most studies have pointed out with evidence the contrasting and/or competing relationships between separation capacities or rates, and corresponding efficiencies even within the unit operations themselves," he adds.

Rotich says that while selecting optimal operating parameters for gravity systems could be extremely difficult and tedious, it might soon be a thing of the past with the advent of the fast computers and computational algorithms currently available. "It is now possible to vividly model these dynamics within a shorter time," he comments.

In the past few years, researchers have attempted to come up with various computational models that could soon allow optimisation, and possible improvement both in performance and understanding.

"[But] the bitter truth about computer models is that correctness in the mathematical description of the systems is crucial to modelling. Incomplete information will definitely cause mis-description to the model, and consequently poor performance," concludes Rotich.

Lappeenranta University of Technology in Finland is carrying out timely research into gravity separation

Weighing up the options

Gravity separation played an important role in the pre- and post-industrial revolution era, and prior to the development of advanced gravity separation, hand picking was used for well over 2,000 years.

In fact, sources refer to separation by density difference as being as old as recorded history. Yan and Gupta date it back to 3,000BC as recorded in writings from ancient Egypt (Yan & Gupta, 2006).

Thinking the industrial revolution to have been a spontaneous phenomenon might suggest that the adoption of gravity separation was simultaneous and widespread throughout the world. However, chronological records show a slowdown in development of gravity separation after the first half of the last century, due to partial replacement by novel methods such as flotation, magnetic separation and leaching (Richards & Palmer, 1997).

Despite the advance of these replacement technologies, gravity separation has not only survived over the years but also thrived, kept pace with, and grown with what is now a competitive industry.

Issues such as the extra cost of grinding particles to flotation sizes and the addition of reagents, as well as environmental concerns about alternatives, have contributed to a resurgence in interest and development for gravity separation.

Nicolus Rotich

There are a number of other obvious reasons for a reluctance to move away from gravity-separation techniques, including the fact that it is generally highly energy-efficient as it uses the natural force of gravity; it is environmentally friendly (no fuels involved, no firing/heating); it can offer quite high separation efficiencies and low cost (e.g. cone and spiral separators), and can handle high capacities of solids up to 272t/h.

Gravity systems can also be quite simple to implement and are based on proven methodologies. They offer numerous and flexible geometry configurations, all with different benefits, many of which have not been properly explored.

On the flipside, gravity separation has not been fully understood in terms of key parameters that determine its performance, such as the motion of particles on different surfaces. Dust control in dry processes can also be challenging, and efficiency and effectiveness in fine particle separation are still questioned (significant losses can occur in rare-earth separation, for example).

There have also been concerns that some new mineral deposits present new challenges, including those hindering the use of gravity as a sole means of concentration. Examples of this group include orebodies bearing rare-earth elements such as bastnäsite, monazite and xenotime, which require the combined efforts of concentration methods, usually froth flotation and magnetic separation, in addition to gravity concentration.

Nicolus Rotich

"Some researchers report new discoveries on gravity separators that have resulted in the successful extraction of particles smaller than 0.5mm"

ACTA UNIVERSITATIS LAPPEENRANTAENSIS

707. AMOUR, IDRISSA. Variational ensemble kalman filtering applied to data assimilation problems in computational fluid dynamics. 2016. Diss.

708. SHESTAKOVA, MARINA. Ultrasound-assisted electrochemical treatment of wastewaters containing organic pollutants by using novel Ti/Ta2O5-SnO2 electrodes. 2016. Diss.

709. OLEKSIIENKO, OLGA. Physico-chemical properties of sol-gel synthesized titanosilicates for the uptake of radionuclides from aqueous solutions. 2016. Diss.

710. PATALA, SAMULI. Advancing sustainability-oriented innovations in industrial markets. 2016. Diss.

711. KUORIKOSKI, TERO. Kohti resonoivaa urheilujohtamista – Tavoitteen muodostuminen urheilun kentässä. 2016. Diss.

712. LAHTELA, VILLE. Improving the properties of solid Scots pine (Pinus sylvestris) wood by using modification technology and agents. 2016. Diss.

713. NEVARANTA, NIKO. Online time and frequency domain identification of a resonating mechanical system in electric drives. 2016. Diss.

714. FANG, CHAO. Study on system design and key technologies of case closure welding for ITER correction coil. 2016. Diss.

715. GARCÍA PÉREZ, MANUEL. Modeling the effects of unsteady flow patterns on the fireside ash fouling in tube arrays of kraft and coal-fired boilers.

716. KATTAINEN, JARI. Heterarkkisen verkostoyhteistyön johtamistarpeet verkoston muotoutumisvaiheessa. 2016. Diss.

717. HASAN, MEHDI. Purification of aqueous electrolyte solutions by air-cooled natural freezing. 2016. Diss.

718. KNUTAS, ANTTI. Increasing beneficial interactions in a computer-supported collaborative environment. 2016. Diss.

719. OVASKA, SAMI-SEPPO. Oil and grease barrier properties of converted dispersion-coated paperboards. 2016. Diss.

720. MAROCHKIN, VLADISLAV. Novel solutions for improving solid-state photon detector performance and manufacturing. 2016. Diss.

721. SERMYAGINA, EKATERINA. Modelling of torrefaction and hydrothermal carbonization and heat integration of torrefaction with a CHP plant. 2016. Diss.

722. KOTISALO, KAISA. Assessment of process safety performance in Seveso establishments. 2016. Diss.

723. LAINE, IGOR. Institution-based view of entrepreneurial internationalization. 2016. Diss.

724. MONTECINOS, WERNER EDUARDO JARA. Axial flux permanent magnet machines – development of optimal design strategies. 2016. Diss.

725. MULTAHARJU, SIRPA. Managing sustainability-related risks in supply chains. 2016. Diss.

726. HANNONEN, JANNE. Application of an embedded control system for aging detection of power converter components. 2016. Diss.

727. PARKKILA, JANNE. Connecting video games as a solution for the growing video game markets. 2016. Diss.

728. RINKINEN, SATU. Clusters, innovation systems and ecosystems: Studies on innovation policy's concept evolution and approaches for regional renewal. 2016. Diss.

729. VANADZINA, EVGENIA. Capacity market in Russia: addressing the energy trilemma. 2016. Diss.

730. KUOKKANEN, ANNA. Understanding complex system change for a sustainable food system. 2016. Diss.

731. SAVOLAINEN, JYRKI. Analyzing the profitability of metal mining investments with system dynamic modeling and real option analysis. 2016. Diss.

732. LAMPINEN, MATTI. Development of hydrometallurgical reactor leaching for recovery of zinc and gold. 2016. Diss.

733. SUHOLA, TIMO. Asiakaslähtöisyys ja monialainen yhteistyö oppilashuollossa: oppilashuoltoprosessi systeemisenä palvelukokonaisuutena. 2017. Diss.

734. SPODNIAK, PETR. Long-term transmission rights in the Nordic electricity markets: An empirical appraisal of transmission risk management and hedging. 2017. Diss.

735. MONTONEN, JUHO. Integrated hub gear motor for heavy-duty off-road working machines – Interdisciplinary design. 2017. Diss.

736. ALMANASRAH, MOHAMMAD. Hot water extraction and membrane filtration processes in fractionation and recovery of value-added compounds from wood and plant residues. 2017. Diss.

737. TOIVANEN, JENNI. Systematic complaint data analysis in a supply chain network context to recognise the quality targets of welding production. 2017. Diss.

738. PATEL, GITESHKUMAR. Computational fluid dynamics analysis of steam condensation in nuclear power plant applications. 2017. Diss.

739. MATTHEWS, SAMI. Novel process development in post-forming of an extruded wood plastic composite sheet. 2017. Diss.

740. KÄHKÖNEN, TOMMI. Understanding and managing enterprise systems integration. 2017. Diss.

741. YLI-HUUMO, JESSE. The role of technical dept in software development. 2017. Diss.

742. LAYUS, PAVEL. Usability of the submerged arc welding (SAW) process for thick high strength steel plates for Arctic shipbuilding applications. 2017. Diss.

743. KHAN, RAKHSHANDA. The contribution of socially driven businesses and innovations to social sustainability. 2017. Diss.

744. BIBOV, ALEKSANDER. Low-memory filtering for large-scale data assimilation. 2017. Diss.